LATVIAN JOURNAL of PHYSICS and TECHNICAL SCIENCES

ISSN 0868 - 8257

4

(Vol. 57)

2020

CONTENTS

S. Arhun, Yu. Borodenko, A. Hnatov, A. Popova, H. Hnatova, N. Kunicina, A. Ziravecka, A. Zabasta, L. Ribickis.
Choice of Parameters for the Electrodrive Diagnostic System of Hybrid Vehicle Traction 3

A. Gasparjans, A. Terebkov, V. Priednieks, R. Klaucans.
Spectral Analysis of Output Voltages and Currents as a Criterion for Technical Diagnostics of Synchronous Generators of Ship Diesel Engine 12

K. Vilcane, S. Matsenko, M. Parfjonovs, R. Murnieks, M. Aleksejeva, S. Spolitis.
Implementation of Multi-Wavelength Source for DWDM-PON Fiber Optical Transmission Systems 24

J. Savickis, L. Zemite, N. Zeltins, I. Bode, L. Jansons, E. Dzelzitis, A. Koposovs, A. Selickis, A. Ansone.
The Biomethane Injection into the Natural Gas Networks: The EU's Gas Synergy Path 34

I. Zeroual, K. Hami, A. Talhi, A. Touhami.
Geo Electric Study in Hydrogeology according to the Axis Hassi Naga – Hassi Khebi of Tindouf (Southwestern Algeria) 51

I. Barmina, A. Kolmickovs, R. Valdmanis, S. Vostrikovs, M. Zake.
The Effect of Electric Field Configuration on the Thermo-Chemical Conversion of Straw Pellets 65

LATVIAN JOURNAL of PHYSICS and TECHNICAL SCIENCES

LATVIJAS FIZIKAS un TEHNISKO ZINĀTŅU ŽURNĀLS

ЛАТВИЙСКИЙ ФИЗИКО-ТЕХНИЧЕСКИЙ ЖУРНАЛ

Published six times a year since February 1964
Iznāk sešas reizes gadā kopš 1964. gada februāra
Выходит шесть раз в год с февраля 1964 года

4 (Vol. 57) • 2020

RĪGA

Language Editor: O. Ivanova
Computer Designer: I. Begicevs

INDEXED (PUBLISHED) IN

www.scopus.com
www.sciendo.com
EBSCO (Academic Search Complete, www.epnet.com), INSPEC (www.iee.org.com).
VINITI (www.viniti.ru), Begell House Inc/ (EDC, www.edata-center.com).

Issuers: Institute of Physical Energetics,
Institute of Solid State Physics, University of Latvia
Registration Certificate Number: 000700221

Editorial Contacts:
11 Krivu Street, Riga, LV - 1006
Ph.: + 371 67551732
E-mail: leo@lza.lv
www.fei-web.lv

sciendo

LATVIAN JOURNAL OF PHYSICS
AND TECHNICAL SCIENCES
2020, N 4

DOI: 10.2478/lpts-2020-0017

CHOICE OF PARAMETERS FOR THE ELECTRODRIVE DIAGNOSTIC SYSTEM OF HYBRID VEHICLE TRACTION

S. Arhun[1]*, Yu. Borodenko[1], A. Hnatov[1], A. Popova[2]**, H. Hnatova[1], N. Kunicina[3]***, A. Ziravecka[3], A. Zabasta[3], L. Ribickis[3]

[1]Department of Vehicle Electronics, Kharkiv National Automobile and Highway University, Khrakiv, UKRAINE
[2]Department of Accounting, Audit and International Economic Relations, Kharkiv National Automobile and Highway University, Khrakiv, UKRAINE
[3]Riga Technical University, Faculty of Power and Electrical Engineering, Institute of Industrial Electronics and Electrical Engineering, Riga, LATVIA
e-mail: shasyana@gmail.com; angelikapopova@meta.ua**; Nadezda.Kunicina@rtu.lv***

When operating a hybrid vehicle (HEV), it is important to reduce maintenance and repair costs. The HEV electric drive (ED) consists of electronic, electrical and mechanical parts and is considered a complex diagnostic model. The availability of an electrical part greatly simplifies the process of monitoring and obtaining information about the state of the system. In order to create a hybrid diesel-electric propulsion system (HDEPS), the choice of structural and functional parameters as diagnostic ones is justified, the control points are chosen, and the necessary accuracy and unambiguity of measurements are determined. Qualitative evaluations of the electrical processes occurring in the power supply circuit of ED from a high-voltage accumulator battery for the selection of diagnostic parameters according to the criteria of sensitivity, informative character, stability and manufacturability of measurements are presented. It has been revealed that during HDEPS diagnostics both stable and transient modes of operation of electric machines should be considered; for analysis of ED technical state it is necessary to have information about current mode of HDEPS load; for measurement of instantaneous values of supply voltage and consumption current it is necessary to select the sensors with short response time and linear conversion function. In terms of sensitivity to structural changes in the circuit and parametric deviations, it is necessary to choose, as diagnostic parameters, the voltage or current, depending on the mode of operation of the ED and the point of measurement of the electrical value. The obtained results are the basis for creating a new system of diagnostics of electric power supply HDEPS in this direction.

Keywords: *diagnostics, hybrid electric vehicle, hybrid power plants, simulation model, traction electric drive.*

1. INTRODUCTION

Deterioration of the environmental situation and a significant reduction in natural resources not only accelerated the development of energy-efficient technologies and alternative sources of electrical energy, but also became the root cause of the popularization of vehicles on electric traction – electric vehicles [1], [2]. Electric vehicles can be divided into two types: those that use only electric motors (EM) and those that drive a hybrid electric vehicle and ICE (plug-in hybrid electric vehicle (PHEV), hybrid electric vehicle (HEV)). A few years ago it seemed that hybrid electric vehicles were a temporary option before the total introduction of EM [3]. Several IoT methods are widely used in the vehicle operation, control, diagnostics, as well as for interconnection with other participants of traffic flow [4]–[6]. However, scientists from many countries continue to work on improving hybrid power plants (HPP) [7], improving their technical and operational characteristics [8], [9], [7], [10], [11], and car manufacturers continue to produce them. At present, cars, trucks and buses with HPP are mass-produced by automobile manufacturers of the world (Honda, General Motors, Toyota, Lexus, Ford, Volkswagen), large energy companies and national laboratories (EPRI, General Electric, NREL, INEEL, ISE Research). This is explained by the advantages of hybrid vehicles, namely their ecological and economic efficiency in comparison with cars with internal combustion engines; independence from electric fueling stations in contrast to EM [12], [13], [7].

However, PHEV and HEV have a significant drawback that constrains their production and application – this is a complex design, which increases the likelihood of failure of components and parts of the HPP, and makes it difficult to diagnose and repair them. Therefore, although the technical and economic characteristics of HPP vehicles are improving every year, their production technology is improving and becoming cheaper, and the relevance of problems associated with the maintenance of hybrid concepts is increasing.

When creating the HPP, it is extremely important to choose power and energy elements, the principle of energy accumulation, the basic scheme, the type of thermal engine, its capacity and operating modes. The second aspect of improving hybrids is to reduce operating costs in terms of their maintenance and repair, where the diagnosis of the technical condition of HPP has the dominant part.

Toyota cars (Camry Hybrid, Highlander Hybrid, Prius, Lexus RX - 400h, Lexus GS - 450h) and Ford (Escape Hybrid, Mercury Mariner Hybrid) use a mixed layout of HPP, which is based on two electric machines operating in engine and generator modes [15].

The electric (ED) hybrid drive consists of electronic (control and power), electric (winding circles of machines and apparatus) and mechanical (transmission) parts and is considered a complex diagnostic model. Malfunctions of such a system can be caused by failure of electronic components, destruction of electrical circuits and wear and tear of mechanical parts. Meanwhile, the presence of an electrical part greatly simplifies the process of monitoring and obtaining information about the state of the system.

When diagnosing ED of general structure, known methods [16]–[18] and approaches are applied: sequential check “from end to beginning”; simulation of

intermediate signals; opening of feedback circuit; replacement and exclusion of separate elements; vibration method [19], [10], [20].

When checking the control part of EV, it is expedient to use the signature analysis method [20]–[22].

In most cases, the following points define the diagnostic method (technology):

- the purpose of the check (regulatory, emergency);
- the depth of fault location (according to the initial or structural parameters);
- the level of qualification of the operator and diagnostic tools;
- actual state of ED system for the period of diagnostics (presence of signs of malfunction).

In general, the check of the electric part of the ED starts with the control of the voltage levels of all power supplies at idling speed and under the rated load in static modes (without input signals). The control equipment of the drive is checked for adequacy of the output signals under initial conditions without changing the conditions at its inputs. Further localization of faults consists in checking of voltages and signals in control circuit control points (localization up to the level of functional block) and modes of power and signal electronics components (localization up to the level of component). Further, the function of the drive in dynamic modes (start, reverse braking, loading, unloading) is checked. After detection of faulty ED element (unit, apparatus, electric machine) it is diagnosed by structural parameters.

For electric machines, structural diagnostics consists of the following operations: measuring the working gap between the stator and the rotor, the insulation resistance of the armature winding and excitation; checking the connection of the neutral; checking the windings for the absence of closed loops and closing to the body; measuring the force of pressing the brushes of the collector unit; checking the axial and radial backlashes of the rotor shaft [23], [15].

Modern vehicle control systems use onboard self-diagnostic systems based on expert programs integrated into the basic control algorithms. Diagnostic information in such systems is read from the on-board computer by means of diagnostic scanners in the form of error codes, current values of mode parameters, reference values of parameters from the data library [15]. The self-diagnostic system is able to control the technical condition of the control system elements (peripheral devices), which are directly connected to the electronic control block (ECB), but does not allow controlling the actuators, which have galvanic isolation from the ECB, and observing the object of mechatronic system control.

To monitor the technical condition of rotating units of the vehicle (ICE, electric motors, pneumatic engines, components and units of the transmission) during maintenance, it is necessary to use methods in which the information about the state of the object of diagnosis is obtained on the basis of harmonic analysis (vibro-acoustics, analysis of the rotation irregularities of the shaft) [10], [24]–[27]. Due to a high level of modern measuring technology, the designated methods can also be used for the current monitoring of the state of the vehicle power units in transport mode.

The aim of the research is to study the electric drive in order to create a system of diagnostics of hybrid power plant of the car with the justification of the choice of its structural and functional parameters.

2. BACKGROUND OF THE STUDY AND SETTING THE TASK OF DIAGNOSTICS OF ELECTRIC VEHICLE OF HPP

Power circuits of hybrid car ED contain reactive elements and they are switching processes. As a result, power supply circuits are subject to transient processes, the nature of which can be used to determine the technical condition of the power plant. Frequency of transients in ED power supply circuits creates preconditions for harmonic analysis of functions of voltage and current change for the purpose of damaged element localization or electronic circuit installation, as well as electromechanical part of ED. Constant voltage converters, inverters, rectifiers should be referred to the electronic devices that make up the power part of the drive. In the mechanical part of the transmission, mechanical torque converters are used.

Presence of reactive components (capacitors, battery, winding of electric machines and inductive reactors) in the ED scheme, on the one hand, cause slowing down of transients (inertial links), on the other hand, increase the dynamics of changes in electrical signals (differential links), depending on the modes of electrical circuit, the nature of load and circuit connection of reactive components.

At present, the electric drive systems of HPP provide sensors of integral parameters (temperature, average or effective values of electrical signals), characterising the general condition of its power elements. Signals of such sensors inform the control system about the regime state of the electric drive elements in order to optimize the power redistribution between the drive units of HPP. At the same time, the obtained information does not allow identifying the technical state of ED elements and localizing the malfunction. To solve this problem, it is necessary to have a system of monitoring of diagnostic parameters. On the basis of its analysis, it is possible to localize the malfunction, ensure accident-free operation, anticipate the emergency state of the HPP and predict its residual lifetime.

Thus, in order to create a system of diagnostics of the HPP electric drive it is necessary to justify the choice of structural and functional parameters as diagnostic ones, to choose the points of their control, to determine the necessary accuracy and unambiguity of measurements.

As alternative diagnostic parameters, the average and instantaneous values of voltage and currents at the outputs of ED functional blocks are considered during the operation of the HPP according to various schemes of power element power distribution and in all operational modes of HPP load.

At the first stage of the research, the task is to give a qualitative assessment of the electrical processes occurring in the power supply circuit of ED from a high-voltage battery (HVB) in order to select diagnostic parameters according to the criteria of sensitivity, informative character, stability and manufacturability of measurement [15], [28].

3. ANALYSIS OF THE STRUCTURE OF THE DIAGNOSIS SUBJECT

Let us consider the typical functional structure of the hybrid car electric drive with the use of the GM valve machine, which is able to work in the modes of engine

"M" and generator "G" and for the control actions absorbs the positions of the accelerator pedal α and the rotation of the machine shaft n (Fig. 1). On the scheme, thick solid arrows indicate the direction of power transfer in mode "M", thick dotted – in mode "G". Thin arrows symbolise the control signals, while three-dimensional arrows symbolise information signals. The controller of electric machines (KEM) transmits to HVC the data on the current at the output of the inverter and its temperature. The KEM receives data for controlling the MG machine from the HVC. The output voltages of the converters are regulated by the corresponding signals f_1 and f_2. The output power of the inverter and, correspondently, of the electric motor, is guided by the signal f_3 and the switching signals fn, which are formed on the basis of the rotor angle signal of the machine ω. The HVC monitors the charging level of the HVB I_3 U_{ch}, its temperature then. HVC also receives information about the temperature of the electrical power devices and the value of the electrical load of the HVB [12].

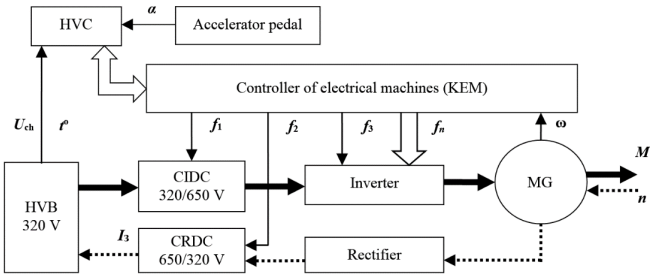

Fig. 1. Scheme of functional electric drive: HVC – a high voltage controller; HVB – a high voltage battery; CIDC – a converter that increases DC voltage; CRDC – a converter that reduces DC voltage.

The level and the value of the pulse pressure on the vortex of the CIDC is the same as the value of the navantagenna (electric motor and inverter mill). Inconsistencies in the electrical field phase will be the victimization of the periodic program function, and in the case of the mechanical transmission – the victimization of the HVB.

4. APPROBATION RESULTS OF THE SIMULATION MODEL

To simulate the processes in the circles of the valve motor system, an imitation model of its circuitry in the application package "Matlab/Simulink" was built (Fig. 2).

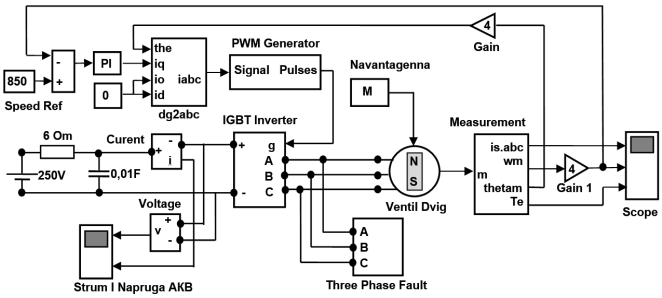

Fig. 2. Simulation model of a valve motor system.

The model contains a three-phase magnetoelectric synchronous machine (Ventil Dvigatel) controlled by a three-phase inverter (IGBT Inverter), inverter control unit (PWM Generator) and coordinate converter dq2abc.

The speed of the drive is set by the Speed Ref unit. The measurement of the machine variable state is carried out by the measurement unit, and the analysis of the instantaneous values of the electrical parameters of the power supply circuit is carried out by the Strum i Napruga AKB oscilloscope.

The model does not take into account the influence of distributed installation parameters of the device, and examines only the modes of electric drive and considers the scheme without a pulse converter of direct voltage CIDC.

Figure 3 represents the time diagrams: phase current i_p, rotor speed n and torque on the shaft M of the valve motor; current i_B and voltage u_B in the power supply circuit of the inverter (high-voltage battery).

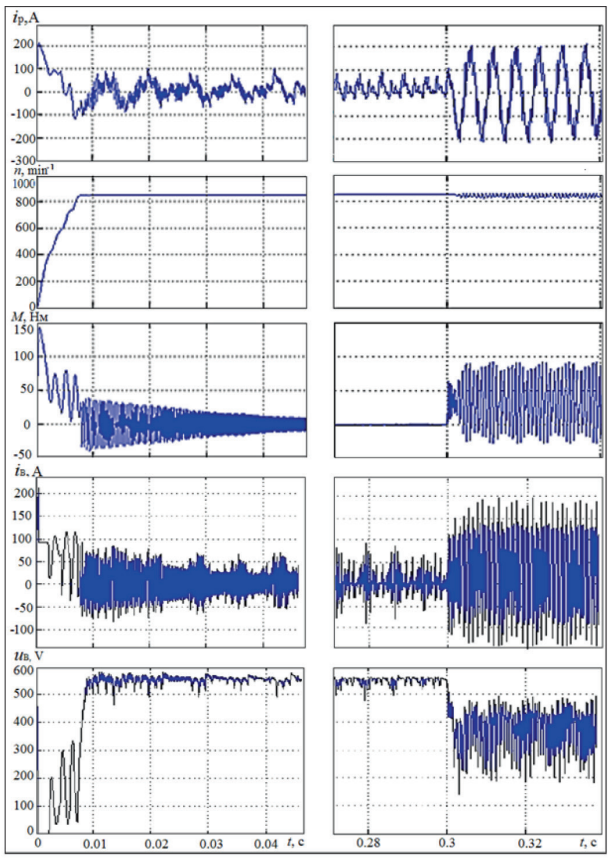

Fig. 3. Time diagrams of electromechanical processes of a drive with the valve electric motor: a – at acceleration without loading; b – at connection of loading.

The analysis of the oscillogram (Fig. 3) shows that both stable and transient modes of operation of electric machines should be considered when diagnosing the actuator.

Fragmentally combined diagrams give an idea of the complexity of transients in the circuits of the valve motor system in different modes of operation of a functional electric drive system. It is obvious that at occurrence of malfunctions in system, character of transients will change.

System malfunctions that do not cause

the drive to shut down, but degrade its performance, include

- loss of HVB capacity and filter capacitor;
- the inverter key exit saturation mode;
- punching of individual keys;
- increased transient resistance at the mounting connections;
- interturn faults in traction motor windings;
- breakdown of power supply circuits on the body and other.

5. CONCLUSIONS

When operating a hybrid vehicle, it is important to reduce maintenance and repair costs. The HEV electric drive (ED) consists of electronic (control and power), electric (winding circles of machines and apparatus) and mechanical (transmission) parts and is considered a complex diagnostic model. The presence of an electrical part greatly simplifies the process of monitoring and obtaining information about the state of the system.

To create the HDEPS diagnostic system, the choice of structural and functional parameters as diagnostic ones was justified, the points of their control were chosen, and the necessary accuracy and unambiguity of measurements were determined.

The analysis of oscillograms shows that during diagnostics of the electric drive it is necessary to consider both stable and transient modes of operation of electric machines.

When measuring the diagnostic parameters, it is necessary to have information about the current load mode of the HPP in order to analyse the technical state of the ED.

Functions of current and voltage changes are characterised by harmonics caused by switching of the inverter keys, the frequency of which is hundreds of hertz (Fig. 3). Therefore, sensors with short response times and a linear conversion function should be selected to measure the instantaneous values of supply voltage and consumption current.

In the case of sensitivity to structural changes in the circuit (element faults) and parametric deviations (change of nominal values), it should be chosen as diagnostic, voltage or current parameters, depending on the operation mode of the actuator and the measuring points of the electrical value.

Faults in the electrical and mechanical parts of the actuator cause changes in the current values of signals and the spectral composition of their time functions. Therefore, for structural and parametric identification of the technical state of the HPP it is advisable to apply methods of harmonic analysis.

The obtained results of the research confirm a hypothesis about the possibility of creation of a new system of diagnostics of electric power supply of a traction electric drive of the hybrid car and they serve as a basis for the further studies in this area.

ACKNOWLEDGEMENTS

The present research has been conducted under the scientific research “Development of the System of Energy Saving and Electric Energy Generation for Vehicles”, 0219U100696, funded by the Ministry of Education and Science of Ukraine.

REFERENCES

1. Arhun, S., Hnatov, A., Dziubenko, O, & Ponikarovska, S. (2019). A Device for Converting Kinetic Energy of Press into Electric Power as a Means of Energy Saving. *J. Korean Soc. Precis. Eng.*, *36* (1), 105–110.
2. Patļins, A., Arhun, S., Hnatov, A., Dziubenko, O., & Ponikarovska, S. (2018). Determination of the Best Load Parameters for Productive Operation of PV Panels of Series FS-100M and FS-110P for Sustainable Energy Efficient Road Pavement. In *2018 IEEE 59th International Scientific Conference on Power and Electrical Engineering of Riga Technical University (RTUCON 2018): Conference Proceedings* (pp. 1–6), 12–13 November 2018, Riga, Latvia.
3. Mahmoud, M., Garnett, R., Ferguson, M., & Kanaroglou, P. (2016). Electric Buses: A Review of Alternative Powertrains. *Renew. Sustain. Energy Rev.*, *62*, 673–684.
4. Patļins, A., & Kuņicina, N. (2015). The new approach for passenger counting in public transport systems. In: Proceedings of the 2015 IEEE 8th International Acquisition and Advanced Computing Systems: Technology (pp. 53–57), 24–26 September, 2015. Warsaw: IDAAC 2015. ISBN 978-1-4673-8359-2.
5. Patļins, A., & Kuņicina, N. (2014). The Use of remote sensing technology dynamics study and analysis. In: Transport Means 2014: International Conference (pp. 63–66), 23–24 October 2014, Lithuania, Kaunas. ISSN 2351-4604.
6. Patļins, A., & Kuņicina, N. (2015). Real-time data collection and easy passenger counting method for public transport system In: Transport Means 2015: Proceedings of the Conference (pp. 329–332), 22–23 October, 2015, Lithuania, Kaunas, ISSN 1822-296X.
7. Dvadnenko, V., Arhun, S., Bogajevskiy, A., & Ponikarovska, S. (2018). Improvement of economic and Ecological Characteristics of a Car with a Start-Stop System. *Int. J. Electr. Hybrid Veh.*, *10* (3), 209–222.
8. Lanzarotto, D., Marchesoni, M., Passalacqua, M., Prato, A. P., & Repetto, M. (2018). Overview of Different Hybrid Vehicle Architectures. *IFAC-Pap.*, *51* (9), 218–222.
9. Gunji, D., & Fujimoto, H. (2013). Efficiency Analysis of Powertrain with Toroidal Continuously Variable Transmission for Electric Vehicles. In: *IECON Proceedings* (Industrial Electronics Conference), (pp. 6614–6619).
10. Migal, V., Arhun, Shch., Hnatov, A., Dvadnenko, V., & Ponikarovska, S. (2019). Substantiating the Criteria for Assessing the Quality of Asynchronous Traction Electric Motors in Electric Vehicles and Hybrid Cars. *J. Korean Soc. Precis. Eng.*, *10* (36), 989–999.
11. Xie, S., He, H., & Peng, J. (2017). An Energy Management Strategy Based on Stochastic Model Predictive Control for Plug-in Hybrid Electric Buses. *Appl. Energy*, *196*, 279–288.
12. Onat, N. C., Kucukvar, M., & Tatari, O. (2015). Conventional, Hybrid, Plug-in Hybrid or Electric Vehicles? State-Based Comparative Carbon and Energy Footprint Analysis in the United States. *Appl. Energy*, *150*, 36–49.
13. Huang, Y., Surawski, N. C., Organ, B., Zhou, J. L., Tang, O. H., & Chan, E. F. (2019). Fuel Consumption and Emissions Performance under Real Driving: Comparison between Hybrid and Conventional Vehicles. *Sci. Total Environ.*, *659*, 275–282.
14. Ak, N., & Demirbas, A. (2016). Promising Sources of Energy in the Near Future. *Energy Sources Part Recovery Util. Environ. Eff.*, *38* (12), 1730–1738.
15. Borodenko, Yu. N., & Cherevach, A. V. (2012). "Kontseptsiia diahnostyky elektropryvoda hibrydnoho avtomobilia," [Hybrid Car Electric Drive Diagnostics Concept]. *Automobile Transport, 30*.

16. Apse-Apsītis, P., Avotiņš, A., & Ribickis, L. (2014). Different approaches consumption monitoring. In: *Proceedings of the 16th Eur Electronics and Applications* (pp. 1–5), 26 February 2014, Finland, Lappeenranta. Available at: doi:10.1109/EPE.2014.691
17. Deuse, J., Grenard, S., Karoui, K., Samuelsson, O., Gertm Sauhats, A., Ribickis, L., ... & Hager, M. (2006). Sollerkvist Dispersed energy resources with power system in Norma. In: T*he 41st CIGRE Session: Proceedings* (pp. 1–12), 22 February 2006, France, Paris. ISBN 9782858730216.
18. Apse-Apsītis, P., Avotiņš, A., & Ribickis, L. (2013). Self-tuning CoreConverter for Powering Loads on Rotating Shafts. *Electron 2013, 19* (2), 41–44. e-ISSN 2029-5731. ISSN 1 doi:10.5755/j01. eee.19.2.3466
19. Malafeev, S. I., & Novgorodov, A. A. (2016). Design and Implementation of Electric Drives and Control Systems for Mining Excavators. *Russ. Electr. Eng.*, *87* (10), 560–565.
20. Ishkova, I., & Vítek, O. (2015). Diagnosis of eccentricity and broken rotor bar related faults of induction motor by means of motor current signature analysis. In: *2015 16th International Scientific Conference on Electric Power Engineering (EPE)*, (pp. 682–686), 20–22 May 2015, Czech Republic.
21. Verucchi, C., Bossio, J., Bossio, G., & Acosta, G. (2016). Misalignment Detection in Induction Motors with Flexible Coupling by Means of Estimated Torque Analysis and MCSA. *Mech. Syst. Signal Process.*, *80*, 570–581.
22. Gan, C., Wu, J., Yang, S., Hu, Y., Cao, W., & Si, J. (2016). Fault Diagnosis Scheme for Open-Circuit Faults in Switched Reluctance Motor Drives Using Fast Fourier Transform Algorithm with Bus Current Detection. *IET Power Electron.*, *9* (1), 20–30.
23. Chekalin, V. G. (2011). *Diagnosis and adjustment of automated electric drives*, Uchebnoe posobie dlya VTUZov. Dushanbe: TTU im. M. Osimi.
24. Dąbrowski, Z., & Dziurdź, J. (2016). Simultaneous Analysis of Noise and Vibration of Machines in Vibroacoustic Diagnostics. *Arch. Acoust.*, *41* (4), 783–789.
25. Boniecki, R., & Miciak, M. (2018). The Decision Making Process of a State Technical Facilities Based on Rough Set and Vibroacoustic Estimates. *MATEC Web of Conferences 2018, 182*, 02016.
26. Glowacz, A., & Glowacz, Z. (2017). Diagnosis of Stator Faults of the Single-Phase Induction Motor Using Acoustic Signals. *Appl. Acoust.*, *117*, 20–27.
27. Borodenko, Y., Ribickis, L., Zabasta, A., Arhun, Shch., Kunicina, N., Hnatova, H., ... & Kunicins, K. Using the Method of the Spectral Analysis in Diagnostics of Electrical Process of Propulsion Systems Power Supply in Electric Car. unpublished.
28. Fedotovs, J., Žiravecka, A., Bunina, I. (2019). Testing of Technical Indicators of Accumulators by Means of Complex Computer Model of EV. *Electrical, Control and Communication Engineering*, Riga, Latvia – *submitted for publication.*

sciendo

LATVIAN JOURNAL OF PHYSICS
AND TECHNICAL SCIENCES
2020, N 4

DOI: 10.2478/lpts-2020-0018

SPECTRAL ANALYSIS OF OUTPUT VOLTAGES AND CURRENTS AS A CRITERION FOR TECHNICAL DIAGNOSTICS OF SYNCHRONOUS GENERATORS OF SHIP DIESEL ENGINE

A. Gasparjans*, A. Terebkov, V. Priednieks, R. Klaucans

Latvian Maritime Academy,
5b Flotes Str., Riga, LV-1016, LATVIA,
*e-mail: aleksandrs.gasparjans@latja.lv

Diesel generator sets (DGU) are very widely used in autonomous power supply systems. An example is marine power plants, diesel locomotives with electric power transmission, uninterruptible power supply units, etc. The power of ship DGUs reaches 2–6 or more MW in one unit. The number of units on ships can be different, but, as a rule, at least two. In this paper, we propose a method of monitoring the dynamic electromechanical system "diesel synchronous generator". The method aims at using a synchronous generator machine as a multifunctional accurate and sensitive sensor for diagnostic parameters of the electromechanical system. The proposed method of technical diagnostics is based on continuous monitoring of non-uniformity of diesel torque, fluctuations in the instantaneous angular velocity and instantaneous angular acceleration of the diesel crankshaft. These data are the results of a spectral analysis of stator currents and voltages of a synchronous generator.

Keywords: *acceleration, angular velocity, diagnostics, diesel, generator, spectrum, stator current, voltage,.*

1. INTRODUCTION

Currently, there are a lot of autonomous DGUs operating in transport (river and sea vessels, drilling platforms, diesel locomotives with electric power transmission, etc.), uninterruptible power supply units and emergency units, the normal functioning of which depends on people's lives, economic efficiency and environmental

protection. These diesel generator sets are not connected to an industrial centralized power supply network. In this regard, it is very important to maintain the diesel generator set in a normal, technical condition, in accordance with the given parameters. A decisive role is played by timely technical diagnostics, which can timely prevent the development of emergency situations. It can convert sudden failures into a gradual discharge, determine the residual motor resource of the unit. For example, the issues of monitoring and diagnosing of diesel plant are discussed in detail [1]–[5] and diesel generator sets with synchronous generators are considered in [6], [7], [14], [15]. A significant part of the works [8]–[12] describes the application of vibration diagnostics methods. Along with the advantages of this method, there are some disadvantages. For example, access to the necessary components and assemblies is not always available; highly qualified personnel are required. Not all mechanisms and units are prepared at the factory for vibrodiagnostics.

The proposed version of technical diagnostics for monitoring the spectral energy composition of stator currents and voltages of a synchronous generator allows for diagnostics of both a synchronous generator and a diesel engine. The article proposes a method for the technical diagnosis of diesel power plants, in which the spectral and energy characteristics of higher harmonics of the output voltage and current are used as diagnostic parameters. The fundamentals of this method were presented by the authors in articles [8]–[11]. It became possible in connection with the rapid development of measuring, storage and processing of information, including microprocessor technology. Previously, such an analysis was carried out most often up to 5–7 harmonics of voltage and current. Harmonics of higher orders in view of their insignificant size and measurement difficulties were usually not considered. The advent of modern high-speed multi-bit analogue-to-digital converters (ADCs) makes it possible to measure the spectral energy characteristics of higher order harmonics up to 11 ... 15th with an amplitude of 2 % ... 0.2 % of the amplitude of the fundamental harmonic. The use of mathematical methods makes it possible to identify the place and cause of their occurrence. Thus, the spectral energy characteristics of higher harmonics can be taken as diagnostic parameters. Comparison of the parameters of higher harmonics with reference values can significantly expand the capabilities of technical diagnostic systems. The unevenness of the torque, instantaneous fluctuations in the angular velocity and instantaneous angular frequency lead to a change in the parameters of the electromagnetic process in the generator, changes in the nature of the interaction of the rotor and stator of the generator. In this case, the spectral composition of the output currents and voltages changes. Higher harmonic components are the product of the electromagnetic interaction of the rotor and stator of an electric machine. The nature of this interaction depends not only on the parameters of the electric machine, but also on the mechanical characteristics of the drive motor – its instantaneous angular frequency of rotation and instantaneous angular acceleration. These parameters characterise the technical condition of the drive motor. Such measurements have their own specifics and, in terms of accuracy, are, in fact, laboratory measurements.

The uneven torque, instantaneous oscillation angular velocity and the angular frequency lead to a change in electromagnetic flow process parameters in the generator, the changing nature of interaction of the rotor and stator of the generator. In this case, the spectral composition of the

output currents and voltages changes. The present article proposes a method of technical diagnostics based on continuous monitoring of non-uniformity of diesel torque, fluctuations in instantaneous angular velocity and angular acceleration for one or two revolutions of the diesel crankshaft. The data obtained are compared either with reference values or with values obtained as a result of mathematical modelling. Deviations of the parameters of these irregularities from the reference characterise the state of the cylinder-piston group (CPG) of the diesel engine and the quality of the working process in its cylinders. The second feature of this method is the use of a standard generator of a diesel-electric installation as a multifunctional sensor. It is possible to diagnose by the balance of the instantaneous power of the diesel engine and the generator — to determine the instantaneous power of the diesel engine, to compare it with the reference values corresponding to the given position of the rail of the fuel pump depending on the generator load. The unevenness of the torque, fluctuations in the angular velocity and angular acceleration of the diesel crankshaft are due to both the specifics of the flow of the working process and its quality in its cylinders, and the specifics of converting the reciprocating motion of the piston into a rotary motion of the crankshaft. The proposed method refers to non-destructive testing methods, most often it does not require a long shutdown of equipment and is performed in real-life conditions. Connection to the generator output terminals is made either on the generator itself or on its control panel.

For technical diagnostics, it is required to install a top dead centre sensor (TDC) and an instantaneous angular velocity sensor in the diesel flywheel area. TDC sensor signals can also be obtained from the electronic control system of the diesel generator itself. In most cases, the DGU control system does not determine the instantaneous angular velocity. Usually it is considered as the transit time of the TDC of the first cylinder for a certain period of time. However, the instantaneous angular velocity and instantaneous angular acceleration, even in multi-cylinder diesel engines, are not constant for one revolution of the crankshaft. It is the oscillations of the instantaneous angular velocity of rotation and angular instantaneous acceleration that are the diagnostic parameters adopted in this method. Knowing the number of engine cylinders and the order of their operation, it is possible to accurately determine in which cylinder the fuel combustion process is damaged, to identify defects in the generator bearings, braking of the generator rotor and engine crankshaft due to partial windings (distortion of the magnetic field in the generator air gap), etc. The instantaneous angular velocity sensor can be installed against the teeth of the gearwheel of the engine flywheel or the teeth of the gear shaft mechanism on ships. Installing voltage sensors and current sensors is not complicated. Often, one can use existing sensors in the existing control circuit of the diesel generator set.

2. MATHEMATICAL MODEL OF THE SYSTEM DIESEL ENGINE GENERATOR

The equation of motion of a diesel generator in general form can be written as follows (the basic equation of the electric drive):

$$\left(J_d + J_{gen}\right) * \frac{d\omega_{gen}(t)}{dt} = T_d(t) - T_{gen}(t), \quad (1)$$

where $T_{gen}(t) = k_{mgen}\Phi_{gen}(t) \cdot i(t)$ – the torque formed by the synchronous generator (SG);
T_d – rms value of the rotational torque of diesel;
J_d – the moment of inertia of diesel reduced to the crank shaft;
J_{gen} – the moment of inertia of generator;
$\omega_{gen}(t)$ – angular velocity of diesel generator;
k_{mgen} – the constructive constant of the generator;
Φ_{gen} – magnetic flux of generator.

3. MATHEMATICAL MODEL OF DIESEL

In this case, the model [6], [17], [18] with the corresponding changes can be taken as the basis of the mathematical (differential) model of a diesel engine with gas turbine supercharging. The basis of the mathematical model is a system of differential equations of the mass and energy balance of the working fluid and the equation of state. In general, the mathematical model can be represented as follows:

$$\left.\begin{array}{ll} \text{Turbocharger:} & J_k \dfrac{d\omega_k}{dt} = T_t - T_k \\ \text{Diesel engine:} & \dfrac{d(\omega + \varepsilon(t))}{dt} = T_i - T_p - T_{gen} \\ \text{Intake manifold:} & \dfrac{V_{i.m}}{R_в T_к^{\,0}} \cdot \dfrac{dp_k}{dt} = G_k - G_d \\ \text{Exhaust manifold:} & \dfrac{V_{e.m}}{R_g T_g^{\,0}} \cdot \dfrac{dp_t}{dt} = G_g - G_t \end{array}\right\}, \quad (2)$$

where J_k – moment of inertia of the compressor;
T_t – turbine torque, $T_t = T_t(\omega, \omega_k, B)$;
T_k – moment of resistance of the compressor, $T_k = T_k(Q, \omega_k)$;
T_i – indicator torque of the diesel;
T_p – moment of diesel loss;
T_{gen} – braking torque on the diesel shaft from the generator (load moment);
ω_k – angular velocity of the rotor of the turbo compressor;
ω – angular velocity of the crankshaft of the diesel engine (generator shaft);
ε – deviation of the angular velocity of the crankshaft;
$V_{i.m}$ – intake manifold volume;
$V_{e.m}$ – exhaust manifold volume;
$R_в$ – gas constant of charge air;
R_g – gas constant of the exhaust gases;

T_k^0 – temperature of the charge air;
T_g^0 – temperature of the exhaust gases;
G_k – air flow through the compressor of the turbocharger;
G_d – air flow through the engine;
G_g – exhaust gas flow through the engine;
G_t – flow rate of exhaust gases through the turbine of the turbocharger.

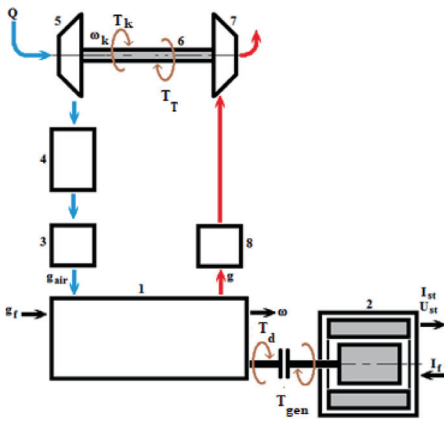

Fig. 1. Block diagram of a diesel generator set.

1 – diesel; 2 – synchronous generator; 3 – diesel intake manifold; 4 – intermediate air cooler; 5 – compressor; 6 – turbocharger shaft; 7 – gas turbine; 8 – exhaust manifold; g_{air} – cyclic dose of air; g_f – cyclic fuel supply; g – cyclic dose of exhaust gases.

The deviation of the angular velocity of the diesel crankshaft (SG rotor) ε:

$$\varepsilon = \omega_{max} - \omega_{min} = A_{\omega}. \quad (3)$$

It characterises the uneven flow of the working process along the cylinders of the diesel engine. It is determined by the technical condition of the fuel equipment, piston group, crank mechanism, valve system of the gas distribution mechanism. It causes oscillations of the angle Θ of the magnetic flux vector of the synchronous generator. The unevenness of the instantaneous angular velocity of the crankshaft of the diesel shaft of the synchronous generator (i.e., the angle Θ) leads to a significant distortion in the spectral composition of the voltage and current of the generator. Therefore, the spectral composition of voltage and current can be a diagnostic parameter of both the generator itself and the primary diesel engine.

Coefficient of intra-cycle non-uniformity of change in angular velocity δ:

$$\delta = (\omega_{max} - \omega_{min})/\omega_{middl}. \quad (4)$$

This coefficient is an integral indicator of the efficiency of an internal combustion engine (ICE).

When determining the indicator torque of a diesel engine T_i, the coefficient of technical condition K_1, which depends on the quality of the fuel system and the cylinder-piston group of the diesel engine, should be taken into account:

$$T_i = T_i\,(B, h_i, \omega, t, K_1), \quad (5)$$

where:
t – the operating time;
h_i – the position of the high-pressure fuel pump rail;
B – determines the amount of fuel (hourly consumption) entering the diesel cylinders. It is determined by the position h of the rail of the high-pressure fuel pump. It characterises the current technical condition of the fuel equipment.

With regard to T_p – the torque of diesel losses, the coefficient K_2 must be taken into account; it characterises losses due to pumping strokes, ventilation losses, friction losses in moving parts of a diesel engine:

$$T_p = T_p(\omega, K_2).$$

These coefficients determine the uniformity of power distribution across the cylinders and characterise the unevenness of the instantaneous angular velocity of the crankshaft (and, therefore, the synchronous generator shaft), the deviation of the angular velocity of the crankshaft ε:

$\varepsilon = \varepsilon\ (\varepsilon, K_1, K_2)$.

The effective torque T_d of the diesel engine is pulsating due to outbreaks of fuel in the engine cylinders. It also causes deviation ε of the angular velocity of the crankshaft of the diesel engine and oscillations of the angle Θ of the synchronous generator [16]. Therefore, it is obvious that the fluctuation of the angle Θ depends on the generator load current, the current and the instantaneous angular velocity of the diesel crankshaft.

4. MATHEMATICAL MODEL OF SYNCHRONOUS GENERATOR

The basis for the SG mathematical model is the system of equations for voltages in phase coordinates [19]–[21]. The basis for the mathematical model of synchronous generator is the system of Park-Goreva equations. As a high level of harmonics exists, the transient and emergency regimes are necessary to be investigated. Its mathematical model is reasonable to be realised in phase frame for stator and in d-q frame for rotor. The voltage equations for the phase values are for all phases of the stator winding (A, B, C) and for the phases of the reduced three-phase circuits of rotor (*f* – the circuit of the excitation winding, *D* – circuits of the damping winding along the axes *d* and *q*) (Fig. 2).

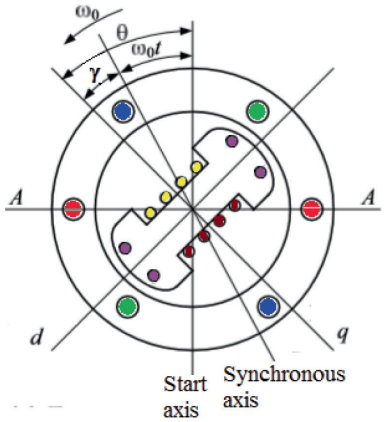

Fig. 2. Coordinate system of windings of the synchronous silent-pole generator.

$$\begin{cases} U_A(t) = R_A * i_A(t) + \frac{d\psi_A(t)}{dt}; \\ U_B(t) = R_B * i_B(t) + \frac{d\psi_B(t)}{dt}; \\ U_C(t) = R_C * i_C(t) + \frac{d\psi_C(t)}{dt}; \\ U_f(t) = R_f * i_f(t) + \frac{d\psi_f(t)}{dt}; \\ U_{D\,d}(t) = R_{D\,d} * i_{D\,d}(t) + \frac{d\psi_{D\,d}(t)}{dt}; \\ U_{D\,q}(t) = R_{D\,q} * i_{D\,q}(t) + \frac{d\psi_{D\,q}(t)}{dt}, \end{cases} \quad (6)$$

where *U(t)* – the voltage of the circuit windings (A, B, C);
R – resistance of the circuit windings;
i (t) – current in the circuit windings;
ψ (t) – flux linkage of the circuit windings.

System (6) is fulfilled with the last equation of the motion of diesel generator (1).

The flux linkages are expressed by means of the currents of stator phases, the currents of the rotor phases and correspondent inductances. For example, the flux linkage of the stator A phase is:

$$\psi_A(t) = L_A \cdot i_A(t) + M_{AB} \cdot i_B(t) + \\ + M_{AC} \cdot i_C(t) + M_{Af} \cdot i_f(t) + \\ + M_{AD\,d} \cdot i_{D\,d}(t) + M_{AD\,q} \cdot i_{D\,q}(t), \quad (7)$$

where *L* – the self-inductances of the machine windings;
M – the mutual inductances of the machine windings.

The flux linkages of *B, C, f,* D_d, and D_q phases are similar.

In accordance with the reciprocity principle and assuming that steel has an infinitively high magnetic permeability the mutual inductances are equal. The constant inductances are those inductances the configuration of magnetic system of which stays constant at any position of the rotor. These are the inductances of all circuits of the rotor and mutual inductances between the rotor circuits. The rest inductances and mutual inductances are changed in accordance with the position of the rotor in space. Thus, the mutual winding inductances of the synchronous silent-pole generator are the periodic functions of the rotor rotation angle θ. They are the harmonic time functions that should be notably taken into account while investigating transient processes.

$$L_A, L_B, L_C, M_{AB}, M_{AC}, M_{BA}, M_{BC}, M_{CA}, M_{CB} = f(\theta). \quad (8)$$

The electromagnetic torque of the synchronous machine can be calculated as follows:

$$T_{gen}(t) = \frac{3\,p_\tau}{2}\left(\psi_d \cdot i_q(t) - \psi_q \cdot i_d(t)\right). \quad (9)$$

For a reliable diagnosis of the current state of the D-SG electromechanical system, the required measurement accuracy should be at least 0.5^0 ... 1.0^0 from the angle of rotation θ of the engine crankshaft, and the angular velocity measurement accuracy ω should be at least 0.01 rad/s. The frequency resolution for spectral analysis should be at least 0.01 ... 0.02 Hz. To exclude random errors, measurements are carried out for at least 200 ... 300 revolutions of the crankshaft.

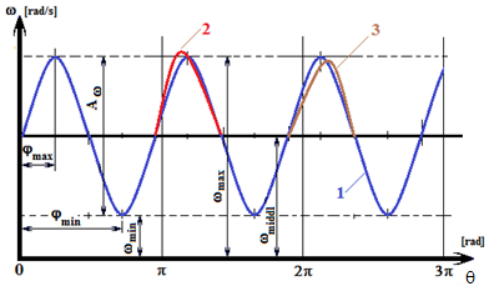

Fig. 3. The dependence of the angular instantaneous velocity ω on the angle of rotation φ (θ) *of* the crankshaft:

1 – with the same work processes in the engine cylinders;

2 – with an early flash and an excessive portion of fuel in one of the cylinders;

3 – with a late outbreak and a small portion of fuel in one of the cylinders.

The sensors of the top dead centre of the first cylinder and the instantaneous angular frequency of rotation are of the frequency type, based on a blocking generator. On the diesel flywheel at the TDC mark, a magnetic pin for the TDC sensor is mounted. The sensor of instantaneous angular rotation frequency (ARF) is placed above the teeth of the ring gear of the diesel flywheel. The number of teeth on the crown of this diesel model is 72, i.e., they are located every 5^0 degrees of the angle of rotation of the diesel crankshaft (SG rotor). Pulses from the ARF sensor go to the counter. At the other input of the counter, filling pulses from a quartz clock generator (5 MHz) are received. Every 5^0 of the angle of rotation of the crankshaft, the counter is reset. In this case, the error in measuring the instantaneous angular speed is not accumulated, and there are no averaging readings per revolution of engine crankshaft. Instant angular acceleration is recalculated for every 5^0 of the rotation angle of the diesel crankshaft. This method allows accurately determining which cylinder causes changes

in the instantaneous angular velocity and instantaneous angular acceleration. The number of diesel cylinders and the order of their operation is known in advance.

Figure 4 demonstrates a structural diagram of the diagnostics of a diesel generator set with a synchronous generator as a diagnostic sensor.

1 – diesel engine (DE); 2 – fuel pump of a high pressure – injection pump (IP); 3 – proportional-integral-differential controller (PID); 4 – angular velocity sensor; 5 – voltage and power regulator of a synchronous generator (PID); 6 – synchronous generator (SG); 7 – voltage sensor; 8 – current sensor; 9 – frequency sensor; 10 – synchronous generator output; 11 – electric drive rail IP – step electric motor; 12 – diesel flywheel; 13 – TDC sensor of the first cylinder; 14 – diesel engine crankshaft angle sensor; 15 – microcontroller; 16 – spectrum analyser.

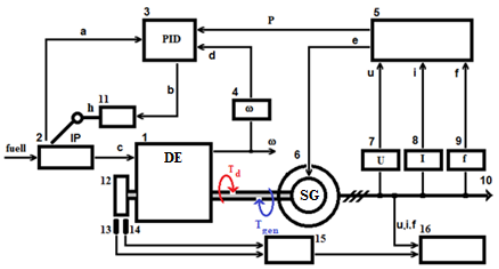

Fig. 4. Block diagram of a diagnostic system of a diesel generator set.

The output parameters of diesel engine 1 is effective torque T_d and the angular velocity ω. The disturbing effect is the torque of resistance T_{gen} of the synchronous generator. The control action for the diesel engine is the h-rail of the injection pump. The control action for the SG is the excitation voltage, the input action (signal) is the effective torque T_d and the angular frequency ω of the diesel engine. The disturbing effect of the SG is the stator phase current and stator voltage. The SG output parameters – current, voltage and frequency – are controlled by sensors 7, 8, 9. Information from them is fed to the voltage and power regulator 5. Regulator 5 controls the excitation voltage of the SG. In controller 5, the active component P of the SG power is calculated, according to which PID 3 regulates the fuel supply to the diesel cylinders using electric drive 11 of injection pump rail 2. Therefore, the fluctuations in the angle Θ of the magnetic flux vector of the synchronous generator are caused not only by a change in the output stator currents, but also by an uneven rotation of the diesel crankshaft.

To carry out a spectral analysis of output voltages and currents, there is a computer with the appropriate software (spectrum analyser) 16. The primary processing of information from TDC 13 frequency sensors and the rotation angle θ of the diesel crankshaft is carried out in microcontroller 15. The signal from it is transmitted to computer (spectrum analyser) 16. Therefore, the resulting spectrum of SG currents and voltages turns out to be tied to the angle of rotation of the diesel crankshaft. Knowing the order of operation of the diesel cylinders, it is possible to judge the technical condition of the cylinder-piston group, fuel equipment and gas distribution mechanism of each cylinder by the appearance of new harmonics and changes in the old ones. When conducting a spectral analysis of stator currents and SG voltages, first of all, it is necessary to take into account the energy–time parameters of the so-called characteristic frequencies. Characteristic frequencies are frequencies that are generated by various defects in the SG-D electromechanical system. For example, the four characteristic frequencies for bearings (the speed of rolling elements along the treadmills of the outer and inner rings of the bearing, the speed of the cage and the natural frequency of rotation of the bodies of rotation) are the frequencies

that occur during the operation of the crank mechanism of a diesel engine, the frequencies that occur in case of misalignment and kink of the axes, violation of the gas distribution mechanism, non-symmetry of the electric load of the SG, etc.

It should be borne in mind that when working in an autonomous shipboard network of a synchronous generator, a load of the type of an asynchronous electric motor with semiconductor converters (frequency converters, etc.) may cause additional harmonics, which will require an additional analysis of the current and voltage spectra.

5. RESULTS OF CALCULATIONS

The results of the presented mathematical apparatus, equations (1, 2, 7, 8, 9), were analysed on the basis of mathematical modelling of the diesel generator model in the MATLAB Simulink software. In order to simplify the modelling process, we will present it in the form of seven stages (blocks).

1. The first block models variable coefficients L, M in equations (7, 8) to determine flux linkage.
2. The second unit simulates the flux values obtained on the basis of the coefficient values L, M.
3. The third block simulates the voltage of the stator windings according to the equations of the system (6).
4. The fourth block simulates the voltage of the rotor windings according to the equations of the system (6).
5. The fifth block simulates the system of equations of a synchronous generator (6).
6. The sixth block simulates the diesel equations (2).
7. The seventh block simulates the diesel generator system according to the equation of motion (1).

Results of calculations and further analysis of the spectrum of voltage harmonics are presented on the spectrogram (Fig. 5).

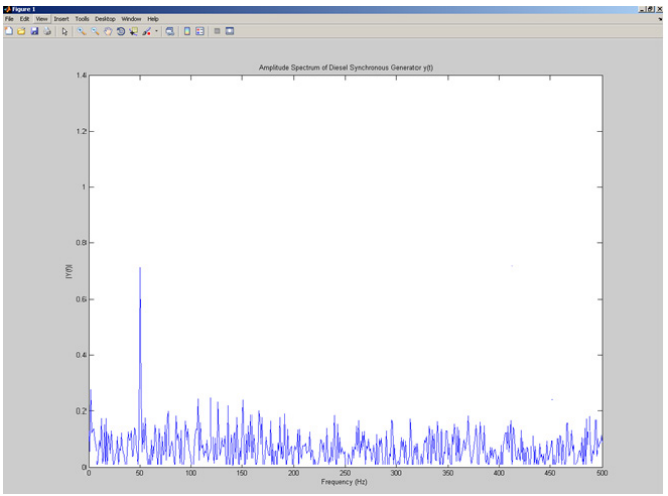

Fig. 5. The spectrogram of the analysis of the model of the diesel generator set.

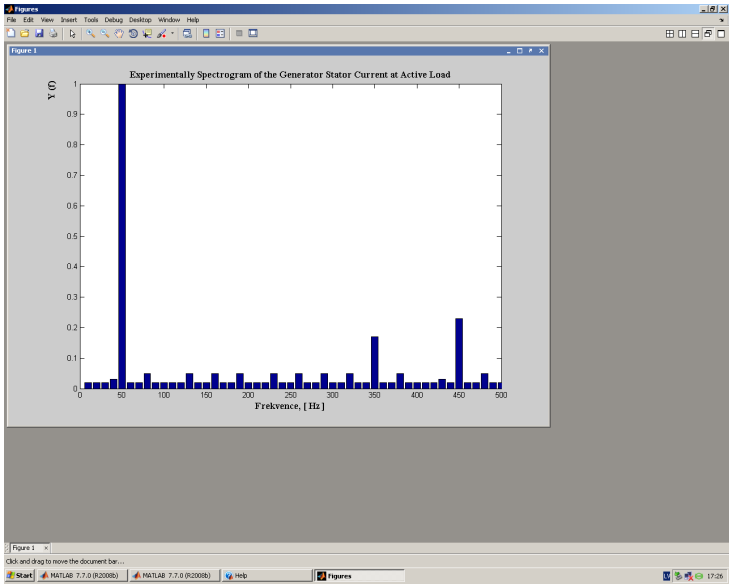

Fig. 6. Experimentally taken from the spectrogram of the stator current of the generator at active load.

In Fig. 6, the appearance of the 7th harmonic (350 Hz) and the 9th harmonic (450 Hz) is clearly visible. The amplitude of the fundamental harmonic at 50 Hz is taken as a conventional unit. The appearance of these harmonics indicates an uneven air gap in the bore of the generator stator. Uneven air gap can be caused by unsatisfactory technical condition of the generator bearings and, as a result, skew of the rotor in the bore of the generator stator.

6. CONCLUSIONS

1. Analysing the received electric parameters of non-uniformity of the rotating moment, angular velocity, angular acceleration and spectral power structure of output currents and pressure and comparing them with reference values, it is possible to evaluate an actual condition of systems and units – both the piston machine and the synchronous machine.
2. The most effective technical diagnostics of electric machines and units mechanically connected to them is carried out in transitive modes.
3. The change in the previous harmonics parameters and the appearance of new ones clearly demonstrate emerging defects in the "engine synchronous generator" system.
4. The use of the synchronous machine in a diesel engine generating and compressor installations as a multipurpose diagnostic sensor is presented. Analysing the received electric parameters of non-uniformity of the rotating torque, angular velocity, angular acceleration and spectral power structure of output currents and pressure, as well as comparing them with reference values, it is possible to estimate an actual condition of systems and units – both the piston machine and the synchronous machine.

REFERENCES

1. Lamaris, V. T., & Hountalas, D. T. (2010). A General Purpose Diagnostic Technique for Marine Diesel Engines – Application on the Main Propulsion and Auxiliary Diesel Units of a Marine Vessel. *Journal of Energy Conversion and Management*, *51* (4), 740–753.
2. Charles, P., Sinha, J. K., Gu, F., Lidstone, L., & Ball, A. D. (2009). Detecting the Crankshaft Torsional Vibration of Diesel Engines for Combustion Related Diagnosis. *Journal of Sound and Vibration, 321*, 3–5.
3. Lus, T. (2012). Marine Diesel Engine Diagnostics in Operating Conditions. *Diagnostika – Applied Structural Health Usage and Condition Monitoring, 2* (62), 43–47.
4. Lus, T. (2011). Vibro-Acoustic Methods in Marine Diesel Engines Diagnostics. *Journal of KONES Powertrain and Transport, 18* (3), 193–200.
5. Zhixiong, L., Xinping, Y., Chengqing, Y., & Zhongxiao, P. (2012). Intelligent Fault Diagnosis Method for Marine Diesel Engines Using Instantaneous Angular Speed. *Journal of Mechanical Science and Technology, 26* (8), 2413–2423.
6. Hansen, J. F., Adnanes, A.K., & Fossen, T.I. (2001). Mathematical Modelling of Diesel-Electric Propulsion Systems for Marine Vessels. *Mathematical and Computer Modelling of Dynamical Systems,* 7 (1), 323–355.
7. Luo, L., Gao, L., & Fu, H. (2011). The Control and Modeling of Diesel Generator Set in Electric Propulsion Ship. *Information Technology and Computer Science, 2*, 31–37.
8. Gasparjan, A., Greivulis, J., & Terebkov, A. (2001). Diagnostic simulator of the marine diesel engines. In *ICERS5 5th International Conference on Engine Room Simulators. Simulator-Aided Education & Training in the New Millennium*. Singapore Polytechnic.
9. Gasparjan, A., & Terebkov, A. (2005). Problems of electric energy quality in ship diesel engine – Generator installations. *Proceedings of the 9th International Conference. Transport Means*. Kaunas University of Technology.
10. Gasparjan, A., & Terebkov, A. (2017). Multifunctional system of the diesel engine – generator diagnostics in ship installations. *Scientific Proceedings of Riga Technical University. Power and Electrical Engineering, 16*. RTU. Riga.
11. Lesinskis, I., Gasparjans, A., & Terebkovs, A. (2009). Results of ship's engine vibromonitoring. *Proceeding of 11th International Conference "Maritime Transport and Infrastructure"*. Riga: Latvian Maritime Academy, 147–151.
12. Nedelko D., Urbahs A., Turko V., Urbaha M., Carjova K., & Nagaraj P. (2019). Assessment of the Limits of Signs of Health and Usage Monitoring System for Helicopter Transmission. *Procedia Computer Science, 149*, 252–257.
13. Urbahs, A., Banovs, M., Carjova, K., Turko, V., & Feshchuk, J. (2017). Research of the Micromechanics of Composite Materials with Polymer Matrix Failure under Static Loading Using the Acoustic Emission Method. *Aviation, 21* (1), 9–16.
14. Trigeassou, J. C. (2011). *Electrical Machines Diagnosis*. Wiley-ISTE.
15. Panadero, R.P, Linares, J.P., Alarcon, V.C., & Sanchez, M.P. (2013). *Review Diagnosis Methods of Induction Electrical Machines based on Steady State Current*. Available at www.aedie.org/11chlie-papers/263-Puche.pdf.

16. Gasparjan, A., Terebkov, A., & Terebkova, M. (2006). The use of results of spectral analysis of synchronous generator output voltage for technical diagnostics. In *International Conference on Industrial Technology ICIT-2006.* Indian Institute of Technology Kharagpur. Bombay.
17. Faris, W. F., Rakha, H. A., Kafafy, R. M., Idres, M., & Elmoselhy, S. (2012). Diesel Engine Analytical Model. *International Journal of Scientific & Engineering Research, 3* (8).
18. Hui, C., Peili, W., & Jundong, Z. (2013). Modeling and Simulation of Working Process of Marine Diesel Engine with a Comprehensive Method. *International Journal of Computer Information Systems and Industrial Management Applications*, *5*, 480–487.
19. Gasparjan, A., Terebkov, A., & Zhiravetska, A. (2017). Monitoring of electro-mechanical system diesel–synchronous generator. In *5th International Conference on Power Engineering, Energy and Electrical Drives*. IEEE P0werENG, IES, May, Riga.
20. Zhiravetska, A., Gasparjans, A., & Terebkov, A. (2017). Monitoring of current technical condition of vessel diesel-generator installation. In *EPE'17, ECCE EUROPE* (pp. 1–7), 11–14 September, Warsaw, Poland.
21. Ivanov-Smolenski, A. B. (1980). *Electric machines*. M.: Energija (in Russian).

sciendo

LATVIAN JOURNAL OF PHYSICS
AND TECHNICAL SCIENCES
2020, N 4

DOI: 10.2478/lpts-2020-0019

IMPLEMENTATION OF MULTI-WAVELENGTH SOURCE FOR DWDM-PON FIBER OPTICAL TRANSMISSION SYSTEMS

K. Vilcane[1]*, S. Matsenko[1,2], M. Parfjonovs[1], R. Murnieks[1,2],
M. Aleksejeva[1,2], S. Spolitis[1,2]

[1]Institute of Telecommunications, Riga Technical University,
12 Azenes Str., LV-1048, Riga, LATVIA
[2]Communication Technologies Research Center, Riga Technical University,
12 Azenes Str., LV-1048, Riga, LATVIA
*e-mail: Klinta.Vilcane 1@rtu.lv

Four-wave mixing (FWM) is one of the well-known nonlinear optical effects (NOE), and it is considered as an adverse impact in fibre optical communication lines. This nonlinear optical effect as a productive one can be used in fibre optical communication systems for various optical processing functions, like wavelength conversion, high-speed time-division multiplexing (TDM), pulse compression, fibre optical parametric amplifiers (FOPA), etc. In most of the fibre optical communication systems, each data transmission channel requires one light source (e.g., laser) as a carrier, which can make these transmission systems expensive. For example, to provide operation of 4-channel dense wavelength-division-multiplexed (DWDM) system four separate lasers at specific operation wavelengths are needed. On the contrary, through the FWM effect, which can be obtained in highly nonlinear optical fibre (HNLF) by using two high-power pump lasers, the generation of new multiple carriers forming the laser array or a multi-wavelength source is possible. Accordingly, within the present research, we investigate the latter approach for FWM light source implementation in DWDM passive optical networks (DWDM-PONs). We analyse up to 16-channel 50 GHz spaced DWDM-PON system with a bitrate of up to 10 Gbit/s per channel, constructed on the basis of two high-power continuous wave (CW) pump lasers. We evaluate the system performance against the number of its channels by changing it from 4 to 16 and in each case find the most optimal HNLF fibre length (for a 4-channel system it is 0.9 km; for an 8-channel system – 1.39 km; and for a 16-channel system – 1.05 km) and laser pump powers (for a 4-channel system it is 20 dBm; for an 8-channel

system – 24.1 dBm; and for a 16-channel system – 26.3 dBm). These optimal parameters were found in order to get the highest system performance, respectively, the lowest BER (threshold BER≤10^{-10}), and minimal power fluctuations among FWM generated carriers. The obtained results show that the proposed transmission system can be a promising solution for next-generation high-speed PONs.

Keywords: *dense wavelength division multiplexed passive optical network (DWDM-PON), four-wave mixing (FWM), highly nonlinear optical fiber (HNLF), nonlinear optical effects (NOE).*

1. INTRODUCTION

An increase in the amount of information transmitted and an ever-growing number of Internet users have increased the demand for network bandwidth and further transition to new architectures and data transmission technologies. High spectral efficiency dense wavelength-division-multiplexed (DWDM) systems are used to increase the rapidly growing demand for the Internet traffic, using multimedia applications, streaming video, file sharing, etc. [1]. Dense wavelength-division-multiplexed passive optical network (DWDM-PON) is compatible with fibre-to-the-home (FTTH) architecture by providing flexibility and far greater capacity. DWDM fibre optical transmission system technology is used for long-distance data transmission; however, DWDM signals are exposed by nonlinear optical effects (NOE). In the process of data transmission, interference, distortion, excessive attenuation of the optical signals may appear due to the nonlinearity of the optical fibre, which leads to a degradation in performance [2]. One of the most common nonlinear optical effects in optical fibre communication systems is Kerr nonlinearities – the influence of frequency modulation or pulse spectral components of the movement. Different effects such as self-phase modulation (SPM), cross-phase modulation (XPM), and four-wave mixing (FWM) occur due to the Kerr nonlinearity [3], [4]. Nonlinear FWM is an effect when two or more different signals with different frequencies propagate next to each other, and because of this effect, new carriers are generated. In addition, existing channels are exposed to power loss and signal distortions. The FWM effect can be used to generate multiple carriers. The FWM effect is adverse for DWDM-PON transmission systems, but nowadays solutions for useful application of this effect are being researched.

The application of the FWM optical effect was researched to create up to a 16-channel DWDM-PON system. FWM multi-wavelength source is based on two continuous wave (CW) lasers and optical highly nonlinear fibre (HNLF). In this article, we developed and analysed setups of up to a 16-channel DWDM-PON system, where optimal power of both pump CW lasers and HNLF fibre span length were determined. The performance of the received signals was analysed in terms of bit error ratio (BER), where we set that the BER threshold according to PON networks was BER ≤10^{-10}.

2. GENERATION OF FOUR-WAVE MIXING NONLINEAR OPTICAL EFFECT

The four-wave mixing may occur in fibre optical systems as the intermodulation phenomenon in which the fourth wavelength arises due to an interaction among three wavelengths. If there are three wavelengths λ_i, λ_j, and λ_k, which are mixed, then it leads to the appearance of the fourth wavelength, as shown in formula 1 below [5]:

$$\lambda_{ijk} = \lambda_i \pm \lambda_j \pm \lambda_k, \tag{1}$$

where λ_{ijk} – may act as an interfering signal to the original signal. The worst-case combination of these wavelengths degrades the performance of a system [5]. Three waves of wavelength λ_i, λ_j, and λ_k (i, j ≠ k) interact to generate a wave with wavelength [6]:

$$\lambda_{ijk} = \lambda_i + \lambda_j - \lambda_k, \ (i, j \neq k), \tag{2}$$

where λ_{ijk} – the wavelength of the generated FWM signal.

Formula (3) describes how many new channels intend to be in a system. For N wavelength channels co-propagating through the fibre, the number of new wavelengths that FMW effect generates is [7]:

$$M = \frac{N^2}{2}(N-1). \tag{3}$$

Figure 1 shows the optical signal spectrum before and after transmission along the optical fibre with the impact of FWM. The power of the FWM signal is influenced by such factors as dispersion of the transmission fibre, channel input power and spectral spacing between the carriers or channels.

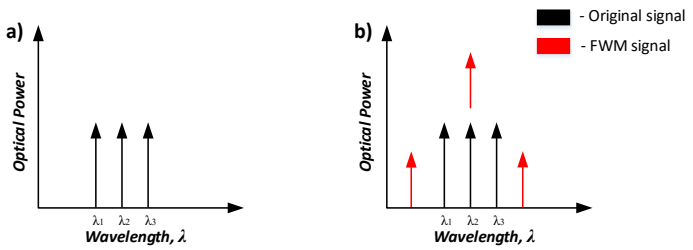

Fig. 1. The spectrum of optical signal a) without FWM and b) with the occurrence of the FWM effect [5].

3. ARCHITECTURE OF DWDM-PON TRANSMISSION SYSTEM WITH FWM SOURCE

DWDM-PON can be used as a multiple channel optical fibre transmission system to be able to serve as many customers as possible at the same time and gain higher power and bitrate [7], [8].

According to ITU-T G.694.1 recommendation for optical C and L bands, the DWDM-PON channel spacing intervals are 100, 50, 25 or 12.5 GHz, and the frequency of the central channel is 193.1 THz [9]. In this article, a DWDM-PON transmission system with channel spacing 50 GHz is

under research. This system uses an FWM multi-wavelength source to provide further information transmission to multiple data channels. Figure 2 shows the architecture of multichannel DWDM-PON transmission system.

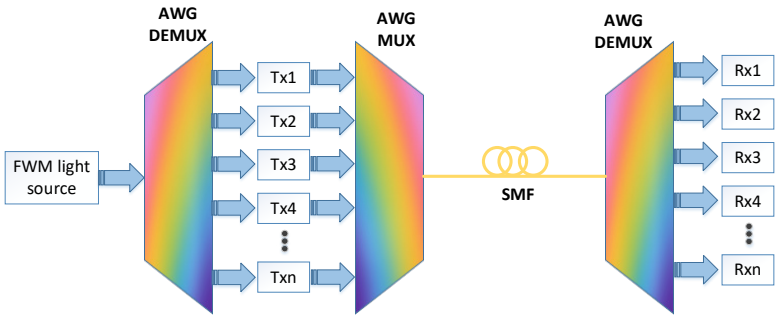

Fig. 2. The architecture of the multichannel DWDM-PON transmission system with FWM multi-wavelength source [10].

As it is shown in Fig. 2, the simulated transmission system employs one arrayed-waveguide grating (AWG) multiplexer (MUX) for the combination of modulated carriers and two demultiplexers (DEMUX) for filtering and separation of carriers generated by FWM multi-wavelength source (transmitter side) and separation of the received DWDM signals at the receiver side.

4. EXPERIMENTAL SIMULATION MODEL AND NUMERICAL ANALYSIS

In this article, the use of the FWM optical effect was researched to create a multi-wavelength source for up to a 16-channel DWDM-PON system. We developed an experimental simulation model with an FWM multi-wavelength source for the DWDM-PON transmission system in the RSOFT OptSim simulation software environment. The power of pumping lasers, as it is shown in Fig. 4, was changed in the range from +15 dBm to +30 dBm. Different HNLF fibre lengths up to 2 km were also studied [11].

As a result of the FWM process, the fourth frequency was generated. To efficiently generate nonlinear FWM in HNLF fibre, the following HNLF parameters were set: the core effective area of 11.6 μm^2, zero dispersion wavelength of 1552.32 nm and the nonlinear coefficient of 11.50 $(W \times km)^{-1}$ [11].

Central frequencies applied in this research for pump CW lasers were 193.10 THz (1552.524 nm) and 193.15 THz (1552.123 nm), attenuation coefficient for a generation of up to 16 carriers in HNLF fibre was 0.8 dB/km at the reference wavelength of 1550 nm [11]. The parameters of AWG MUX/DEMUX employed in DWDM-PON systems were as follows: channel spacing was 50 GHz, optical 3-dB bandwidth was 16.5 GHz and the lowest channel frequency of AWG MUX/DEMUX varied depending on the number of channels used: for 4 channels – 193.05 THz, for 8 channels –192.95 THz, for 16 channels – 192.75 THz. Table 1 shows optimal parameters for both CW lasers and HNLF fibre employed accordingly in 4-, 8- and 16-channel DWDM-PON transmission systems. The optimal power of pumping CW lasers and HNLF fibre length were defined experimentally

by using simulation software. These parameters were found by evaluating the optical spectrum (see Fig. 3) on the output of the first AWG demux, considering the lowest power variation of generated carriers, which did not exceed the range of 3 dB.

Table 1. Optimal Parameters for the Generation of Multiple Carriers

Number of carriers (channels)	CW pump laser power, dBm	HNLF length, km
4	20.0	0.90
8	24.1	1.39
16	26.3	1.05

Figure 3 shows output spectra of FWM multi-wavelength source, where (a) 4-channel, (c) 8-channel, (e) 16-channel after the HNLF output and (b) 4-channel, (d) 8-channel, (f) 16-channel after the AWG multiplexer. Spectrum diagrams can be used to determine the quality of the selected parameters because the spectrum on the HNLF output will be smoother. Then it will be possible to find the lowest BER and maximum uniform carrier capacity for minimal fluctuations.

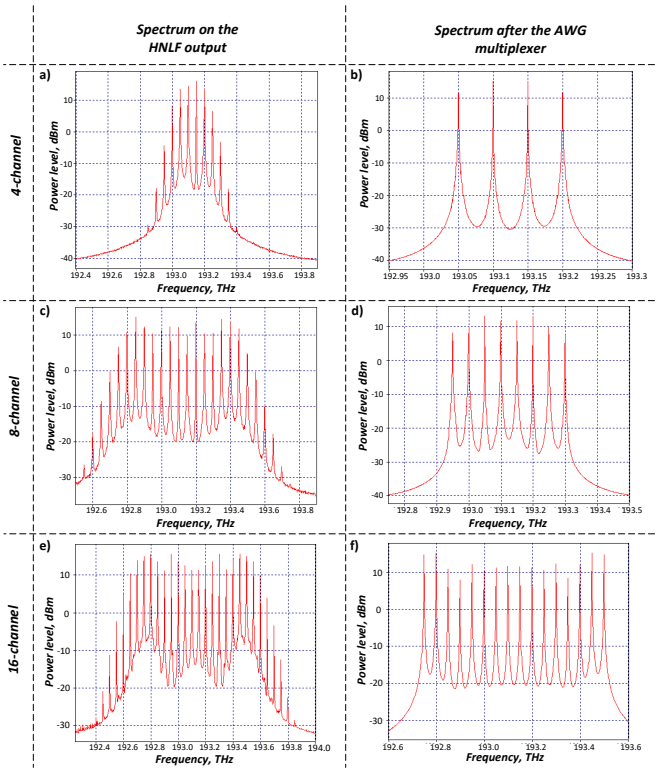

Fig. 3. The measured optical spectra (a, c, e) on the output of HNLF and (b, d, f) after AWG multiplexer at the transmission side of up to 16-channel DWDM-PON transmission system.

We configured the FWM multi-wavelength source, the parameters of which varied depending on the number of channels used in the system. Figure 4 shows the experimental simulation model of (a) up to 8-channel (including 4-channel) and (b) 16-channel DWDM-PON transmission system with the defined FWM multi-wavelength source.

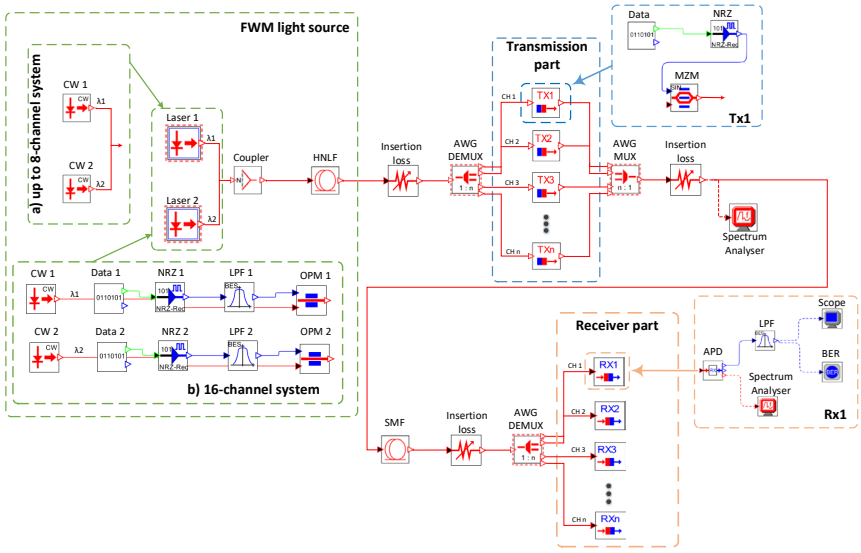

Fig. 4. Experimental simulation model of (a) 4 and 8-channel and (b) 16-channel DWDM-PON transmission system with an FWM multi-wavelength source.

In the DWDM-PON transmission system, some modifications were applied for multi-wavelength light source in the case of 16-carrier generation to obtain event distribution of the generated carrier powers. When the number of data channels increases, the carrier can be specially modulated to reduce the adverse effects of Brillouin scattering (SBS). An increase in the number of data channels increases the nonlinear Kerr effect as well as the stimulated Brillouin scattering [12]. In the case of SBS, energy is pumped from one light wave to another with a larger wavelength. SBS limits the maximum injected power (amplitude manipulation increases the width of the spectrum, as well as the SBS threshold), which is the reason why the use of more powerful lasers can be limited. To reduce SBS effect, the passive optical components with low attenuation are used [13], [14]. Two extra components – optical phase modulators (OPM) are used in multi-wavelength source scheme of the 16-channel system (see. Fig. 4 (b)) to increase SBS threshold and decrease the impact of SBS. Each of the pump laser sources is modulated by a bitrate of 100 Mbit/s [15] (non-return to zero (NRZ) line code, 2.8 GHz 3-dB bandwidth low-pass filters (LPF)).

In addition to the AWG MUX/DEMUX, an optical element was added, which simulated optical attenuation that introduced the required loss. This optical element in Fig. 4 is depicted as insertion loss – value is 3-dB. Data transmission channels with the 10 Gbit/s bitrate consist of data source (Data), NRZ coder and optical Mach-Zehnder modulator (MZM), where 3-dB bandwidth is 10 GHz and excess loss is 3-dB. During the research, the number of data transmission channels varied from 4 to 16 channels. Optical ITU-T G.652 single-mode fibre (SMF) was used as transmission media; its length was 20 km, the attenuation coefficient was 0.2 dB/km and the dispersion coefficient was 16 ps/nm/km at 1550 nm reference wavelength.

The receiver of the DWDM-PON system was formed of a sensitivity optical receiver where avalanche photodiode (ADP) was used with sensitivity of -24 dBm

at reference error probability 10^{-9}. After the sensitivity receiver, Bessel low-pass filter (LPF) with 3-dB bandwidth of 7.5 GHz was used to reduce noise in the received signal. The BER estimator, the electric scope, as well as the optical spectrum analyser were used to study information obtained about the data and the quality of the propagated signal.

5. RESULTS AND DISCUSSION

While performing simulation, all of the above parameters were abiding, but optimal parameters such as CW power and HNLF length were defined experimentally. Results were analysed by the obtained spectrum of the optical signal at the HNLF output, the signal spectrum after the AWG multiplexer and the spectrum after the transmission line (where SMF span length was 20 km). The quality of the transmitted signal was evaluated for the worst channel of the DWDM-PON transmission system based on the eye diagram and BER results (where BER$\leq 10^{-10}$). The worst channel for a 4-channel and 16-channel DWDM system was the fourth channel, but for an 8-channel system, it was the first channel.

Using the optimal parameters as defined in Table 1, different spectra were obtained for FWM optical effect for up to 16-channel DWDM-PON transmission system (see Fig. 5) with data channels.

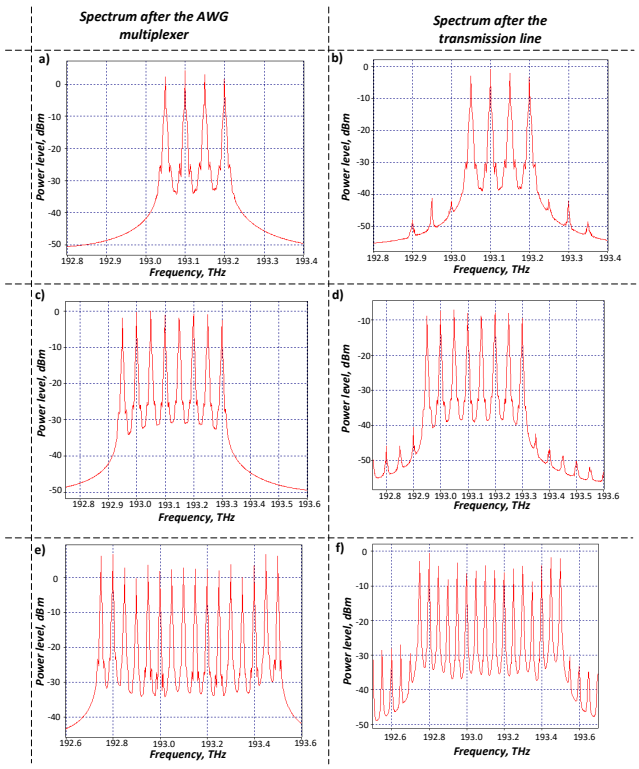

Fig. 5. The output spectrum of the DWDM-PON transmission system with FWM multi-wavelength source – (a) 4-channel, (c) 8-channel, (e) 16-channel after the AWG multiplexer, and (b) 4-channel, (d) 8-channel, (f) 16-channel after the 20 km long fibre optical transmission line.

Comparing the optical spectrum at the output of HNLF and AWG MUX, we can conclude that the channel output levels after AWG DEMUX/MUX are evenly distributed (Fig. 3 (a, c, e) generated harmonics before demultiplexing). In Fig. 5 (b, c, e) depending on the number of channels, we can see that in this case the demultiplexer separated 4, 8 and 16 channels at frequencies from 192.75 to 193.5 THz with a channel spacing of 50 GHz. The average calculated channel peak power output for 4 channels was 3.3 dBm. The largest difference between the calculated average channel peak power and the measured channel power levels was in the fourth channel, which was 0.5 dBm. However, in an 8-channel system the average channel peak power was 0.7 dBm where the difference between the worst channel was 1.3 dBm (for the first channel). However, in a 16-channel DWDM-PON transmission system, the average channel peak power was 2.8 dBm, and the difference between the calculated average channel peak power and the measured channel peak power was 2.9 dBm (for the fourth channel). The obtained values are acceptable because they fall within the 3 dBm range. Figure 5 shows the spectrum for the DWDM-PON transmission system with (a) 4-channel, (c) 8-channel, (e) 16-channel after the AWG multiplexer, (b) 4-channel, (d) 8-channel, (f) 16-channel after the transmission line.

The quality of the following eye diagrams was evaluated (up to a 16-channel DWDM-PON system with transmission length of 20 km and the bitrate of 10 Gbit/s) using the electrical scope. Figure 6 shows eye diagrams of the received signal in the (a) 4-channel, (b) 8-channel and (c)16-channel DWDM-PON transmission system with an FWM multi-wavelength source.

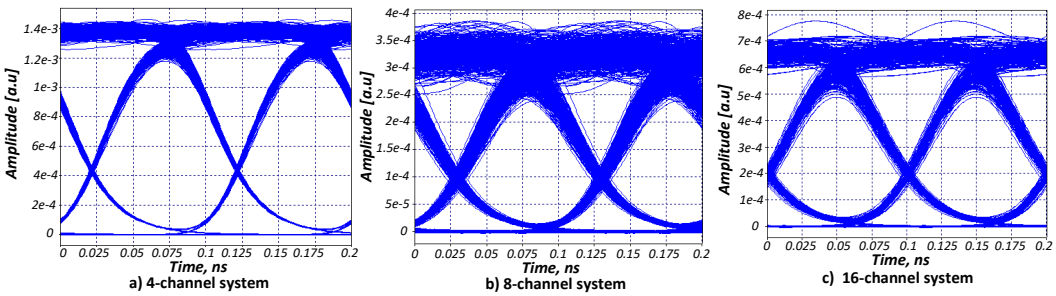

Fig. 6. Eye diagrams of the DWDM-PON transmission system with an FWM multi-wavelength source for (a) 4-channel, (b) 8-channel and (c) 16-channel.

As we can see from Fig. 6, the quality of the eye diagram decreases due to the increased dispersion and nonlinear effects (like FWM, SBS), and as more channels should be generated, the higher power fluctuations and therefore the overall performance of the system are lower. Table 2 shows BER values for up to 16-channel of the DWDM-PON transmission system, where the worst channel for a 4-channel and a 16-channel system is the fourth channel, but for an 8-channel system – the first channel. However, it is considered that the transmission lines will perform qualitatively with low losses because the "eye" opening is wide in all cases and the BER is below the threshold. According to ITU-T G.984.2 related to the recommended BER value for fibre optical transmission systems with a bitrate of 10 Gbit/s per channel, BER should be less than 10^{-10} [16].

Table 2. Summary of BER Values of the Received Signals in up to 16-Channel DWDM-PON Transmission System after 20 km Transmission through SMF Fibre Span

	4-channel system	8-channel system	16-channel system
BER value for the worst performing system channel	1×10^{-40}	2.5×10^{-23}	6.5×10^{-14}

6. CONCLUSIONS

Within the framework of research, we investigated up to 16-channel DWDM-PON transmission system with an FWM multi-wavelength source. FWM effect was used to generate a multi-carrier (multi-wavelength) light source for 4-, 8- and 16-channel DWDM-PON transmission system. The first step was to find the optimal power of CW pump lasers and HNLF fibre length for FWM carrier generation, which could be further used for modulation and transmission of data. It was found that for the simulated DWDM-PON transmission system with 10 Gbit/s bitrate and 50 GHz channel spacing, the CW pumping power level for both lasers in the case of a 4-channel system was +20 dBm and the HNLF fibre length was 0.9 km. To increase the number of DWDM-PON system channels from 4 channels to 8 and 16 channels and, accordingly, to generate more carriers, it was necessary to increase the power of pump CW lasers. Thus, for an 8-channel system, CW power was 24.1 dBm, and the length of HNLF was 1.39 km, but for a 16-channel system it was 26.3 dBm and 1.05 km, respectively. The SBS threshold must be taken into account to increase the number of FWM generated carriers for the DWDM-PON system with 8 to 16 channels; otherwise, the carrier output power is uneven and, as a result, a 16-channel system cannot be created. Therefore, for the generation of 16 carriers and SBS suppression, we used additional phase modulation. BER values and eye diagrams were evaluated for the worst channel of the DWDM-PON system. Through the analysis of the received signal after 20 km transmission, it was observed that in a 4-channel DWDM system the BER value of the worst-performing channel was 1×10^{-40}. Nevertheless, in an 8-channel system, the BER value for the worst-performing channel was 2.5×10^{-23}, but in a 16-channel system, the BER value of the worst-performing channel was 6.5×10^{-14}.

ACKNOWLEDGEMENTS

This work has been supported by the project "Generation of Kerr Combs in a Nonlinear Microresonator and Its Applications in Fiber Optical Communication Systems" No. MP-2019/4, for strengthening scientific personnel capacity in the year 2019/2020 at Riga Technical University.

REFERENCES

1. Bobrovs, V., Porins, J. & Ivanovs, G. (2007). Influence of Nonlinear Optical Effects on the NRZ and RZ Modulation. *Electronics and Electronica Engineering Signal Technology*, *4* (76), 55–58.

2. Olonkins, S., Spolitis, S., Lyashuk, I., & Bobrovs, V. (2014). Cost effective WDM-AON with multicarrier source based on dual-pump FOPA. In: *6th International Congress on Ultra Modern Telecommunications and Control Systems and Workshops (ICUMT),* (pp. 23-28), 6–8 October 2014, St. Petersburg, Russia.
3. Gómez, F., Puerto, K., & Guevara, D. (2015). Effect of nonlinear four-wave mixing in optical fibre transmission. In: *2015 IEEE Thirty Fifth Central American and Panama Convention (CONCAPAN XXXV),* (pp. 1–6), 11–13 November 2015, Tegucigalpa, Honduras.
4. Dilendorfs, V., Spolitis, S., & Bobrovs, V. (2017). Effectiveness Evaluation of Dispersion Compensation Methods for Fiber-Optical Transmission Systems. *Progress in Electromagnetic Research Symposium (PIERS)*, 3759–3763.
5. Selvamani, A., & Sabapathi, T. (2011). Suppression of four wave mixing by optical phase conjugation in DWDM fiber optic link. In: *International Conference on Recent Advancements in Electrical, Electronics and Control Engineering* (pp. 95–99), 15–17 December 2011, Sivakasi, India.
6. Sugumaran, S., & Arulmozhivarman, P. (2013). Effect of chromatic dispersion on four-wave mixing in WDM systems and its suppression. In: *International Conference on Emerging Trends in VLSI, Embedded System, Nano Electronics and Telecommunication System (ICEVENT)* (pp. 1–5), 7–9 January 2013, India.
7. Cheng, M.C., Tsai, C.T., Chi, Y.C., & Lin, G.R. (2014). Direct QAM-OFDM Encoding of an L-band Master-to-Slave Injection-Locked WRC-FPLD Pair for 28 × 20 Gb/s DWDM-PON Transmission. *IEEE Journals & Magazines*, *32* (17), 15724–15736.
8. Kachhatiya, V., & Prince, S. (2016). Wavelength division multiplexing-dense wavelength division multiplexed passive optical network (WDM-DWDM-PON) for long reach terrain connectivity. In: *International Conference on Communication and Signal Processing (ICCSP)* (p. 1), 6–8 April 2016, Madras, India.
9. Telecommunication Standardization Sector of ITU. (2012). *Spectral grids for WDM applications: DWDM frequency grid*. Recommendation ITU-T G.694.1.
10. Spolitis S., Bobrovs, V., Berezins, S., & Ivanovs, G. (2013). Optimal design of spectrally sliced ASE seeded WDM-PON system. In: *2012 15th International Telecommunications Network Strategy and Planning Symposium (NETWORKS)* (pp. 1–5), February 2013. Rome, Italy.
11. OFS Specialty Photonics Division. (2013). *Highly Non-Linear Fiber (HNLF*). Product Sheet, Version: 20131210, Denmark, 1, 2013.
12. Cerqueira Arismar, Jr. S., Chavez Boggio, J. M., Hernandez-Figueroa, H. E., Fragnito, H. L., & Knight, J. C. (2008). Highly efficient generation of cascaded four-wave mixing products in a hybrid photonic crystal fiber. In: *European Conference on Optical Communications – ECOC* (pp. 16–20), 16–20 September 2007, Berlin, Germany.
13. Kartalopoulos, S. V. (2008). *Next generation intelligent optical networks*. USA: Springer Science Business Media.
14. Agrawal, G. (2002). *Fiber-optic communication systems* (3rd ed.). New York: John Wiley & Sons.
15. Dakin, J. P., & Brown, R. G. W. (2018). *Handbook of optoelectronics: Enabling technologies* (Volume Two). USA: CRC Press Taylor & Francis Group.
16. Telecommunication Standardization Sector of ITU. (2003). *Gigabit-Capable Passive Optical Networks (GPON): Physical Media Dependent (PMD) Layer Specification*. Recommendation ITU-T G.984.2.

sciendo

LATVIAN JOURNAL OF PHYSICS
AND TECHNICAL SCIENCES
2020, N 4

DOI: 10.2478/lpts-2020-0020

THE BIOMETHANE INJECTION INTO THE NATURAL GAS NETWORKS: THE EU'S GAS SYNERGY PATH

J. Savickis[1], L. Zemite[2]*, N. Zeltins[2], I. Bode[2], L. Jansons[2],
E. Dzelzitis[2], A. Koposovs[2], A. Selickis[2], A. Ansone[2]

[1]ITERA Latvija
50 Skanstes Str., Riga, LV-1013, LATVIA
[2]Riga Technical University,
Faculty of Power and Electrical Engineering, Institute of Power Engineering
12-1 Azenes Str., Riga, LV-1048, LATVIA
*e-mail: laila.zemite@rtu.lv

Biomethane is one of the most promising renewable gases (hereafter – RG) – a flexible and easily storable fuel, and, when used along with the natural gas in any mixing proportion, no adjustments on equipment designed to use natural gas are required. In regions where natural gas grids already exist, there is a system suitable for distribution of the biomethane as well. Moreover, improving energy efficiency and sustainability of the gas infrastructure, it can be used as total substitute for natural gas. Since it has the same chemical properties as natural gas, with methane content level greater than 96 %, biomethane is suitable both for heat and electricity generation, and the use in transport.

Biomethane is injected into the natural gas networks of many Member States of the European Union (hereafter – the EU) on a regular basis for more than a decade, with the Netherlands, Germany, Austria, Sweden and France being among pioneers in this field. In most early cases, permission to inject biomethane into the natural gas grids came as part of a policy to decarbonize the road transport sector and was granted on a case-by-case basis. The intention to legally frame and standardise the EU's biomethane injection into the natural gas networks came much later and was fulfilled in the second half of the present decade.

This paper addresses the biomethane injection into the natural gas grids in some EU countries, highlights a few crucial aspects in this process, including but not limited to trends in standardisation and legal framework, injection conditions and pressure levels, as well as centralised biogas feedstock collection points and the biomethane injection facilities. In a wider context, the paper deals with the role of biomethane in the EU energy transition and further use of the existing natural gas networks.

Keywords: *biomethane, injection, natural gas girds, renewable gases, synergy.*

INTRODUCTION

During the energy transitions, the role of biomethane and other RGs in the EU is closely related to future prospects, and, to some extent, even physical survival of the natural gas infrastructure. Long-term strategies need to emerge in order to help secure the EU's energy future, as well as to add the diversification dimension to its energy security. Bearing in mind the limited timeframe of energy transition initiatives, which barely covers two decades, there is an urgent necessity to explore all possible synergy paths involving natural gas and RG across energy production, distribution, storage and consumption spectrum [1]–[3]. Among these paths, increasing presence of RGs, and, firstly and foremostly, biomethane in existing natural gas transportation and distribution networks should be studied more extensively.

The general trends of all deep decarbonisation strategies in the EU are centred around low-carbon energy systems as the backbone of the future energy supply, in which an expansion of renewable or maximally carbon neutral electricity generation is accompanied by widespread electrification of industrial processes. Electric heating takes over market share from the conventional natural gas in buildings, and e-mobility becomes more and more popular worldwide [4], [5]. Global investment in electricity generation, networks and storage in 2018 exceeded USD 770 billion, more than combined investment in oil and gas supply for the same period [6]. However, there are limits to how quickly and extensively electrification can develop, as it is not yet well suited to deliver all types of energy services. Even if the complete technical potential for electrification were deployed, there would still be sectors requiring other energy sources, including gaseous fuels.

Maintaining a parallel natural gas or RG infrastructure adds a layer of resilience compared with an approach that relies exclusively on electricity. This was rather obvious in Japan, when gas-fired generation stepped in to provide power after shutdown of its nuclear reactors following Fukushima Daiichi nuclear power plant disaster on 11 March 2011 [7]. It also provides a useful hedge against the risks that electrification and the development of new electricity networks do not increase at the pace needed to displace existing fuels while meeting energy service demands. However, if natural gas infrastructure is to secure the role in post energy transition EU, it will need to deliver much bigger share of RG, one of which is biomethane. In a long run, the future of the natural gas infrastructure in the EU is largely dependent not only on diversification of gaseous fuel sources by gradually increasing percentage of RGs, but also on ability of the existing natural gas grids facilitate this diversity in a safe, cost effective and sustainable manner [8].

Increasing sustainability and carbon neutrality of the natural gas infrastructure all over the EU means more intensive presence of RGs into the natural gas sector. Here biomethane stands out as one of the most promising RGs to be blended with natural gas in large volumes, which can be done in a relatively short period of time [8]. Biomethane is a flexible and easily storable fuel that can be used wherever natural gas grids exist without significant improvements to any parts of the natural gas transportation and distribution networks. In those EU regions where a natural gas grid already exists, there is a system suitable for the distribution of biomethane as well. It can be used as a direct substitute for natural gas and as a fuel in heating, transport and electricity

generation since it has the same properties as natural gas – achieving methane content levels greater than 96 % [9]. However, this methane content level benchmark is not legally or technically binding to all the EU Member States, as they can make their own decisions on how pure biomethane must be in terms of methane content to be injected into the grid. For example, the Netherlands let biomethane with methane content of only 85 % be injected, but Switzerland and Sweden require 96 % and 97 % of methane content [10].

Biomethane has been injected into the natural gas grids of many Member States of the EU for about a decade, with the Netherlands, Germany, Austria, Sweden and France being the pioneers in the field [11], [12]. In most early cases, however, permission to inject biomethane came as part of policy to attempt to decarbonize road transport only and was granted on a case-by-case basis. But, since 2003, Directive 2003/55/EC of the European Parliament and of the Council of 26 June 2003 concerning common rules for the internal market in natural gas and repealing Directive 98/30/EC has granted the injection of gases from non-conventional sources into the natural gas network when technically possible and when safety is maintained. In period that followed Directive 2009/73/EC of the European Parliament and of the Council concerning common rules for the internal market in natural gas and repealing Directive 2003/55/EC (hereafter – Directive 2009/73/EC) and Directive 2009/28/EC of the European Parliament and of the Council on the promotion of the use of energy from renewable sources and amending and subsequently repealing Directives 2001/77/EC and 2003/30/EC (hereafter – Directive 2009/28/EC) set out an all-EU legal framework for injection of biomethane into natural gas grids. Recital 26 of the preamble to Directive 2009/73/EC states that Member States should take concrete measures to assist the wider use of biogas and gas from biomass, the producers of which should be granted non-discriminatory access to the gas system, provided that such access is compatible with the relevant technical rules and safety standards on an ongoing basis. Additionally, point (e), Article 40, of Directive 2009/73/EC also specifies that Member States should facilitate access to the network for new production capacity, in particular removing barriers that could prevent access for new market entrants and of gas from renewable energy sources [13].

Recital 62 of the preamble to Directive 2009/28/EC provides a further clarification on how new connections should be handled, as it states: the costs of connecting new producers of electricity and gas from renewable energy sources to the electricity and gas grids should be objective, transparent and non-discriminatory and due account should be taken of the benefit that embedded producers of electricity from renewable energy sources and local producers of gas from renewable sources bring to the electricity and gas grids. Article 16.7 and Article 16.9 of Directive 2009/28/EC also read that Member States shall ensure that the charging of transmission and distribution tariffs does not discriminate against gas from renewable energy sources, and that where relevant Member States shall assess the need to extend existing gas network infrastructure to facilitate the integration of gas from renewable sources [14].

The intention to standardise the EU's biomethane injection into the natural gas network came much later and was fulfilled in the second half of this decade. Part 1 of Standard EN 16723–2 "Natural gas and biomethane used in transport as well as biomethane injected into the natural gas network" (hereafter – Standard EN 16723–2)

was published in 2016, and it concerned the requirements of biomethane injected into the natural gas grids [15]. Part 2, published in 2017, specifies the requirements and test methods for natural gas, biomethane and blends of both for use as vehicle fuels (standardisation applies to these fuels irrespective of the storage state (compressed or liquefied)) [16].

Standard EN 16723–2 includes the following general parameters:

- The natural gas, biomethane and blends of those intended for injection into natural gas networks shall be free from any constituents or impurities other than the ones described in this standard, to the extent that it cannot be transported, stored or utilized without quality adjustment or treatment. In the case of such other constituents and/or impurities, it may be necessary to obtain an approval from the competent and legitimate authority to define the acceptable risk in the territory of the injection point;
- Health criteria assessment for biomethane is complex and dependent upon the biogas feedstock and upgrading and purification process. As a result, it is recommended that contaminants to be specified and limits to be applied are assessed at national level using an appropriate methodology;
- Biomethane shall meet the requirements of the Standard EN 16726 "Gas infrastructure – Quality of gas – Group H for common parameters" that specifies gas quality characteristics, parameters and their limits, for gases classified as group H that are to be transmitted, injected into and from storages, distributed and utilized [17].

At the national level, where access to the grid infrastructure is equal and non-discriminatory, additional quality requirements have been set on biomethane and regasified LNG for injection into the natural gas grids (both transportation and distribution networks) [18].

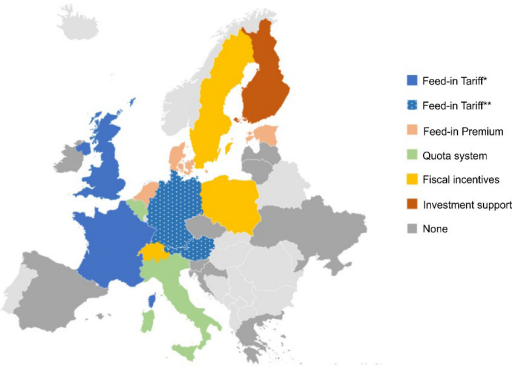

**In Austria and Germany, the support schemes apply only if the end-use of the biomethane is electricity production.

In Belgium, the support scheme is only applicable in Wallonia

Source: regatrace.eu

Fig. 1. Support schemes in place per country.

Several different subsidy or market schemes in the field of biomethane are used in the European countries, which include but are not limited to tax exemptions, feed-in tariffs, investment subsidies or grants, preferential financial conditions for loans, reduction or exemption of grid tariffs, obligation of grid operator to take over connection costs, exemption for penalties for balance energy and quota systems [19]. Figure 1 shows the current variety of the biomethane production support schemes in Europe.

2. SEVERAL TRENDS OF BIOMETHANE SECTOR DEVELOPMENT IN THE EU

In Europe landfill and sewage gases account for around a quarter of total biogas

production, while most of the resources come from another source: anaerobic fermentation of agricultural feedstock. Up to 70 % of the feedstocks – such as energy crops, manure and agricultural residues used for biogas production – emerges from the agricultural sector [20]. The use of agricultural residues is particularly important in countries like Denmark, France and Italy, but energy crops are mainly grown and used in Germany and Austria. The municipal and industrial organic waste still has a potential to be developed for use in biogas production, like it is done in the Nordic countries [21].

By the end of 2012 biogas was upgraded to biomethane in eleven EU countries, and in nine countries it was injected into the natural gas grids. Sweden and Switzerland have the longest experience with biomethane injection into natural gas distribution networks and closed local networks, which started back in the 1990s [22]. In 2018, the European countries with the biggest production of the renewable gases, mostly biomethane, were Germany with 10 018 GWh, the United Kingdom with 3300 GWh, the Netherlands with 2226 GWh, Denmark with 1425 GWh, Sweden with 1281 GWh and France with 1207 GWh. Apart from Sweden and Germany, no country reported production of renewable gases via gasification or power-to-methane process. Sweden reported gasification production of 15 GWh in 2018, but renewable gas production in Germany via gasification or power-to-methane was negligible [23].

As the leading biogas producing region, the EU has around 20 000 biogas plants, with the majority of them located in Germany. Most are built for on-site electricity generation and co-generation, with around 500 plants dedicated to the upgrading of biogas [8]. The analysis of the latest data shows that the number of the biomethane plants in Europe has increased by 51 % in 2 years, from 483 in 2018 to 729 in 2020. There are currently eighteen countries producing biomethane in Europe. Germany has the highest share of biomethane production plants (232), followed by France (131) and the United Kingdom (80) [24].

The biomethane production in Germany begun in 2006, and since then, the number of biomethane plants and the total annual production capacity have been growing constantly. In 2018, the number of plants reached 213 units, but in 2020 – 232 units with approximately 10 TWh of yearly maximum biomethane output capacity [23]. Theoretically, the whole amount of biomethane produced in Germany can be injected into the natural gas grids, with costs for the injection shared between the plant operator and the gas grid operator in the proportion 25 % to 75 %. Moreover, if the length of the connecting pipelines is less than 1000 m, share of the biomethane plant operator must not exceed EUR 250 000, but if connecting pipelines are longer than 10 km, the plant operator bears additional costs. The connecting pipelines, including the injection unit, are normally a property of the gas grid operator [23].

Fig. 2. Biomethane piping and measurement equipment in the grid connection station, Germany.

Source: dena.de

France is one of a few EU countries that has specific biomethane target: to produce 8 TWh of biomethane by 2023. Biomethane was granted regular access to the natural gas grids only in 2011, and after this date the growth in a field was considerable, with the number of new biomethane plants going from 7 to 107 between 2015 and 2019. According to an overview of France's renewable gas sector, the amount of biomethane injected into the French natural gas networks almost doubled between 2016 and 2017. Figures in the report from GRTgaz show that 406 million kWh of RGs were injected into the network over this period, which is equivalent to the consumption of nearly 34 000 homes [25].

Around 100 new biomethane projects were declared in France in 2017 alone, increasing the biomethane production capacity by 3 billion kWh/year. With a total of 361 biomethane projects registered, the country's prospected total capacity now stands at 8 billion kWh/year. The growth of the biomethane sector strengthens the role of the agricultural sector in France's economy, while also helping to develop a competitive industrial sector [26].

Over 1000 projects are currently at different stages of development, meaning that France is fulfilling its ambition to become a leader in the European biomethane sector by the mid and late 2020s [23].

An analysis of the biomethane life cycle carried out by the gas distribution system operator (hereafter – DSO) GRDF demonstrated that the development of the biomethane sector could prevent emission of 750 000 tonnes of CO_2 for the year 2020 alone. Cumulatively, the emission of over 2 million tonnes of CO_2 would therefore be avoided thanks to the development of the biomethane sector between 2018 and 2020. In other words, for each MWh of biomethane produced, injected and consumed, savings of 188 kilogrammes of CO_2 equivalent would be made. The French Environment & Energy Management Agency anticipates that 500 to 1400 plants could inject between 12 and 30 TWh/year of biomethane into the natural gas transportation and distribution networks around 2030 [27].

In the United Kingdom, biomethane is already being injected into the gas grid at a number of biogas upgrading facilities: for example, in "AB Agri" anaerobic digestion plant in North Yorkshire, which has the capacity to process 60 000 tonnes of waste a year. At the same time, its EU Member State neighbour – Ireland – plans to achieve 20 % renewable gas in the natural gas network by 2030. To achieve this ambitious goal, its first biomethane injection facility was built in Nurney, Kildare, and the first portion of biomethane was injected into the grid in 2019. In upcoming years, it is planned to implement a network of injection facilities throughout Ireland [28].

In most cases, national production and consumption of biomethane are well balanced, and currently only some EU countries demonstrate slight disbalance between the two. For instance, as shown in Fig. 3, Denmark is producing more biomethane than it consumes, whereas Sweden is consuming more than double the amount it is producing. This is mainly because in Sweden incentives are focused on the consumption side, of which tax exemption is the most important one, whereas in other EU Member States subsidies are focused on production or injection of biomethane. It means that imported biomethane in Sweden can be double subsidized. In 2016, Sweden imported 200 GWh from Denmark, which increased to 1132 GWh in 2018. At the same time, in Germany production of biomethane in 2018 was 1498 GWh higher than its consumption. Germany exported some of these resources to the Netherlands

and Switzerland, but the biggest share of leftover biomethane is still stored in the natural gas grids for later use [23].

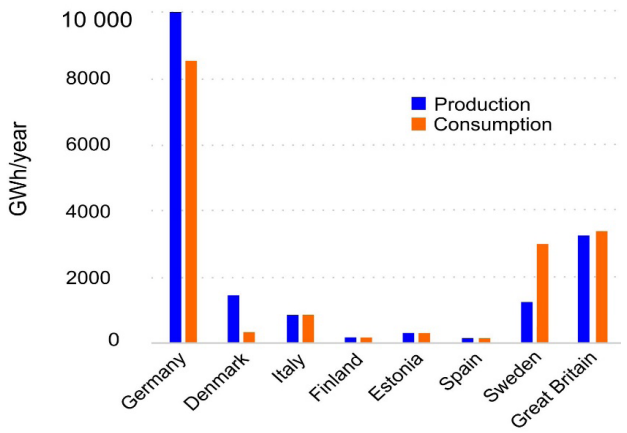

Fig. 3. Biomethane production compared to total biomethane consumption (per country, GWh/year).

Source: regatrace.eu

If there is a successful introduction of gasification, optimal use of anaerobic digestion potential and options for cross-border trade, volumes of the biomethane injected into the EU natural gas grids could reach up to 10% – 20% of all gaseous fuel consumption. Even more, the estimates have been made that during energy transition, biomethane could provide total gradual replacement of the conventional natural gas in the so-called mature gas markets, such as the United Kingdom, Germany and the Netherlands [29].

3. THE CASE OF LATVIA

Latvia has biogas production, but biomethane upgrading and its injection into the natural gas grids are still absent. At the same time, the legal and regulatory framework for injection of biomethane into the natural gas grids is already in place. Namely, paragraphs 6 and 7 of Regulation of the Cabinet of Ministers No. 650 "Requirements for the Injection and Transport of Biomethane and Gaseous Liquefied Natural Gas in the Natural Gas Transmission and Distribution System" (hereafter – Regulation No. 650) clearly state that in Latvia injection of biomethane is possible in both natural gas transmission and distribution networks. If biomethane is injected into the natural gas transmission system, where a minimum pressure is 25 bar, its pressure must not exceed the actual pressure of the system by more than 5 bar. On the other hand, if biomethane is injected into the natural gas distribution system, its operating pressure must exceed the pressure of the system by not more than 10 % of the actual pressure at the connection point. The Appendix of Regulation No. 650 also shows the purity or chemical composition requirements that must be met in order to inject biomethane into the natural gas systems [18].

Table 1. Quality Characteristics of the Substitute Gas to be Injected and Transported in the Natural Gas Transmission and Distribution System

Parameter	**Unit**	**Value**
Wobbe index - WI, b at base temperature conditions (combustion / measurement) 25/20 ° C	MJ/m^3 $kcal/m^3$ kWh/m^3	47.02–51.98 11231–12415 13.06–14.44
Maximum heat of combustion (GCV) at a base temperature of 20 ° C and 101.325 kPa (combustion / measurement) 25/20 ° C	MJ/m^3 $kcal/m^3$ kWh/m^3	≥ 34.87 ≥ 8329 ≥ 9.69
Minimal heat of combustion (GCV) at a base temperature of 20 ° C and 101.325 kPa (combustion / measurement) 25/20 ° C	MJ/m^3 $kcal/m^3$ kWh/m^3	≥ 31.82 ≥ 7600 ≥ 8.83
Relative density – d		0.55–0.70
Total sulfur - S (without odorant)	g/m^3	≤ 0.03
Hydrogen sulfide + carbonyl sulfide H_2S + COS	g/m^3	≤ 0.007
Mercaptans - RHS (without odorant)	g/m^3	≤ 0.016
Methane – CH_4	mol %	≥ 90
Nitrogen - N_2	mol %	≤ 3
Oxygen – O_2	mol %	≤ 0.02* ≤ 1.0**
Carbon dioxide – CO_2	mol %	≤ 2.5* ≤ 4.0**
Methane number		≥ 65
Mechanical impurities	g/m^3	≤ 0.001
The hydrocarbon dew point HC DP, pie 1–70 bar	°C	≤ –2
The water dew point H2O DP, pie 40 bar	°C	≤ –10
Hydrogen - H_2	mol %	≤ 0.1
Odorant	mg/m^3 points	≥ 3 ≥ 3

* Quality characteristics of the substitute gas to be fed into and transported in the natural gas transmission system.

** Quality characteristics of the substitute gas to be fed into and transported in the natural gas distribution system, if the distribution system is not connected to the underground gas storage and is not connected to the gas supply system of other countries.

In both cases, the supply of biomethane to the gas pipelines of the natural gas transmission system must take place in such a way that the requirements of the natural gas transmission system operator regarding the supply/mixing point are met [18].

Latvia has a significant potential for development of biomethane injection into the natural gas grids, but it has not been started yet. There are 59 biogas plants in operation in Latvia, and in most cases biogas is used locally – for the production of electricity. However, according to present estimates, production of biomethane with its subsequent injection into the natural gas grids would be a more cost-effective option in terms of economy and sustainable transformation of the natural gas sector [2].

About 12 % of Latvia's biogas plants rely on landfill resources for biogas production, 2 % are sewage sludge substrate biogas plants, 5 % are plants producing biogas

from produce residues or wastewater, and the major share – 81 % – run on agricultural waste. Figure 4 shows biogas plant proximity to the natural gas grids, and most of them are located rather close to both natural gas transport and distribution networks. Injection of biogas into those grids is currently prevented by quite a few obstacles, like private land ownership, rough terrains and lack of clearly defined and transparent support schemes, and in future these obstacles should be adequately addressed [2].

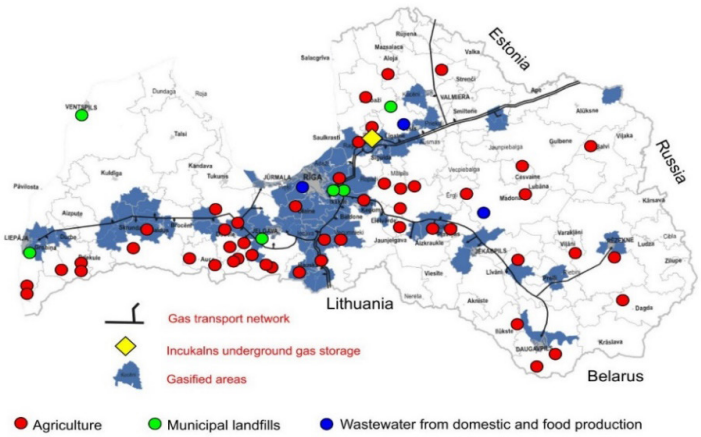

Fig. 4. Location and type of biogas plants in Latvia with respect to the natural gas network.

Source: JSC "Gaso", the Latvian Biogas Association

The comparative research has been made, which established that on average the Latvian biogas plants operate at between 60 % and 70 % of installed capacity rate. Only twenty-three out of fifty-nine plants have average operational capacity of 80 % or more, and almost the same number – nineteen plants – have average operational capacity of less than 50 %. The remaining biogas plants operate at average capacity between 50 % and 80 %. If the connections between biogas plants and the natural gas grids are constructed where possible and economically feasible, they could be used not only for transportation of biomethane from plants to grid, but also, if necessary, for delivery of natural gas to the plants, thus ensuring the maximum productivity of cogeneration facilities. If distance from a biogas plant to a possible connection point with the natural gas distribution grid is considered the main criterion, seventeen biogas plants can relatively easily be connected to grids, as five of them are located less than 1 km, nine are located less than 5 km and three – up to 10 km away from the natural gas grid. Another seven plants are located within 10 to 15 km distance from possible grid connection points, and at the moment it is rather questionable whether their connection to the grids would be technically and financially feasible. Additionally, all these distances can deviate by about 10 %, as actual, precise measurements are taken.

As for five plants located less than 1 km to the natural gas grid, their total installed cogeneration capacity is 3.72 MW and, they have an average operational capacity rate of 78 %. While operating at a maximum capacity rate of 95 %, the amount of energy

produced there is about 30 950 MWh, with possible additional electricity production of 6 735 MWh. For approximate calculation of the connection costs, the natural gas flows and approximate pipeline diameters were estimated. The natural gas pipeline connection flows range from 63 to 141 m^3/h, but mostly are above 280 m^3/h. The required nominal diameters of connection pipelines therefore are 32 mm to 50 mm. The approximate total costs of the pipelines and gas control points are estimated at EUR 188 247. Assuming that the plants, when operating at 70 % capacity rate, are upgrading all produced biogas to the biomethane level and injecting it into the natural gas grids, the specific current biogas purification costs for three closest plants would be around 0.132 EUR /m^3, and for two – around 0.204 EUR/ m^3. The total estimated cost of construction, including pipelines, gas control points and injection facility, for plants up to 1 km from the natural gas distribution network would reach about EUR 2 947 114.

Fourteen biogas plants within a distance of up to 5 km from the natural gas grids with total installed cogeneration capacity of 16.09 MW operate at an average capacity rate of 64 %. In this case, if the plants operated with the maximum capacity rate of 95 %, the amount of electricity produced would reach about 133 859 MWh. The required nominal diameters for connection pipelines range from 25 to 100 mm, with average diameter of <65 mm. The estimated cost for the pipeline and gas control point construction is about EUR 1 698 000, but the estimated cost of installation of the biogas upgrading facility – EUR 12 603 000.

Seventeen biogas plants with a distance of up to 10 km to the natural gas grid with total installed cogeneration capacity of 18.33 MW operate at an average capacity rate of 65 %. If plants operated at a maximum capacity rate, the possible amount of electricity produced would be 152 542 MWh. In order to make connection with the natural gas grid, the required nominal diameters of pipelines in this case again range from 25 to 100 mm. The approximate cost of the pipelines and gas control points is EUR 2 871 991, but the total estimated cost of the project, including biomethane production facility, is EUR 15 113 551.

Twenty-four biogas plants within a distance of up to 17 km to the natural gas grid with the total installed cogeneration capacity of 24.87 MW operate at an average capacity rate of 69 % and produce about 142 938 MWh of electricity. The maximum possible amount of electricity produced during the year is 206 960 MW. By constructing gas pipeline connections, thus ensuring maximum cogeneration productivity, it is possible to produce additional 64 022 MWh of electricity per year. The total estimated cost of the pipelines and gas control points is EUR 7 735 419, but construction of the biogas upgrading facility – 28 492 525 EUR.

As a result, the conclusion was drawn that for plants located 5–10 km from the natural gas grids, the cost of the pipeline connection was on average 7 times lower than the cost of biogas upgrading technology. The construction costs of the natural gas connection would begin to dominate over the costs of the upgrading facility only when the length of the natural gas connection would reach:

- 25 km, and the plant capacity would be 250 m^3/h;
- 30 km, and the plant capacity would be 500, 650 and 950 m^3/h;
- 35 km, and the plant capacity would be 1400m^3/h;
- 45 km, and the plant capacity would be 2000m^3/h.

The introduction of centralised points

to produce or inject biomethane into the natural gas grid is quite promising option, especially in areas with rather dense clustering of biogas plants, which could have particular advantage in countries such as Latvia. Centralised biomethane injection points could provide a relatively easy and less costly alternative to installing separate injection points for numerous producers. It would facilitate biomethane production particularly in places where separate, direct connections of the distributed biogas plants are not feasible due to technical or other reasons [30].

There are two principal options to organise centralised biomethane injection into the natural gas grids. The first option is a centralised feedstock collector, where separate producers of biogas feedstock deliver the raw product. Digestion, scrubbing and injection would be all carried out at this central location for multiple producers. This option is favourable, if biogas producers are not interested in the development of full-scale biogas production and consumption of their respective sites, or they have access to large stock of raw products, which can be split between biogas production and consumption on site and raw material delivery to a centralised feedstock facility. This possibility would be especially interesting in regions, where there are no full-scale biogas plants, or to farmers, who produce large amount of agricultural waste with no intension to invest in separate biogas production. However, estimates made by some research groups show little financial benefit in centralised biogas production [30].

The second option is to establish a centralised biogas upgrade and injection facility, where all the delivered biogas is treated and scrubbed to convert it to biomethane and then injected into the natural gas grid [31]. Producers of biogas would deliver their product to a centralised facility via pipelines or by specialised gas carrier trucks [32]. If gas carrier trucks are used to transport biomethane to a centralised facility, it would need to be compressed and collected from multiple sites according to a certain schedule, but, if pipeline connections are installed between a centralised facility and separate biogas plants, such a schedule would not be required.

In many cases, overall capital and operating costs for centralised biomethane injection points would be lower per unit of biomethane injected, and it would be easier to monitor biomethane quality and enforce safety standards. If such injection points were available, it could lead to more interest in biomethane production and its distribution via the natural gas grids in Latvia. Needless to add that with correctly balanced incentives, biomethane is a commercially viable transport fuel as well: it can rely on existing natural gas infrastructure and contribute to reaching the European climate targets in reduction of CO_2 and other greenhouse gas emissions [20].

4. THE PRINCIPLES OF BIOMETHANE INJECTION INTO THE NATURAL GAS GRID

The technical rules and legislative framework of injection of biomethane into the natural gas grids vary in different EU Member States, and responsibilities are attributed to the different parties, including but not limited to regulatory authorities, energy suppliers, biogas producers, natural gas transmission system operators

(TSOs), DSOs and the third parties. The owners or operators shall be clearly defined for biogas upgrading and compression unit, biomethane injection facilities and biomethane quality control systems (chemical composition monitoring, metering, etc.). The following responsibilities should also be allocated between the different parties: the biogas production environmental safety control, the compliance with the technical specifications which correspond to the injection conditions, odorization and deodorization of biomethane (when necessary), obligation to informing the adjacent TSOs, natural gas storage system operators and customers that they may be supplied with biomethane [33].

In order to supply information to policy makers, interested parties, potential customers and society at large on the biomethane production status in a certain country or region, the 2020 edition of biomethane map suggests adding three more points to a regular information list, which are:

- the type of connection to the grid: some biomethane plants are connected to the natural gas transport grid, others to the distribution grid, and a few are not connected as they use biomethane for their own consumption;
- the type of gas transported in a specific grid: it depends on national specifications and can be low caloric or high caloric (does not apply to Latvia);
- availability of on-site production of bio-CNG or bio-LNG, which can be used as an all-purpose sustainable fuel [24].

The natural gas transmission system, transporting large volumes of the natural gas at high pressure, is the main element of every national or regional natural gas grid. The physical characteristics of the transmission system vary for technical or safety reasons with pipeline diameters in most cases from DN80 up to DN1400 and a natural gas pressure between approximately 16 bar up to the maximum operating pressure of 50 bar and higher [33].

High-power compression plants ensure that there is sufficient pressure in the system to deliver natural gas to all parts of the network in order to meet the daily demand. Biomethane injected at the transmission level, therefore, must be at a higher pressure than that injected at the distribution level [18]. Accordingly, its compression costs would be higher for the producers injecting into the transmission system. Theoretically, it might be possible to accept at the transmission level small volumes of biomethane, which do not meet the normal natural gas quality standards, as small quantities of such biomethane would be mixed with a much larger volume of standard quality natural gas, resulting in dilution of impurities present in RG. However, in ordinary circumstances, biomethane purity requirements must be met at all times and regardless of amount of biomethane injected into the grids. Table 2 lists the main contaminants of biogas that should be maximally removed from biomethane before its further use.

Odorization may not be necessary if the quantities being injected are small relative to the volumes of natural gas in the transmission system, which is already odorised, and this could result in some operational savings for biomethane producers. In some European countries, the distribution systems require odorization only at quite low pressures – for instance, in Great Britain natural gas must be odorized when delivered at 7 bar or lower [34].

There are very few situations, when it is justified to require biomethane injection into the grid at the transmission level, and these cases are normally dealt with individually. In the future, if there are numerous

large-scale biomethane upgrading facilities coming online, it may be necessary to turn to this option more regularly.

Table 2. Contaminants of Biogas, Their Sources and Impact on Plant Operation

Impurity	**Source**	**Impact**
Carbone dioxide – CO_2	Mineralization of carbon from organic biomass (the main component of biogas)	Reduces overall calorific value; promotes corrosion of metallic parts by formation of weak carbonic acid
Hydrogen sulfide – H_2S	Proteins, manure, organic waste	Acts as corrosive in pipelines; causes SO_2 emissions after combustion or H_2S emissions in case of incomplete combustion; poisons the catalytic convertor
Water – H_2O		A major contributor to corrosion in aggregates and pipelines by forming acid with other compounds; formation of condensation leading to the damage of instruments; freezing of accumulated water in high-pressure low temperature conditions
Ammonia – NH_3	Proteins	Leads to an increase in antiknock properties of engines; causes formation of NO_x.
Dinitrogen – N_2	Air input, e.g., by desulphurization with air	Leads to an increase in antiknock properties of engines; leads to a reduction in calorific value as well
Siloxanes	Cosmetics, antifoaming agents, washing agent, hydraulic fluent	They are mainly present in biogas formed out of landfill or sewage gas. This hydrocarbon acts as quartz of silica, grinding motor part
Dust		Damages vents and exhaust by clogging

Source: dena.de

From the practical standpoint, it is more likely, that biomethane plants would connect to the natural gas distribution systems, which is a common practice in the EU countries [35]. The natural gas distribution system operates at a lower pressure and is designed to move smaller volumes of gas than the transmission system. Many natural gas distribution pipelines in the European countries feed residential customers and small businesses, where natural gas use is weather dependent and, therefore, has very low demand in summer months [36]. In small, strictly localized systems, if quantities of the biomethane injected exceeded the demand of distribution system and could not physically take the gas away from the injection point, pressures would rise and this could pose a safety risk in the pipeline where biomethane was injected. The minimum demand levels on the distribution network, therefore, limit the size of the biomethane plant or amount of simultaneous injection capacity that can be accommodated at any particular point on the networks [37]. As experience shows, in some countries only the biomethane facilities that have their own gas storages on site [38] may be permitted to connect to the distribution pipelines where the minimum demand level is very low. For instance, it is a practice in Great Britain that biomethane plants are limited in size to the minimum demand levels of the downstream pipeline. Areas where direct connection is most cost-effective must have some or all of the following criteria: proximity to the distribution network and proximity to year-round

gas consumption points (industrial estates, hospitals, swimming pools, sport and community centres etc.). Parts of the natural gas distribution network that currently require reinforcement could especially benefit from the addition of the local biomethane injection.

The cases of biomethane injection at both transportation and distribution levels in pipelines, which are connected to underground storages, should be treated separately, as storage system operators should give their own specifications, if different from general requirements of biomethane injection into the grid. In most EU countries, currently there are no formal limitations for biomethane injection into the grids with subsequent placement in different types of gas storages.

5. CONCLUSION

The current state of development of the biomethane sector in the European countries, including the EU Member States, and corresponding legislative frameworks are rather various. Many countries treat biomethane as a viable alternative for raw biogas plants, as it can decarbonise the natural gas grids and trigger energy transition at the natural gas infrastructure level. For most countries, production and consumption of biomethane are well balanced, but cross-border trade – rather limited [23].

As for Latvia, injection of biomethane into the natural gas grids can bring a valid option for decarbonisation of the natural gas supply chain and provide local, renewable resources with wider market accessibility [2]. Among biogas plants currently in operation in Latvia, five are located within 1 km radius around possible gas grid connection points, nine – within 5 km radius and three – within 10 km radius. Additional seven biogas plants are located between 10 and 15 km distance around the natural gas grids. Biomethane injection legally can be performed both in the natural gas transportation and distribution networks [18].

The most promising connections can be built with the biogas plants located within 10 km radius; thus, costs of the pipeline connections tend to grow significantly in comparison with biomethane injection facility costs, when biogas plants are located further than 10 km around the natural gas grid. At the same time, centralised biomethane injection can be a viable solution for regionally clustered biogas plants, where owners are not willing to subsidise separate biomethane upgrading and injection projects.

Benefits from biomethane injection into the natural gas grid in Latvia include:

- liquidation of biogas "locality": use of raw biogas in Latvia relates exclusively to electricity generation on-site, where leftover heat energy is rarely utilised at all. If biogas is upgraded to the level of biomethane, it can be used anywhere: for instance, in efficient modern domestic gas boilers or remote modern micro-CHPs, allowing one to improve overall efficiency of biomethane up to 90 %;
- support of the "green gas" delivery to every household and business customer: effective and widespread delivery of renewable fuel and heat, as biomethane injection into the natural gas grid enables renewable resources to reach over 444 400 homes in Latvia, where natural gas is physically available. The same applies to all scale business customers;

- more active market participation: injection of biomethane into the natural gas grid gives a producer direct access to a much larger spectrum of potential clients than if biomethane was to be sold and used only locally. From the perspective of the biogas producer, injecting biomethane into the natural gas grid can, therefore, give access to a higher price than available locally. Depending on commercial factors, including the associated costs, this may mean a higher net price.
- returning biogas from "electricity domain" to "gas domain": a vast majority of the local biogas projects were created and are actively used as a source of subsidised electricity production, which means that, unlike many EU countries, in Latvia the biogas sector focuses only on electricity, without much interest to turn to RGs. The fiscal incentives or other support schemes should be developed in order to trigger the biomethane production with its subsequent injection into the natural gas grid. This is one of the most viable ways to ensure the gas synergy for sustainable future of the existing natural gas infrastructure in Latvia.

ACKNOWLEDGEMENTS

The research has been supported by the National Research Programme, project "Trends, Challenges and Solutions of Latvian Gas Infrastructure Development" (LAGAS) (No. VPP-EM-INFRA-2018/1-0003).

REFERENCES

1. Wellinger, A., Murphy, J., & Baxter, D. (2013) *The Biogas Handbook: Science, Production and Applications*. Elsevier.
2. Savickis, J., Zeltins, N., & Jansons, L. Synergy between the Natural Gas and RES in Enhancement of Security of Energy Supply in the Baltic Countries (Problem Statement). *Latvian Journal of Physics and Technical Sciences*, *56* (6). DOI: https://doi.org/10.2478/lpts-2019-0032
3. International Energy Agency. (2019). The Role of Gas in Today's Energy Transitions. World Energy Outlook Special Report.
4. Herring, H. (2012). *Living in a Low-Carbon Society in 2050*. Springer.
5. Lombardi, P., & Gruenig, M. (ed.). (2016). *Low-carbon Energy Security from a European Perspective*. Academic Press.
6. International Energy Agency. (2019). World Energy Investment 2019. [Online]. [Accessed: 12 June 2020] https://www.connaissancedesenergies.org/sites/default/files/pdf-actualites/WEI2019.pdf
7. Vivoda, V. (2016) *Energy Security in Japan: Challenges after Fukushima*. Routledge.
8. Outlook for Biogas and Prospects for Organic Growth. World Energy Outlook Special Report Biomethane. (2020). [Online]. [Accessed: 12 July 2020] https://www.euneighbours.eu/sites/default/files/publications/ 202003/Outlook_for_biogas_and_biomethane.pdf
9. European Biogas Association. (n.d.). *EBA's Biomethane Fact Sheet*. [Online]. [Accessed: 20 March 2020] https://www.europeanbiogas.eu/wp-content/uploads/files/2013/10/eba_biomethane_factsheet.pdf
10. Koonaphapdeelert, S., Aggarangsi, P., & Moran, J. (2020). *Biomethane: Production and Applications*. Springer.

11. Raboni, M., & Urbini, G. (2014). Production and Use of Biogas in Europe: A Survey of Current Status and Perspectives. *Rev. Ambient. Água*, *9* (2). Apr./June 2014. https://doi.org/10.4136/ambi-agua.1324.
12. Etudes de l'Ifri. (2019). *Biogas and Biomethane in Europe. Lessons from Denmark, Germany and Italy*. [Online]. [Accessed: 20 May 2020] https://www.ifri.org/sites/default/files/atoms/files/mathieu_eyl-mazzega_biomethane_2019.pdf
13. Directive 2009/73/EC of the European Parliament and of the Council of 13 July 2009 concerning common rules for the internal market in natural gas and repealing Directive 2003/55/EC. [Online]. [Accessed: 20 June 2020] https://eur-lex.europa.eu/legal-content/EN/ALL/?uri=CELEX%3A32009L0073
14. Directive 2009/28/EC of the European Parliament and of the Council of 23 April 2009 on the promotion of the use of energy from renewable sources and amending and subsequently repealing Directives 2001/77/EC and 2003/30/EC. [Online]. [Accessed: 16 June 2020] https://eur-lex.europa.eu/legal-content/EN/ALL/?uri=CELEX%3A32009L0028
15. EN 16723-1:2016. Natural gas and biomethane for use in transport and biomethane for injection in the natural gas network—Part 1: Specifications for biomethane for injection in the natural gas network. [Online]. Accessed: 10 July 2020] https://infostore.saiglobal.com/en-gb/Standards/EN-16723-1-2016-342125_SAIG_CEN_CEN_783563/
16. EN 16723-2:2017. Natural gas and biomethane for use in transport and biomethane for injection in the natural gas network–Part 2: Automotive fuel specifications.
17. Report on the practical experiences with the application of European Biomethane Standards. (2017). [Online]. [Accessed: 5 July2020]http://www.ergar.org/wp-content/uploads/2018/07/BIOSURF-D3.7.pdf
18. Ministru kabineta noteikumi Nr. 650. (prot. Nr. 50 5. §) "Prasības biometāna un gāzveida stāvoklī pārvērstas sašķidrinātās dabasgāzes ievadīšanai un transportēšanai dabasgāzes pārvades un sadales sistēmā". [Online]. [Accessed: 26 June 2020] https://likumi.lv/ta/id/285189-prasibas-biometana-un-gazveida-stavokli-parverstas-saskidrinatas-dabasgazes-ievadisanai-un-transportesanai-dabasgazes-parvades-...
19. Status Review of Renewable Support Schemes in Europe for 2016 and 2017. [Online]. [Accessed: 2 July 2020] https://www.ceer.eu/documents/104400/-/-/80ff3127-8328-52c3-4d01-0acbdb2d3bed
20. Bioenergy Europe Statistical Report. Energy Brief: Biogas (2019). [Online]. [Accessed: 8 June 2020] https://bioenergyeurope.org/article/103-statistical-report-2019-biogas.html
21. Bioenergy Europe. (2019). *Statistical Report: Report Biogas.* [Online]. [Accessed: 12 May 2020] https://bioenergyeurope.org/article.html/103
22. Centre on Regulation in Europe. (2019). *Future Markets for Renewable Gases and Hydrogen: What Would Be the Optimal Regulatory Provisions?* [Online]. [Accessed: 8 June 2020] https://www.cerre.eu/sites/cerre/files/cerre_futuremarketsforrenewablegasesandhydrogen.pdf
23. Renewable Gas Trade Centre in Europe. (2020). *Mapping the state of play of renewable gases in Europe.* [Online]. [Accessed: 10 July 2020] https://www.regatrace.eu/wp-content/uploads/2020/02/REGATRACE-D6.1.pdf
24. European Biogas Association. (2020). *Biomethane Map*. [Online]. [Accessed: 6 July 2020] https://www.europeanbiogas.eu/wp-content/uploads/2020/06/GIE_EBA_BIO_2020_A0_FULL_FINAL.pdf
25. Biomethane Injection Surges in France. (2018). [Online]. [Accessed: 14 June 2020] https://www.bioenergy-news.com/news/biomethane-injection-surges-in-france/
26. Panorama du gaz renouvelable 2017. [Online]. [Accessed: 9 July 2020] http://www.grtgaz.com/en/press/press-releases/news-details/article/panorama-du-gaz-renouvelable-2017.html
27. Biomethane. A Renewable Gas that is a Source of Energy. [Online]. [Accessed: 1 July 2020] http://www.grtgaz.com/en/

solutions-for-the-future/energy-solutions-with-a-future/biomethane.html

28. The Role of Biomethane towards Decarbonizing the Heat and Transport Sectors. (2019). [Online]. [Accessed: 19 June 2020] https://actionrenewables.co.uk/news-events/post.php?s=the-role-of-biomethane-towards-decarbonising-the-heat-and-transport-sectors
29. Van Forees, F. (2012). Perspectives for Biogas in Europe. [Online]. [Accessed: 29 June 2020] https://www.oxfordenergy.org/wpcms/wp-content/uploads/2012/12/NG-70.pdf
30. Hengeveld, E. J., Bekkering, J., van Gemert, W. J. T., & Broekhuis, Antonius A. (2014). When does Decentralized Production of Biogas and Centralized Upgrading and Injection into the Natural Gas Grid Make Sense? *Biomass and Bioenergy, 67*, 363–371. DOI: 10.1016/j.biombioe.2014.05.017
31. Havrysh, V., Nitsenko, V., & Štreimikienė, D. (2018). Assessment of Optimal Location for a Centralized Biogas Upgrading Facility. *Energy & Environment.* DOI:10.1177/0958305X18793110
32. Balaman, S. Y. (2019). *Decision-Making for Biomass-Based Production Chains: The Basic Concepts and Methodologies*. Academic Press.
33. ENTSOG. (2011). *Technical Paper on the Injection of Biogas into the Natural Gas Networks*. [Accessed: 16 June 2020] https://www.entsog.eu/sites/default/files/files-old-website/publications/INT%20Network%20Code/2011/INT010-10_Rev4_Paper%20on%20the%20positioning%20of%20European%20transporters%20on%20the%20injection%20of%20biogas%20into%20the%20natural%20gas%20networks.pdf
34. Department of Energy and Climate Change. (2009). *Biomethane into the Gas Network: A Guide for Producers.* [Online]. [Accessed: 20 May 2020] http://www.organics-recycling.org.uk/uploads/category1060/Biomethane%20into%20the%20Gas%20Grid%20a%20Guide%20for%20producers.pdf
35. Zillman, D., Roggenkamp, M., Paddock, L., & Godden, L. (ed.). (2018). *Innovation in Energy Law and Technology: Dynamic Solutions for Energy Transition*. Oxford.
36. Hallac, M. (2013). Gas Demand: The Role of Gas-fired Power Plants. In Glachant, J.-M., Hallac, M., & Vazquez, M. (eds.), *Building Competitive Gas Markets in the EU*.
37. Commission for Energy Regulation. (2013). *Biogas injection into the Natural Gas Grid. Consultation Paper*. [Online]. [Accessed: 5 July 2020] https://www.cru.ie/wp-content/uploads/2013/07/cer13209-biogas-injection-consultation-paper.pdf
38. Storage and Transportation of Biogas and Biomethane. [Online]. [Accessed: 10 July 2020] http://www.suscon.org/pdfs/news/biomethane_report/Chapter_4.pdf
39. Zemite, L., Kutjuns, A., Bode, I., Kunickis, M., Zeltins, N. Consistency Analysis and Data Consultation of Gas System of Gas-Electricity Network of Latvia (Open Access), (2018) *Latvian Journal of Physics and Technical Sciences, 55* (1), pp. 22-34. Cited 6 times. http://www.degruyter.com/view/j/lpts.2012.49.issue-5/issue-files/lpts.2012.49.issue-5.xml, doi: 10.2478/lpts-2018-0003
40. Zemite, L., Bode, I., Zeltins, N., Kutjuns, A., Zbanovs, A. Analysis of the Power System Damage Hazard from the Point of View of the Gas Supply System (2018) *Proceedings - 2018 IEEE International Conference on Environment and Electrical Engineering and 2018 IEEE Industrial and Commercial Power Systems Europe, EEEIC/I and CPS Europe 2018*, art. no. 8494380. Cited 3 times.http://ieeexplore.ieee.org/xpl/mostRecentIssue.jsp?punumber=8476917, ISBN: 978-153865185-8, doi: 10.1109/EEEIC.2018.8494380
41. Zemite, L., Kutjuns, A., Bode, I., Kunickis, M., Zeltins, N. Risk Treatment and System Recovery Analysis of Gas System of Gas and Electricity Network of Latvia (Open Access) (2018) *Latvian Journal of Physics and Technical Sciences, 55* (5), pp. 3-14. Cited 2 times. http://www.degruyter.com/view/j/lpts.2012.49.issue-5/issue-files/lpts.2012.49.issue-5.xml, doi: 10.2478/lpts-2018-0031

sciendo

LATVIAN JOURNAL OF PHYSICS
AND TECHNICAL SCIENCES
2020, N 4

DOI: 10.2478/lpts-2020-0021

GEO ELECTRIC STUDY IN HYDROGEOLOGY ACCORDING TO THE AXIS HASSI NAGA – HASSI KHEBI OF TINDOUF (SOUTHWESTERN ALGERIA)

I. Zeroual[1,2]*, K. Hami[1], A. Talhi[1], A. Touhami[1]

[1]Department of Earth Science and the Universe,
University Centre Ali KAFI, Tindouf, 37000, ALGERIA
[2]Laboratoire Géoressources et Risques Naturels (GEOREN),
Université d'Oran2,
BP: 1510, Oran, 31000, ALGERIA
*e-mail: zeroual_ib@yahoo.fr

The hydrogeological environment of the Saharan North East region of Tindouf is of utmost interest, particularly in agriculture. In fact, exploitation and exploration processes must be analysed to ensure sufficient water production. This study demonstrates the value of spatial processing and exploitation of geoelectric and geological data in the study area and facilitates interpretation. The results of the electrical survey and the spatial analysis of the data allowed us to design a complete model that met the needs of hydrogeology. The applied methodology consists in breaking down our subject into three (3) classes of entities: geomatics, geophysics and hydrogeology. Synthetic mapping based on continuity is the result of studying two sites (Hassi Naga and Hassi Khebi) for geological analysis. Knowing that the electrical resistivity is between 0 and 3000 Ohm-meter, we were able to construct thematic maps showing the spatial distribution of the facies and the probable positions of the boreholes. The study provided with a geo-spatial model highlighting the impact of measurements in hydrogeology of the area considered that was called SIHE (Information System for Environmental Hydrogeology).

Keywords: *cartography, electrical resistivity, spatial processing, Tindouf.*

1. INTRODUCTION

The use of the electrical method for the recognition of the subsoil is of great importance due to great variability of the resistivity of the components of the subsoil and its ease of implementation. The chosen arrangement is of the pole-pole type: a

current electrode and a potential electrode are rejected to infinity. This configuration makes it possible to simplify the calculation of the apparent resistivity and to have a depth of recognition approximately equal to the distance separating the two remaining electrodes. In this study, the analysis of the electrical resistivity for groundwater resource recognition is applied to the Hassi Naga and Hassi Khebi area, located in the north-eastern part of the Tindouf basin (SW Algerian). Taking into account all the existing studies and the confrontation with the results of geophysics, we used the inverse process analysis. By measuring the resistivity of the layers, from which the lithology and the structure of the region are determined, we defined the aquifer levels, geometry and thickness [1].

In the field of cartography, cognitive mapping and spatial processing tools are paramount for studying the surface of the earth. The data are indispensable for any surveillance, photographic analysis and morphological modelling, whatever the scale. The new solutions are attractive, fast, and usable in any type of morphological configuration and provide easily integrable data in Geographical Information Systems (GIS), at resolutions ranging from hundreds of meters to centimetres [2], [3]. In several fields, the interest in spatial processing plays a central and fundamental role in the dissemination and communication of metadata as well as the visualization and implementation of the management processes using thematic maps. Water and energy are intimately associated with the energy process [4]. The amplifications by the international energy trade and studies show that international incarnated water flows averaged 6298 Mm3 yr-1 from 1992 to 2010, which represented 10 % of the water used for energy production, including oil, coal, gas and electricity production [4], [5].

On the other hand, models of the spatial distribution of wind speed and wind energy that were used to analyse the density were developed using the spatial interpolation method based on the genealogical measurement results and presented in cartographic form with a resolution of 1x1 km [4], [6].

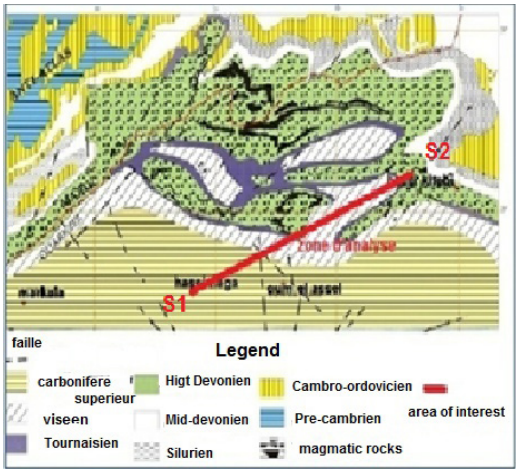

Fig. 1. Geological map of the North East zone of Tindouf [7], study area Hassi Naga (S1) – Hassi Khebi (S2).

Spatial tools for geology and the hydrogeological environment are integrated with geophysical measurements in order to establish the exploration cognition of aquifers. In the present research, we insist on the contribution of topography, photogrammetry and GIS to develop thematic maps and synthesis maps. The geology of the study area is defined on the following map (Fig. 1). The syncline of Tindouf, better known in literature as Tindouf basin, whose surface is about 200000 km², is the residue of a basin connecting the West – West Craton to the south, with the Mediterranean Sillon to the North. The Tindouf syncline, whose axis is west-east, is asymmetrical: in fact, the southern flank is represented by a monoclinal dipping gently towards the north (1°–5°), while the north flank is narrower and is affected by many secondary folds.

On the southern flank of the syncline, there are Paleozoic deposits ranging from Cambrian to Upper Carboniferous overlain in an unconformable way by the Hamadian Tertiary – Quaternary continental deposits. The electrical profiles, carried out along toposéquences and lithosequences previously identified, make it possible to establish a parallelism between the anomalies of resistivity and the different units of grounds; this on a very large scale.

On the Precambrian basement series, there is the formation of the Cambro-Ordovician, consisting of conglomeratic sandstones at the base, compact quartz sandstones and coarse-grained sandstones with a thickness of 40 to 70 m. The Paleozoic formations are covered by Tertiary and Quaternary deposits of Hamada, consisting of whitish to greenish-grey argillaceous sandstones with conglomerates at the base, and a limestone dolomitic limestone slab with flint beds at the top. Its thickness can reach 80 m. The study area concerns the north east of Tindouf with a surface coverage of 20 000 km².

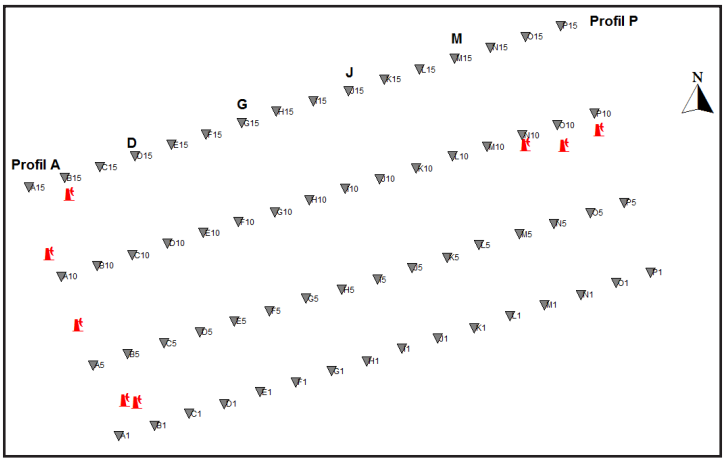

Fig. 2. Hassi Naga site profiles.

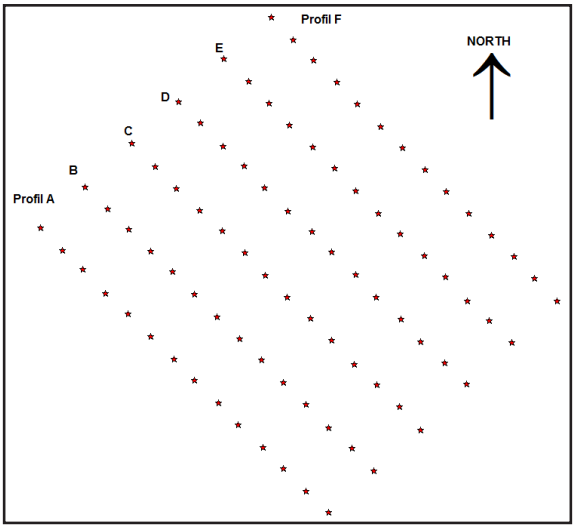

Fig. 3. Hassi Khebi site profiles.

2. METHODOLOGICAL APPROACH

The inverse electrical problem is complex due to its non-linearity [8]: the measured apparent resistivities do not depend linearly on the real resistivities of the computational cells. It is then necessary to perform a parametric study to determine the factors that have a significant weight in the measurement. The least-squares inversion scheme is a classic but convenient concept for reversing 3-D resistivities. With a sufficient amount of data, the reconstruction of the distribution of true resistivity is possible. In order to overcome the problems of resolution and inversion of linear and non-linear systems, the mapping approach of spatial distributions is used.

2.1. Observation Model

The electrical method consists in injecting a continuous electric current into the ground using two stainless steel electrodes and measuring the potential deference created between the terminals of two other copper electrodes. The set constitutes a quadrupole as it is in Fig. 3, an ammeter is used to measure the electrical current and a voltmeter to measure the potential difference (Fig. 3):

The idea is to move the four AMNB electrodes together and, thus, make profiles and resistivity cards. There is a variety of devices but the quadrupole remains the most widespread. The power source is usually 90v batteries, more rarely a gasoline generator with a rectifier or a car battery, the new devices work with ten (10) batteries in series. This method makes it possible to measure the potential difference ΔV and the electric current I injected and recovered in the subsoil. This leaves for us the calculation of the resistivity in the considered medium with two poles A and B, the combined action of A and B will give:

Potential at a point M and N:

$$V_M = \rho I/2\pi\,(1/AM - 1/BM)\ ;\ V_N = \rho I/2\pi\,(1/AN - 1/BN). \tag{1}$$

Potential difference between M and N:

$$\Delta V = V_M - V_N = \rho I/2\pi\,(1/AM - 1/BM - 1/AN + 1/BN). \tag{2}$$

From where:

$$\rho = (k \cdot dV)/I, \tag{3}$$

where

$$k = \pi \cdot (AM \cdot AN)/MN\,. \tag{4}$$

Resistivity in ohm-meter is calculated by:

$$\rho_a = (k \cdot \Delta V)/I_{AB}, \tag{5}$$

where

k – the geometrical factor that depends only on the relation of the electrodes and is expressed by (4);

ΔV – the potential difference across MN electrodes;

I_{AB} – intensity of the electric current circulating in the circuit AB.

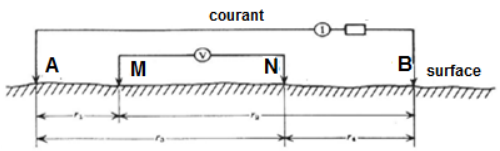

Fig. 3. Scheme of Schlumberger chosen for prospecting sites.

All conventional methods of interpreting electrical soundings are based on the two basic assumptions about vertical variation and horizontal variation. It is essential that both of these conditions are fulfilled for an electrical survey to yield to correct interpretation. Parametric soundings are essential; they are placed near a mechanical drilling or on outcrops. They make it possible to get an idea of the resistivity in a region and they also make it possible to fix the line lengths effective for the execution of the second phase.

Thanks to the resistivity maps established during the second phase that the geophysicist can place the electrical soundings of the third phase in an optimal way, that is to say, in the zones of interest, the resistivity varies less possible horizontally [9], [10].

Tables 1 and 2 present a scale for calibrating geo-electrical measurements in the areas in question.

Table 1. Resistivity Scale Adopted at Hassi Naga

Formation	**Age**		**Résistivité Ohm-m**
Sandstone limestone	Neogene Hamada		211–1070
Sandstone – clay sand			53–137
Sandy clay			30–50
Gypsum intercalation clays			9–28
Clayey sandstone	Paleozoic	Upper Carboniferous	77–102
Silty clay with sandstone			30–71
Clay with intercalation of gypsum		Higher Viseen	8–28
Limestone and anhydrite			230–3622

Table 2. Summary Table of Lithology at Hassi Khebi

Lithology	Age	Resistivity adopted (ohm-m)	Observations
More or less silicified limestone Neogene	Tertiary Continental or TC)	150 –500	Aquifer, low flow
Siltstones, quartzites and argillites	Carboniferous	200–400	Aquifer very unlikely
Argillites, limestones containing pyrite (FeS2), siltstones and quartzose sandstones, dolerites	Upper Devonian	20–40, 50–100 et >120	Probable aquifer if the roof of the formation is close to the ground
Argillites, past siltstone limestones, argilites and massive pyritized marls	Middle Devonian	>500	No aquifer
Clay, fine quartzose sandstone, compact, clay limestone	Lower Devonian	30-150	Aquifer to be collected by shallow drilling (150-300 m).
Argilites and marls massive pyritized Facies dominated clay. Schists and sandstones of "Bani"	Silurian: Ordovician Gothlandian	50 à 90	Aquifer likely when these formations are close to the ground
Quartzitic and Quartzite	Cambro – Ordovician	> 1000	No aquifer

These tables will allow us to set up the spatial analysis function and to create a synthetic cartography on the spatial distribution of electrical resistivity.

2.2. Modelling and Spatial Analysis in Geology

A cognitive map provides a simple visual communication medium for humans analysing a complex system that can be processed through brainstorming phases. These maps have been used in several fields such as biology, ecology and the environment in general [2], [3], [5]. In the present research, cognitive mapping is based on spatially referenced information systems that highlight electrical resistivity. The following steps [11], [12] illustrate an approach based on computer science:

- The brain-ware phase: a conceptual reflection on the model;
- The software phase: a logical transformation of the model;
- The hardware phase: a physical implementation of the model.

Supporting and integrating data from geophysical exploration and groundwater behaviour, and integrating environmental data with GIS require the development of a conceptual data model (CDM). This is the result of the analysis of the existing data and the surveys with the future developments of the GIS [13]. It represents in a synoptic way all the data and the links that exist among them. The MCD questions take up the problems of treatment.

It involves bringing into play many elements for the generation of simulation models; this is possible thanks to the following

concepts:

- The topographic surface;
- The attributes and the physicochemical properties of the places;
- The evolution time in the form of intervals, iterations, or recursive constructions;
- The inference engine that is generated by deterministic or stochastic transformation rules.

It is therefore easy to understand the considerable contribution the geological spatial analysis makes to thematic and simulation mapping by enabling multiple structures at once and facilitating quick visualization of results. The groundwater can be considered a localized area delimited topographically where space operations are carried out. Thus, the classical repertoire of three-dimensional coordinates becomes a table supplemented by indicators of this hydrogeological environment.

We present a general approach for the assimilation of different aspects of management and exploitation of tablecloths. The main objectives of this specification are as follows:

- Integration of different natural and artificial contexts into the same database;
- Homogenization of the local geographic database;
- Production of a data model (maps) without redundancy;
- Standardization of spatial analysis and decision-making;
- Assistance with maintenance and prevention;
- Prediction capability (periodic synthesis of dynamic parameters).

The process begins with the assimilation of the following territorial contexts:

- The geology of the region;
- The topography;
- The agglomeration.

Each context is represented by a digitized layer of the map attached to a class of the database. Then we integrate the hydric aspects where each unit (or hydrogeological subunit) will be characterised according to several contexts, namely:

- Hydrogeology;
- Hydrography and hydrology;
- Hydrodynamics.

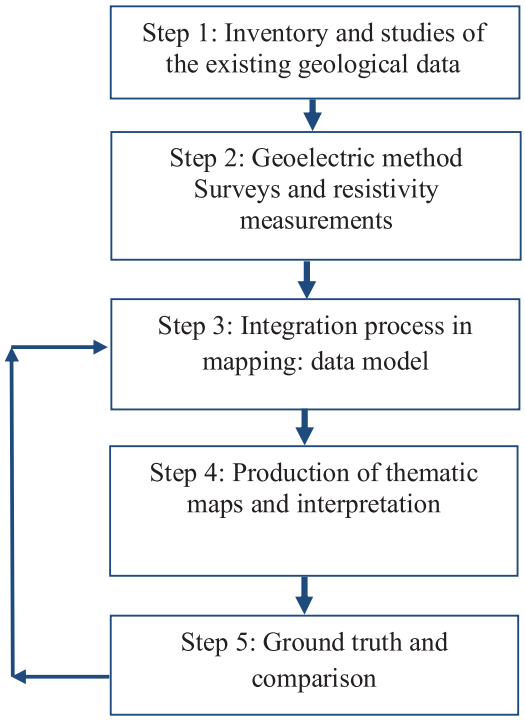

Fig. 4. Summary of different stages of the study.

The analysis and synthesis of the data involve periodic sampling measurements on aquifers, as well as hydrographic and hydrodynamic elements according to the following groups of parameters:

- hydrochemistry, physicochemical, toxic substances, undesirable substances, microbiological parameters and the total rate of pesticides;
- history of flows / consumption of the hydrodynamic elements;
- parameters for calculating vulnerability to pollution according to one or more methods.

A quality assurance program based on the flowchart in Fig. 5 provides alternatives for inventory and analysis. This brings us back to developing a data model that will be appended to different layers of the hydrogeological database (Fig. 5). In this model, the map class is the subject of this article.

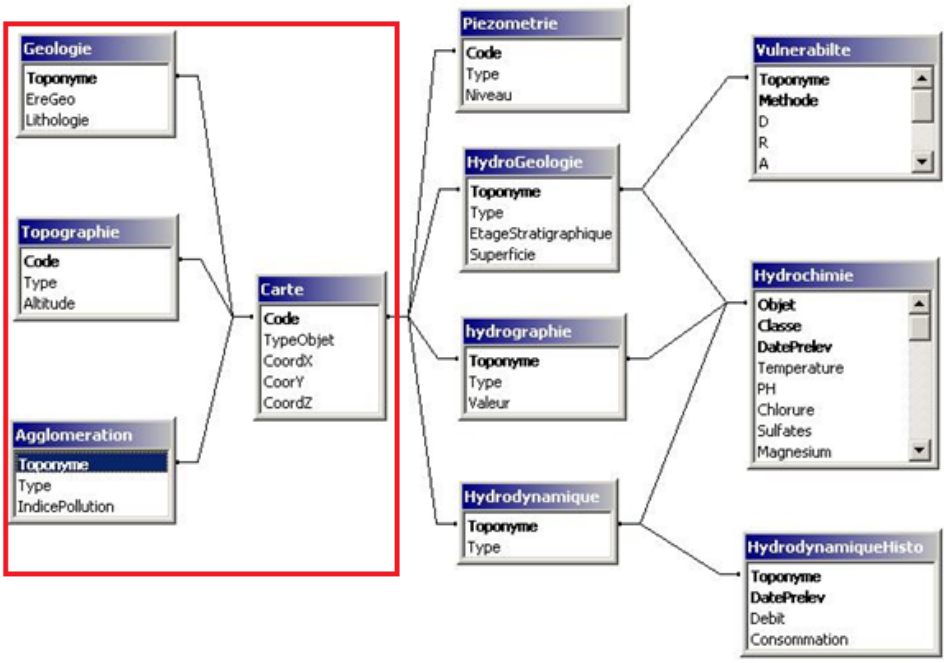

Fig. 5. Logic model (SIHE) of data and focus of study in red.

3. TREATMENTS FOR TWO SITES: HASSI KHEBI AND HASSI NAGA

The treatments are based on an information system for environmental hydrogeology (SIHE – Fig. 5), which poses a double problem related to the inventory of different information and its structuring in the form of diagrams. According to Ruas [14], this inventory step requires taking into account a transfer model, adapting the diagram of the SIHE and looking for equivalence between the technical options and the card elements. Despite knowing that engineering in hydrogeology is expensive, it remains crucial for the success of hydro-environmental projects. In this perspective, the treatments present orthogonal projections of interpretive geoelectric sections and maps of apparent resistivities. All profiles are oriented South-South-East / North-North-West with similarities in their monotonous look and in the thicknesses of the geological formations. Recorded resistivity is almost similar. The measurement campaigns relate to two sites separated by a distance of 200 kilometres: Hassi Naga (S1) and Hassi Khebi (S2). There are 16 and 6 profiles, respectively, for both sites S1 and S2.

The dome-shaped structure of Hassi Khebi deserves to be explored in more detail. Secondary complications may exist in this major structure. For example, near the curbs, the tanks can be emptied. Moreover, the village of Hassi Khebi, on its cur-

rent location (rocky plateau, total absence of vegetation), can logically develop a serious and viable activity. It would be a judicious parallel thinking about a partial relocation of the population in the plain of Oued Khebi 20 km away from the village.

Table 3. Summary of Hassi Naga Profiles

N°. Profile	**Layer 1 C1**	**Layer 2 C2**	**Layer 3 C3**	**Comments**
A	118–571 Ohm-m 25–77 Ohm-m	8–62 Ohm-m	195–1350 Ohm-m	C1: Neogenous C2: Upper carboniferous C3: Lower carboniferous.
B	31–116 Ohm-m	18–52 Ohm-m / 70–102 Ohm-m	190 à 1342 Ohm-m.	C1: Neogenous C2: Upper carboniferous C3: Carbonifère inférieur.
C-D	≥200 Ohm-m	10–57 Ohm-m	234 –1453 Ohm-m	C1: Neogenous C2: Upper carboniferous C3: Lower carboniferous.
E-F	20–200 Ohm-m	15–50/65–73 Ohm-m.	205 et 1216 Ohm-m	C1: Neogenous C2: Upper carboniferous C3: Lower carboniferous.
G-H	21–90 Ohm-m	11 à 41/ 52 à 57 Ohm-m	≥ 229 Ohm-m	C1: Neogenous C2: Upper carboniferous C3: Lower carboniferous.
I-J	≥ 129 Ohm-m	< 100 Ohm-m	< 50 Ohm-m	C1: Neogenous C2: Upper carboniferous C3: Lower carboniferous.
K-L	77–115 Ohm-m	< 50 Ohm-m	≥ 350 Ohm-m	C1: Neogenous C2: Upper carboniferous C3: Lower carboniferous.
M-N	< 43/58 à 265 Ohm-m	< 50 Ohm-m/≥ 400 Ohm-m	≥ 350 Ohm-m	C1: Neogenous C2: Upper carboniferous C3: Lower carboniferous.
O-P	< 30 / ≥ 45 Ohm-m	10–46 Ohm-m	≥ 200 Ohm-m	C1: Neogenous C2: Upper carboniferous C3: Lower carboniferous.

All the data collected are related to the spatial and temporal contexts. It should be noted that all samples must be structured and stored (archived). Thus, we equip our GIS with an effective tool for monitoring the evolution of the water table. This concept, called "object version", is widely used in software engineering [15]. The process of exploitation of the water table is completed (after structuring and data acquisition) and more complex tasks (integration of data, interpolation of measurements taken, homogenization, etc.) are carried out. These synthesis tasks are provided by tools developed and integrated incrementally in the GIS. The current prototype can be enriched by applying it on several real cases.

4. ANALYSIS AND RESULTS ON SITE

Scientific interpretation and visualization bring a new configuration for exploratory analytical cognition of groundwater. The generalization and aggregation of cognitive information allows for a better perception in the context of exploration. The study of the integration of GIS as a decision-making support tool in hydrogeology training and the difficulties that accompany it called for a multidisciplinary approach. It was organised around the following themes:

1. A geometric theme around scientific visualization to predict levels of abstraction;
2. A cognitive approach, which allowed studying the way of thinking of users in cartography, facing the solution of spatial problems using GIS;
3. A didactic dimension, which allowed integrating the expert approaches used in the strategies of resolution of the distribution of resistivity through the formations;
4. Based on cognitive and didactic knowledge, innovative training devices in line with the demands of the professional world.

The analysis of the data from the observations was guided theoretically, by the framework of visual-cognitive mechanisms involved in reasoning, and methodologically by the qualitative and quantitative treatments of the geophysical process protocols. This allowed us to identify components of the reasoning processes involved in the realization and perception of a digital mapping activity. The multidisciplinary approach also facilitated the match between training and profession, combining skills in GIS methods and technologies, to the needs of a specific professional sector (geological sciences). The sections and the geophysical profiles allowed us to build levels of analysis by aggregation of the resistivities of levels R1 to R8. Figure 6 shows level R1.

In this study, we approach a multiscale design using geomatic tools. The GIS approach is launched to validate the structuring model; the following maps provide an overview of the timeline of reassignment operations and the use of profiles. The functions applied take into account the location and parameterization of each variable. Relation 6 summarises the elaborated treatments.

$$G = f(x, y, z, \alpha, \beta, \theta), \tag{6}$$

where

(x, y, z) – represent the location factors (Cartesian coordinates, DTM and DSM);

(α, β, θ) – thematic values related to the application (type, nature, identification).

Univariate and multivalue processing of location and geoelectric parameters reflect repeated effects of classes. The histograms in Fig. 6 show the predominance of these classes. The analysis of the maps shows a sudden geoelectric change, which may suppose a fault or deformation at this level (figure arrows 6C and 6D).

The formulation of the geoelectric analysis is based on a reciprocal function of type:

$$z = F(x,y, \alpha, \beta, \theta). \tag{7}$$

The dissimilarities observed between the maps of apparent resistivity reveal the transition zones between homogeneous soil units and thus specify the notion of progressive limit in space.

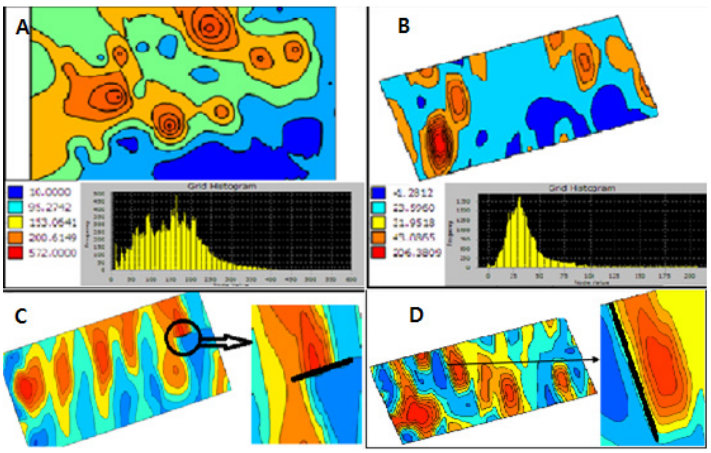

Fig. 6. Thematic maps of electrical resistivity (A and B) and geoelectric discontinuity observed in C and D (Hassi Naga*).*

The spatial representation of the thickness of the geological layers and its histogram highlight structural aspects that can be caused by deep tectonic deformations (Fig. 7A). Piezometry and its histogram in the Hassi Khebi area imply spatial compatibility with the representation of resistivity; this visualization makes it possible to generate a thematic function (thickness–resistivity and piezometry).

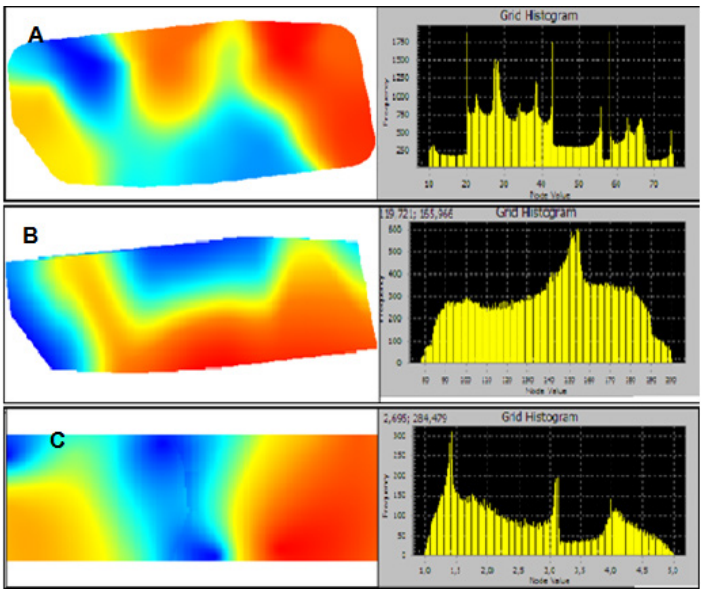

Fig. 7. Themes on thickness A, piezometry B and resistivity C (Hassi Khebi area); the histograms show the impact of the resistivity on thicknesses and piezometry.

The spatial visualization of the flows of the six (6) existing boreholes allowed us to compare the spatial distribution with the existing geological factors. A proposal for drilling is given in Table 4. The spatial representation of existing borehole flows is in line with the geological features of Fig. 8. A geological correlation of surface type is

therefore desirable for a complete geological survey (Fig. 9). The direction S1S2 in Fig. 1 defines the interpolation zone to analyse the layers relating to the resistivities of layers C1, C2 and C3.

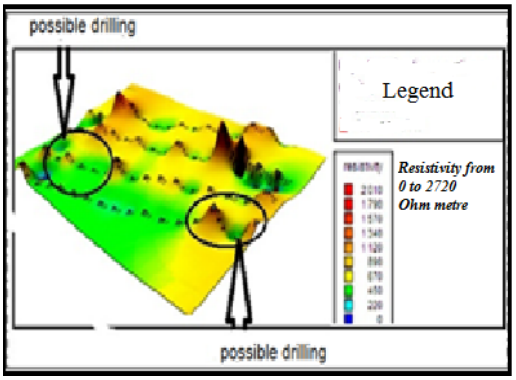

Fig. 8. Resistivity provides two possible drill sites.

A drilling proposal is being established in the Hassi Khebi area. To complete Table 4 of the proposals, it is strongly recommended a geophysical prospection by electrical soundings in the north sector of Hassi Khebi on a strip parallel to the reliefs of Adhim Filou. These profiles would be perpendicular to this line. The depth of investigation should be of the order of 400 to 500 m (AB = 3000 m) [16].

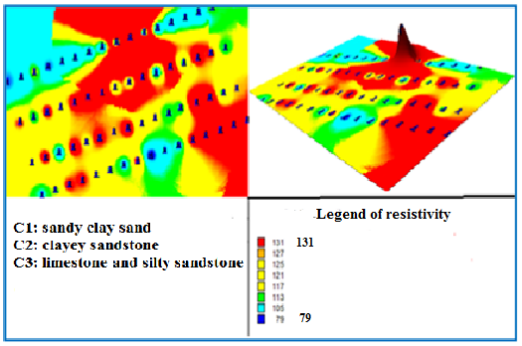

Fig. 9. Aggregated function to obtain the elements of layers C1, C2 and C3.

Table 4. A Drilling Proposal in the Hassi Khebi Area

Cup	Depth(meter)	Training (s) to capture	X	Y
A	100	T C and carboniferous	252.850	3241.459
A	150	T C, carboniferous and upper Devonian	262.625	3231.375
B	150	T C and upper Devonian	264.082	3235.596
B	150	T C and upper Devonian	265.477	3234.121
C	200	T C and lower Devonian	262.887	3242.618
C	200	T C and upper Devonian	269.869	3235.388
D	150	T C and Lower Devonian	268.510	3242.588
E	200	T C and lower Devonian	271.436	3245.350
E	200	T C and lower Devonian	272.785	3243.925
F	150	T C and upper Devonian	264.561	3258.178
F	300	T C, Middle Devonian, and lower Devonian	274.336	3248.095
F	300	T C and lower Devonian	278.432	3243.865

5. CONCLUSION

The execution of the exploration work is based on the methodology of the three-dimensional geological and geophysical model of various hydrogeological indices. These are recognised in exploited aquifers such as Hassi Naga and Hassi Khebi; they will discover new hidden mineralized boreholes and, thus, ensure the economic development of the north eastern region of Tindouf. The proposed model can be used for bettering the field management, prioritizing actions for monitoring groundwater quality and remediation of polluted sites. The integration of other geophysical methods, taking into account all the geological parameters, and the geomatic data available in the region in hydrogeological material, can help us develop and modernise the proposed analysis model towards good exploitation and integrated management of water resources. The SIHE model "Information System in Environmental Hydrogeology" can be extended for the support of structural elements at the level of geological and hydrogeological units. In a multidisciplinary vision, the preservation and protection of aquifers will be indexed to the land planning model. By knowing the genesis of quaternary deposits of the study sites, we can infer the type of deposit and their sedimentary structures that are specific to them from the geometry and spatial relationships of the reflectors visible on the geoelectric profiles [17].

REFERENCES

1. Teibe I., Bendere R., & Arina, D. (2013). Latvian Waste Management Modelling in View of Environmental Impact Reduction. *Latvian Journal of Physics and Technical Science, 50* (6), 36–47. DOI: 10.2478/lpts2013-0039
2. Axelrod, R. M. (1976). *Structure of decision: The cognitive maps of political elites*. N.J.: Princeton.
3. Celik, F. D., Ozesmi, U., & Akdogan, A. (2005). *Participatory ecosystem management planning at Tuzla lake (Turkey) using fuzzy cognitive mapping*. Eprintar Xiv:q-bio/0510015, 2005.
4. Zhang, J. C., Zhong, R., Zhao, P., Zhang, H. W., Wang, Y., & Mao, G. Z. (2016). International Energy Trade Impacts on Water Resource Crises: An Embodied Water Flows Perspective. *Environ. Res. Lett. 11*, 074023.
5. Chauvin, L., Genest, D., Le Dorze, A., & Loiseau, S. (2013). User centered cognitive maps. In Guillet, F., Pinaud, B., Venturini, G., and Zighed, D. A. (eds.), *Advances in Knowledge Discovery and Management*, volume 471 of Studies in Computational Intelligence (pp. 203–220). Springer.
6. Aniskevich, S., Bezrukovs, V., Zandovskis, U., & Bezrukovs, D. (2017). Modelling the Spatial Distribution of Wind Energy Resources in Latvia. *Latvian Journal of Physics and Technical Sciences, 54* (6), 10–20. DOI: 10.1515/Lpts-2017-0037
7. Dida, M., Bentaleb, A., & Zeroual, I. (2017). Master's Memory. Digital Cartography and the Geoelectric Study of Hassi Khebbi Zone, 20–40.

8. Panissod, C. (1997). Prospection electrique et electrostatique a faible profondeur a l'aide de systemes multipoles permettant la description directe des structures. In "3–D".
9. Chandrasekharan, H., Yada, B., Tomar, S., & Sarma, P. (1994). Studies on Salinity and Water Content of Soils. – Geoelectrical Approach. *Journal of The Indian Society of Soil Science*, *42* (3), 430–436.
10. Kalinski, R., & Kelly, W. (1994). Electrical Resistivity Measurements for Evaluating Compacted-Soilliners. *Geotech*., *120* (2), 451–457.
11. Le Dorze, A., Duval, B., Garcia, L., Genest, D., Leray, P., & Loiseau, S. (2013). *Cartes cognitives probabilistes.* Technical report, LERIA – Universited' Angers.
12. Sedki, K., & Bonneau De Beaufort, L. (2012). Cognitive maps and Bayesian networks for knowledge representation and reasoning. In *IEEE 24th ICTAI* (pp.1035–104).
13. Laurini, R., & Milleret-Raffort, F. (1993). Les bases de données en géomatique. *Edition HERMES- France*.
14. Booch, G. (1992). Conception orientée objet & applications. *Edition Wesley*.
15. Ruas, A., & Sanders, L. (2015). Regards croisés sur la modélisation des dynamiques spatiales, *Revue Internationale de Géomatique*, *25* (3), 275–300.
16. Khelifa, H., Zeroual, I., Talhi, A., & Djmila, A. (2017.). Contribution de la géomatique à l'interprétation géoélectrique du bassin de Hassi Naga (Sud-ouest Algérien). In *International Congress on Energetic and Environmental Systems (IEES-2017)*, Djerba, Tunisia.
17. Gousmania, M., Gasmi, M., Mhamdi, A., Bouri, S., & Ben Dhia, H. (2006). Prospection géoélectrique pour l'étude de l'aquifer thermal des calcaires récifaux, Hmeima-Boujabeur (centre ouest de la Tunisie). *C.R. Geosciences, 338*, 1219–1227.

sciendo

LATVIAN JOURNAL OF PHYSICS
AND TECHNICAL SCIENCES
2020, N 4

DOI: 10.2478/lpts-2020-0022

THE EFFECT OF ELECTRIC FIELD CONFIGURATION ON THE THERMO-CHEMICAL CONVERSION OF STRAW PELLETS

I. Barmina*, A. Kolmickovs, R. Valdmanis, S. Vostrikovs, M. Zake

Institute of Physics, University of Latvia,
32 Miera Str., Salaspils, LV-2169, LATVIA,
*e-mail: barmina@sal.lv

With the aim to control and improve the thermo-chemical conversion of straw pellets, the experimental investigations of the DC electric field effect on the combustion dynamics and heat energy production were made. The electric field effect on the gasification/combustion characteristics was studied using three different positions of the positively charged electrode in flame. First, the electrode was positioned coaxially downstream the flame flow. Next, the electrode was positioned coaxially upstream the flame flow and, finally, the electrode was positioned across the downstream flow. The bias voltage of the electrode varied in the range from 0.6 up to 1.8 kV, while the ion current in flame was limited to 5 mA. The results of experimental investigations show that the DC electric field intensifies the thermal decomposition of straw pellets and enhances mixing of volatiles with air causing changes in combustion dynamics and heat energy production, which depend on position and the bias voltage of the electrode. The increase in the average volume fraction of CO_2 (by 6 %) and the decrease in the mass fraction of unburned volatiles in the products (CO by 60 % and H_2 by 73 %) for the upstream field configuration of the electrode and the ion current 0.5–1.8 mA indicate more complete combustion of volatiles.

Keywords: *electric field, composition emissions, heat energy, straw pellets, thermochemical conversion.*

1. INTRODUCTION

The EC 2030 climate and energy targets for the period from 2021 to 2030 require more efficient use of renewable fuels (harvesting, agriculture or herbaceous residues) for energy production (by 32 %) to reduce greenhouse emissions (GHG) by 40 %

and to improve energy efficiency by 32 % [1]. The use of renewable fuels for energy production is related to the formation of "carbon-neutral" emissions by limiting the formation of GHG emission during their thermochemical conversion [2], while it can cause the problems, which are associated with their relatively low heating value, high nitrogen and ash contents, low melting temperatures of ash and relatively high content of heavy metals in biomass, especially in agriculture and herbaceous residues [3], [4]. Different methods and technologies have been developed to improve their combustion characteristics, such as washing, drying, sieving, leaching, granulation, thermal pre-treatment or mw pre-treatment [4]–[6]. The effective tool for an increase in the applicability of problematic renewable fuels (straw, herbaceous residues) for more efficient heat energy production with the reduced NO_x, CO emission is their co-firing with solid [7]–[9] or gaseous fossil or renewable fuels [7]. Besides, the effective control of the thermochemical conversion of biomass and the main combustion characteristics can be obtained using the electric effects on the flame, which can be related to the field-enhanced mass transfer of the flame ions and neutral species in the field direction, determining local variations of the flame temperature and composition [10], [11]. It should be noticed that the electric field-induced variations of the main flame characteristics are observed if the DC and AC electric fields are applied to different flame types (laminar, turbulent) during the combustion of gaseous fuels [10]–[13]. Limited number of experiments were performed to assess the electric field effect on the thermochemical conversion of biofuels, when the field-enhanced interrelated processes of heat and mass transfer promoted the thermal decomposition of biofuels (wood, straw pellets), the formation of combustible volatiles (CO, H_2), their mixing with air, ignition and burnout [14], [15]. Moreover, the results of industrial experiments suggest that the electric field effects on the flame can be used to control the processes developing in the industrial combustion systems [16] determining cleaner and more efficient heat energy production.

The results of complex experimental study and mathematical modelling of DC electric field effects on the thermochemical conversion of solid fuels (straw, wood, peat and their mixtures) confirm that the electric field effects on the flame can be used to improve mixing of the flame components, to control the formation of the flow dynamics, the main flame characteristics, heat energy production and composition of emissions, depending on a lot of factors, such as bias voltage of the electrodes, their configuration and location [14], [15]. With account of the influence of these factors on the thermochemical conversion of biofuels, the goal of this study is to optimise the configuration of the electrodes, their location in the flame reaction zone and potential to achieve the effective control of the gasification/combustion characteristics, produced heat energy and composition of the emission at thermochemical conversion of problematic biofuel – straw pellets with the aim to provide more efficient use of straw as fuel for energy production.

2. EXPERIMENTAL

The experimental study of the electric field effect on the thermochemical conversion of wheat straw pellets was studied using a batch-size pilot device with the heat output up to 4 kW. The experimental device included biomass gasifier (1) and

two-sections of the water-cooled combustor (2) with inner diameter 88 mm and 600 mm of total height (Fig. 1). The gasifier was charged with fixed mass (450 g) of A-quality wheat straw pellets with 9.1 % moisture content. The propane flame flow was used for an additional heat (0.81 kW) input into the device to initiate the thermal decomposition of straw pellets and the formation of combustible volatiles (CO, H_2) and was switched off after ignition of volatiles. The primary air (3) was supplied at the bottom of the gasifier at the constant rate of 30 l/min and was used to support the gasification of straw pellets. The secondary swirling air (4) was supplied above pellet layer at the constant rate of 40 l/min and was used to provide the combustion of volatiles downstream the combustor. The diagnostic sections with openings (5) were used for the local measurements of the flow velocity, flame temperature and composition of products. With the aim to provide DC electric field control of the thermochemical conversion of wheat straw pellets, nichrome wire electrodes with the diameter of 3 mm (7) were located in the flame base, where the peak values of the flame primary flame ions (CHO^+, $C_2H_3^+$, H_3O^+, etc.) were observed [14]. The experimental study of the electric field effect on the gasification/combustion of wheat straw pellets was provided for three different configurations of the electrodes. First, the electrode of length L = 94 mm was inserted through the layer of straw pellets and was positioned axially downstream the flame flow up to the flame reaction zone (Fig. 1, a). Next, the electrode of length 53 mm was inserted into the flame reaction zone at distance L = 65 mm from secondary air supply through the opening in the wall of the combustor and was positioned axially upstream of the flame flow (Fig. 1, b). Finally, the electrode of length 40 mm was inserted into the flame reaction zone at distance L = 65 mm from secondary air supply through the opening in the wall of the combustor and was positioned across the flame flow (Fig. 1, c). The electric field was applied in the space between the electrode and water-cooled walls of the device. The positive bias voltage of the electrode relative to the water-cooled walls could be varied in the range from 0.6 to 1.8 kV by limiting the ion current in the flame to 5 mA.

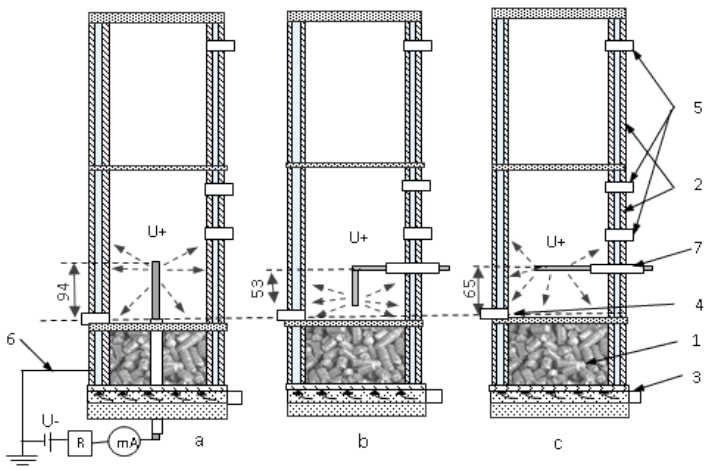

Fig. 1. The laboratory scale device for experimental study of the DC electric field effect on the thermochemical conversion of straw pellets: 1. gasifier, 2. water-cooled sections of the combustor, 3. primary air supply nozzle, 4. secondary swirling air supply nozzle, 5. diagnostic sections with orifices, 6. electric measuring circuit, 7. electrode placement: a- electrode arranged axially downstream of the flow; b- electrode arranged axially upstream of the flow; c- electrode arranged across the flow.

The detailed studies of the DC electric field effect on the thermal decomposition of straw pellets and combustion of volatiles involve the measurements of the weight loss rates of straw pellets, the local measurements of the axial and tangential flow velocity components, the kinetic and radial measurements of the flame temperature, the calorimetric measurements of the cooling water flow from the gasifier and the combustor, the local measurements of the flame composition and composition of polluting emissions. Detailed methodology of the experiments was described in [14].

3. RESULTS AND DISCUSSION

The experimental study of the DC electric field effect on the combustion dynamics and variations of the main combustion characteristics starts with the estimation of the effect of electrode arrangement on the main flame characteristics at the condition U = 0. The results of experimental measurements of the flame velocity and temperature formation field have shown that for all positions of the electrode (downstream, upstream, across) its placement in the flame flow disturbs the formation of the flame temperature and velocity profiles decreasing the average values of the axial velocity with radial expansion of the flow velocity and flame temperature profiles (Fig. 2- a, b).

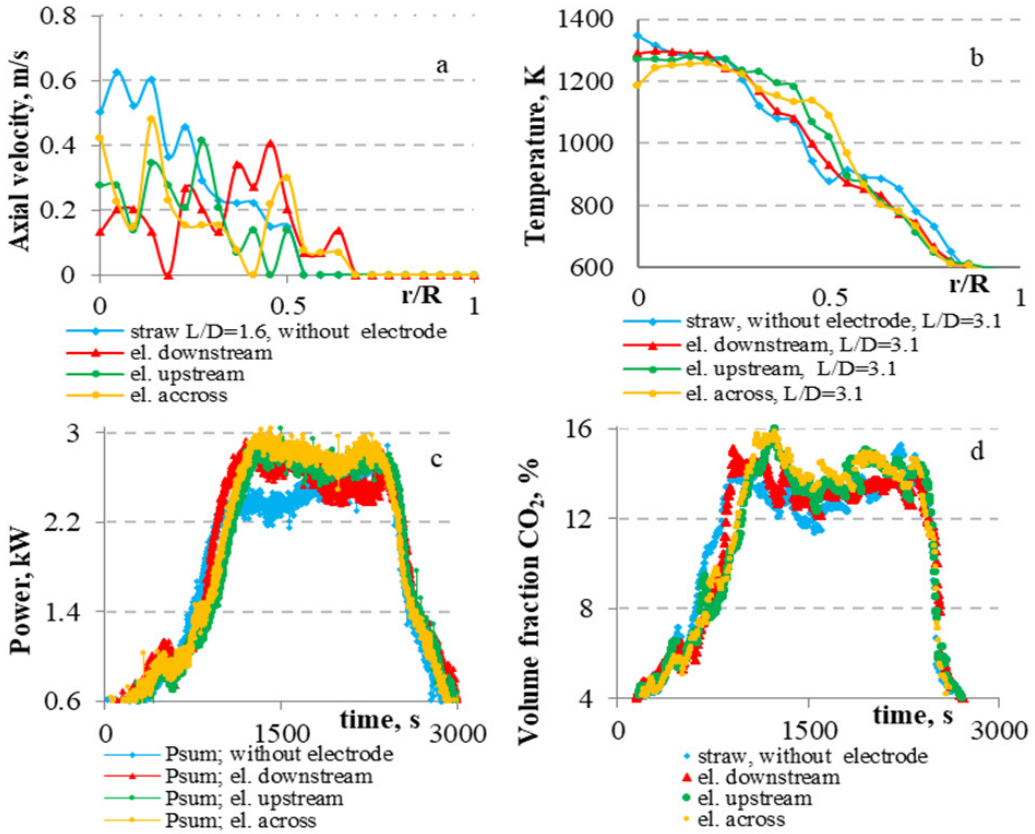

Fig. 2. The effect of the electrode arrangement on the flow axial velocity (a), flame temperature (b) profiles, the total heat output from the device (c) and the volume fraction of CO_2 in the products (d).

Moreover, the time-dependent measurements of the total heat output from the device and the volume fraction of CO_2 in the products (Fig. 2, c-d) confirm that for all electrode configurations inserting the electrode into the flame flow promotes the enhanced burnout of volatiles. Further changes in the main flame characteristics are achieved by increasing the positive bias voltage of the electrode and the current in the flame space between the electrodes, which depends on the formation of flame ions. During the burnout of hydrocarbon fuels the formation of the main flame ions (CHO^+, H_3O^+, $C_3H_3^+$) refers to the development of the chemo-ionization reactions between the flame species:

$$CH + O \rightarrow CHO^+ + e \quad (1)$$

$$CH^* + C_2H_2 \rightarrow C_3H_3^+ + e \quad (2)$$

$$C_2H + O_2^* \rightarrow CO + CHO^+ + e \quad (3)$$

$$CHO^+ + H_2O \rightarrow CO + H_3O^+ \quad (4)$$

H_3O^+ is accepted as the major positive ion [17]. The concentration of positive ions in hydrocarbon/air flames is about 10^{17}–10^{18} m^{-3}. During the thermochemical conversion of straw pellets the maximum value of ion density ($n_i \approx 1.8*10^{17}$ m^{-3}) was observed in the central part of the flame reaction zone, close to the flow axis ($r/R < 0.3$) at distance $L/D \approx 1$–1.5 from the flame base (Fig. 3, a). Therefore, to achieve the most effective field-induced control of the main flame characteristics, the electric field must be applied to this part of the flame flow. The current-voltage characteristics for three different locations of the electrode in the flame are presented in Fig. 3, b.

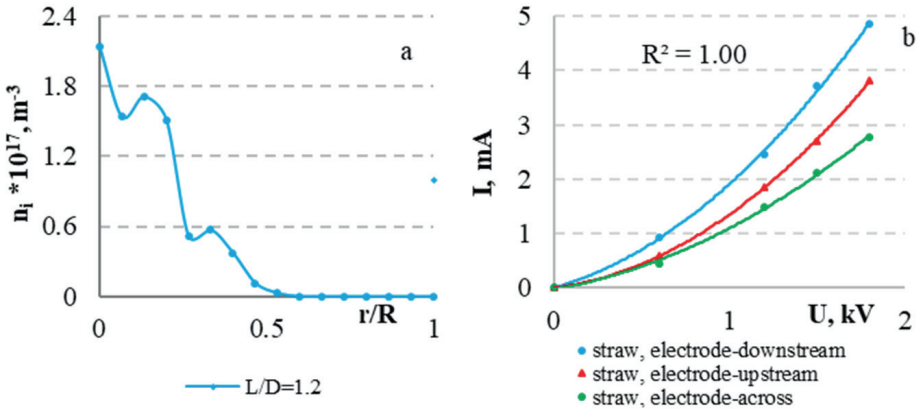

Fig. 3. The radial distribution of ion density at the thermochemical conversion of straw (a) and a current-voltage characteristic depending on the positions of electrode in swirl flame (b).

The results of the previous investigations [14], [15] have shown that the field-induced electric body force ($F = en_iE$), which is produced increasing the positive bias voltage of the axially inserted electrode, promotes field-enhanced drift motion of positive ions (CHO^+, H_3O^+, $C_3H_3^+$, etc.) from the reaction zone outwards – to the water-cooled walls of the combustor [10]. The elastic collisions between the accelerated flame ions and neutral flame species are responsible for the formation of field-enhanced processes of heat/mass transfer (ion wind effect) determining the variations of the local and average values of the flow velocity, flame temperature and composition.

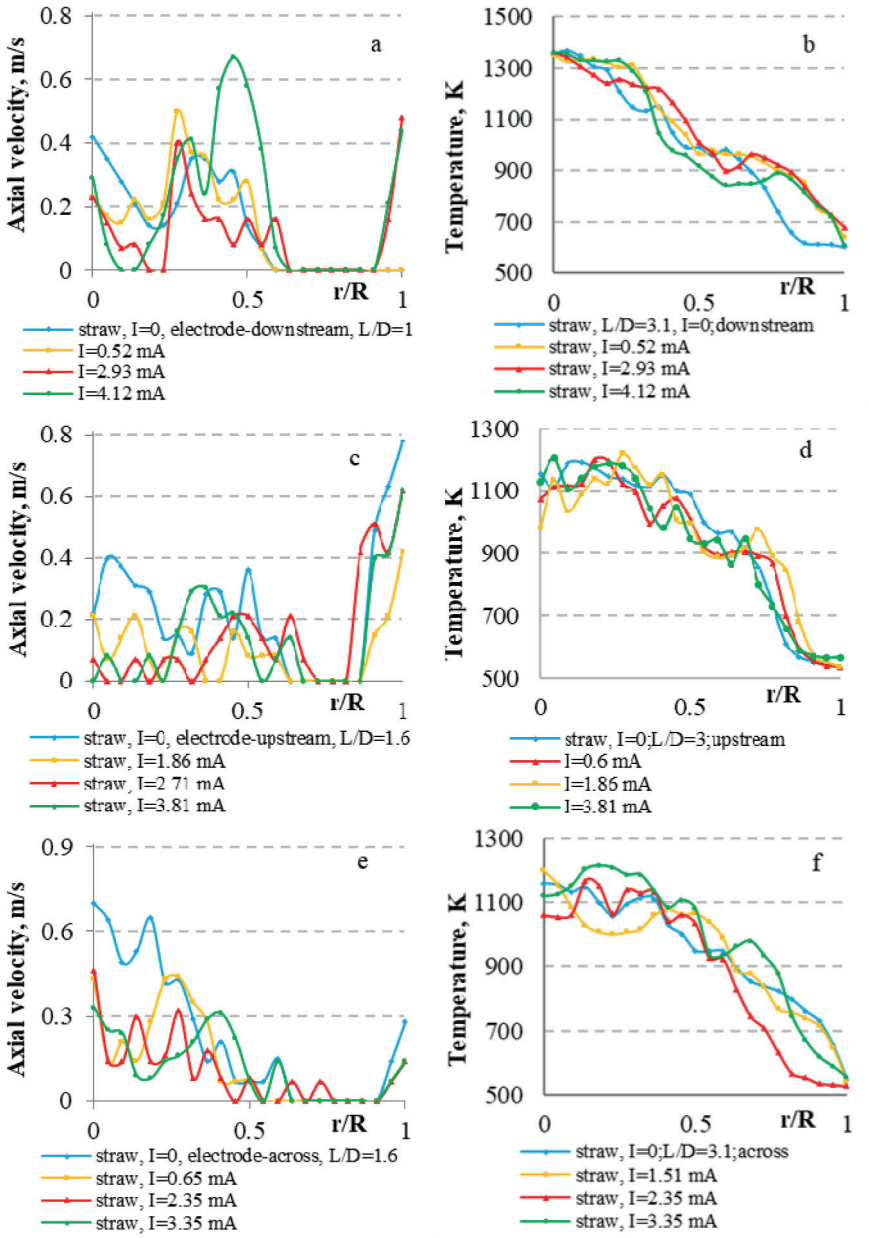

Fig. 4. The electric field effect on the formation of flow velocity and the temperature profiles of the flame reaction zone for different configurations of the electrodes.

The experimental study of the electric field effect on the main flame characteristics has shown that for the downstream position of the electrode the field-enhanced radial mass transfer of the flame ions and neutral flame species from the flame reaction zone outwards dominate. Therefore, for such electrode configuration increasing the positive bias voltage of the electrode causes the evident radial expansion of the reaction zone increasing the axial flow velocity along the airside part of the reaction zone ($r/R > 0.5$) and the flame temperature close to the walls of the combustor (Fig. 4-a, b).

For the upstream configuration of the electrode the field-enhances both the

reverse and radial mass transfer of the flame species. The field-enhanced reverse mass transfer slows down the axial flow velocity, while the field-enhanced radial motion of the flame species promotes the radial expansion of the reaction zone (Fig. 4-c, d). If the electrode is positioned across the reaction zone, the electric field enhanced reverse axial mass transfer of the flame species dominates, which slows down the axial velocity close to the flow centreline (r/R < 0.5) increasing the residence time of reactions and the temperature in this part of the flame (Fig. 4 - e, f).

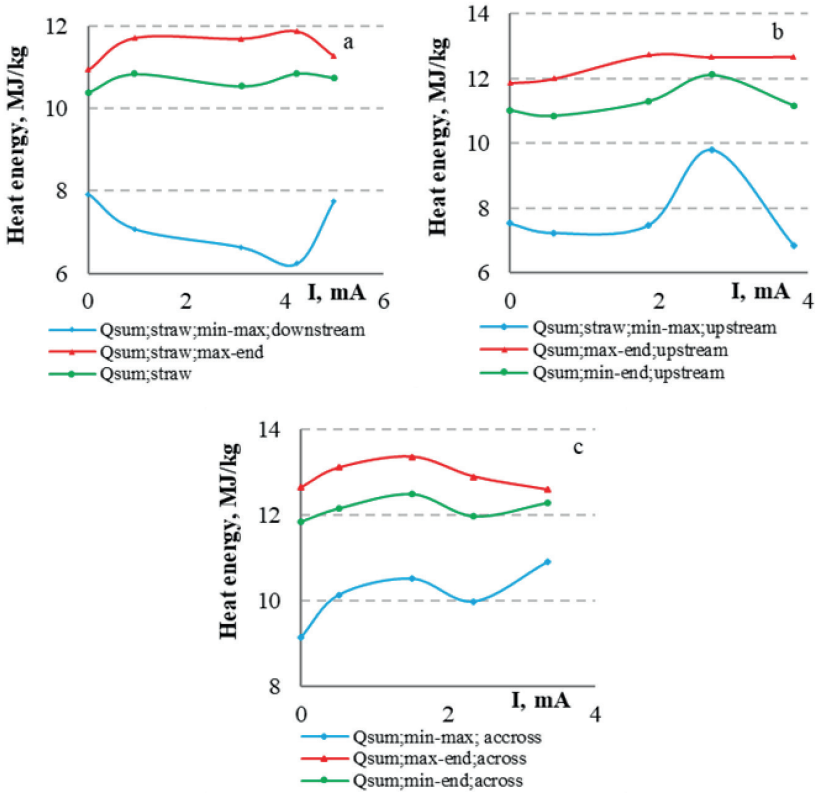

Fig. 5. The effect of electrode configuration on the total amount of the produced heat energy at the thermochemical conversion of straw.

The field-induced variations of the flow velocity and flame temperature profiles are closely linked to variations of the heat output from the device. The field-enhanced radial expansion of the reaction zone for the downstream positioned electrode results in an increase of the heat output from the flame reaction zone by about 12.5 % with an increase of the total heat output from the device by about 9.5 %. The produced heat energy per mass of burned straw for the downstream positioned electrode can be increased by about 12 % (Fig. 5-a), which confirms that the processess of field-induced radial heat/mass transfer complete the thermochemical conversion of straw. For the upstream configuration of the electrode, when the field enhances the reverse axial and radial heat mass transfer of the flame species, the heat output from the reaction zone can be increased by about 12.8 % increasing the total heat output from the device by about 13.3 %, while the produced heat energy per mass of burned straw increases by about 10 % (Fig. 5-b).

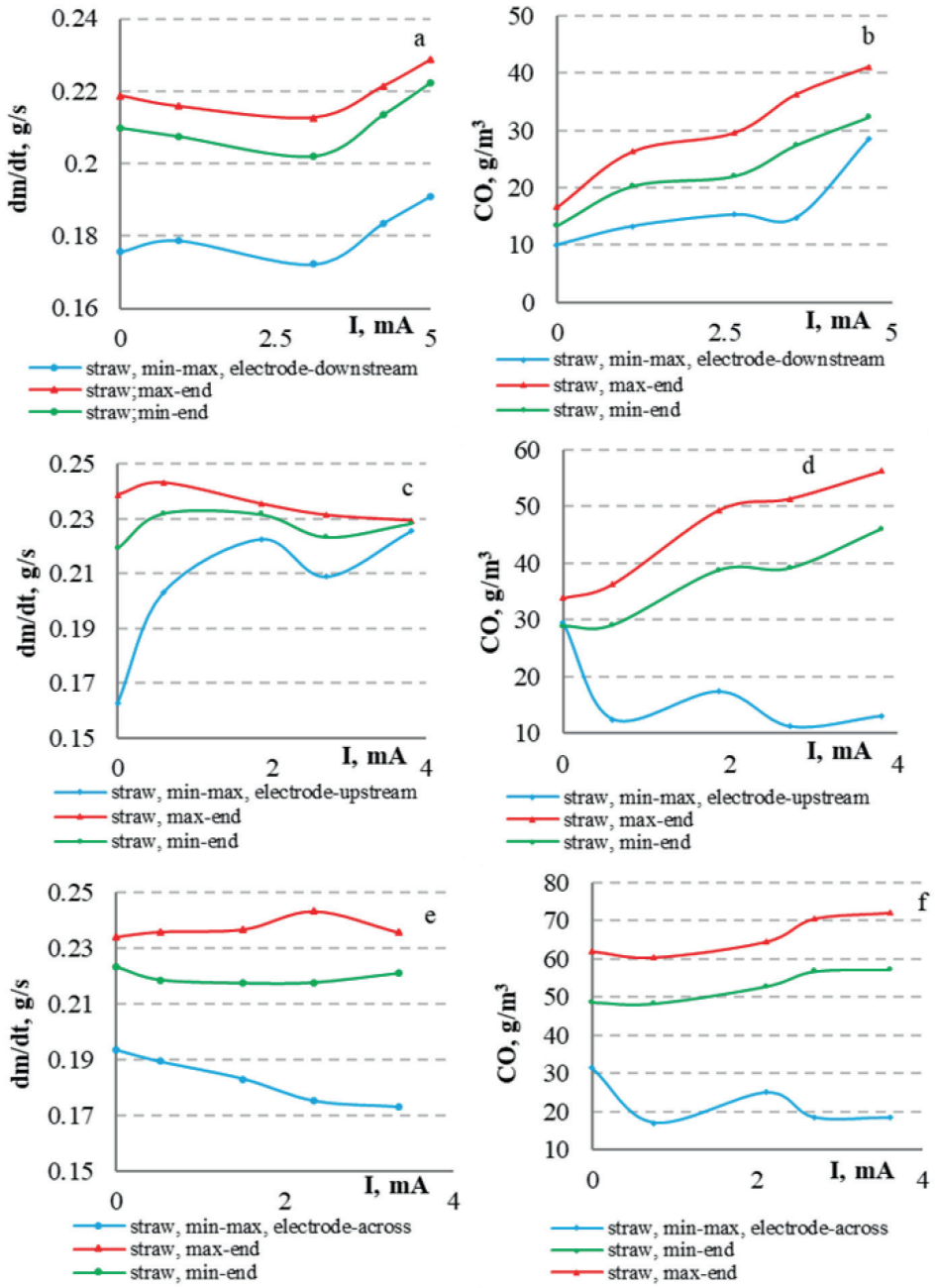

Fig. 6. The field-induced variations of the weight loss rate of straw pellets (a, c, e) and the volume density of combustible volatiles (CO) at the outlet of the gasifier (b, d, f) for different configurations of the electrodes.

Finally, for configuration of the electrode, located across the reaction zone, when the reverse axial heat/mass transfer of the flame species dominates, the heat output from the reaction zone increases by about 1.5 % and the total heat output from the device – by about 2.3 % with an increase in the produced heat energy during the burnout

of straw by about 5.6 % (Fig. 5-c). Hence, by comparing the field-induced variations of the heat output from the device, it can be concluded that upstream configuration of the electrode provides maximum heat output increase from the device and can be recommended for electrodynamic control of the produced heat power.

The analysis of the field effect on the main flame characteristics suggests that the field-induced variations of the flow dynamics, flame temperature and the heat output from the device disturb the heat balance between the flame reaction zone and the processes developing inside of the gasifier determining the complex field-induced variations of the weight loss rate and the composition of emissions at the thermal decomposition of straw pellets (Fig. 6, a-f). For the downstream configuration of the electrode an increase in the ion current provides an increase in the weight loss rate of straw pellets (Fig. 6-a) and the mass flow of volatiles increasing the mass fraction of combustible volatiles at the outlet of the gasifier (Fig. 6-b). For the upstream configuration of the electrode increasing the ion current above 2 mA promotes a decrease in the weight loss rate of straw pellets (Fig. 6-c), while the axial mass flow of volatiles increases (Fig. 6-d) indicating the field-induced recombination of H_3O^+ and the development of the endothermic water-gas reactions, which are responsible for the field-enhanced increase of the mass flow of CO and H_2 at the outlet of the gasifier:

$$H_3O^+ + e \rightarrow H_2O + H \quad (5)$$

$$H_2O + C \rightarrow H_2 + CO \quad (6)$$

The effect of development of the water-gas reactions on the weight loss rate of straw pellets with correlating increase of mass flow of CO and H_2 at the outlet of the gasifier is also observed if the electrode is located across the flame reaction zone (Fig. 6 - e, f) and the field-enhanced reverse mass transfer of positive ions to the carbonized surface of straw pellets slows down the thermal decomposition of straw pellets.

The field-induced variation of the flow dynamics, heat/mass transfer and residence time of reactions for different configuration of the electrodes determine the variation of the product composition. By analogy with the field effect on the produced heat energy at the thermochemical conversion of straw for all configuration of the electrodes increasing the bias voltage of the electrodes and the field-induced ion current results in an increase in the average values of the total amount of CO_2 emissions in the products (by about 5–6 %) during the self-sustaining burnout of volatiles with a correlating decrease in CO emissions in the products (up to 60 % for upstream field configuration), confirming that the electric field completes combustion of volatiles.

Besides, the flame response to field-induced variation of the main flame characteristics results in an increase in combustion efficiency, while the field-enhanced reverse axial and radial heat/mass transfer of the flame species from the flame reaction zone outwards with a correlating decrease in the temperature is limiting the temperature-sensitive NO formation, decreasing the mass fraction of NO_x ($NO+NO_2$) emission in the products for all electric field configurations. The maximum decrease in NO_x mass fraction (up to 10 %) was observed for upstream field configuration. Finally, the results of experiments show that the electric field control can be used as a tool to provide a cleaner and more complete thermochemical conversion of straw.

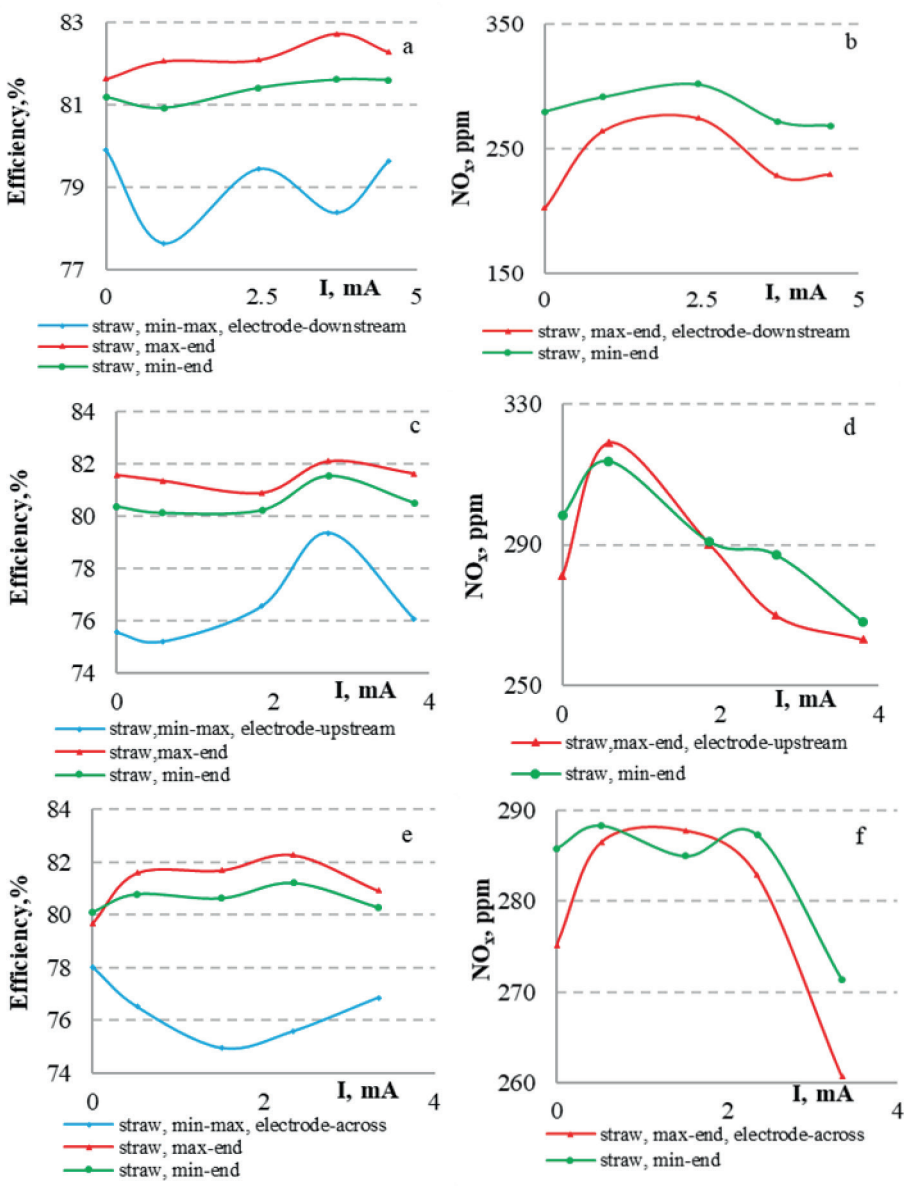

Fig. 7. The electric field effect on the combustion efficiency (a, c, e) and the mass fraction of NOx in the products (b, d, f)) at the thermochemical conversion of straw.

4. CONCLUSIONS

Summarising the results of the complex experimental studies of the DC electric field effect on the development of combustion dynamics and heat energy production during the thermochemical conversion of straw for different positions of the electrode in the flame reaction zone (downstream, upstream, across) the following conclusions are drawn:

For all positions of the electrode its

placement in the flame flow disturbs the formation of the flame temperature and velocity profiles decreasing the average values of the axial velocity with radial expansion of the flow velocity and flame temperature profiles and enhanced burnout of volatiles. Further changes in the main flame characteristics are achieved by increasing the positive bias voltage of the electrode and the current in the flame space between the electrodes. For all positions of the electrode the DC electric field intensifies the thermal decomposition of straw pellets, enhances mixing of volatiles with air and causes changes in the main combustion characteristics by varying heat energy production and composition of the products.

The most pronounced electric field effect on the main combustion characteristics is observed for the upstream configuration of the positively biased electrode, when increasing the bias voltage from 0.6 kV to 1.8 kV and the ion current from 0.5 mA to 1.8 mA, the heat output from the reaction zone can be increased by about 12.8 %, increasing the total heat output from the device by about 13.3 %, while the produced heat energy per mass of burned straw increases by about 10 %. Besides, the average volume fraction of CO_2 increases by 6 %, decreasing the mass fraction of unburned volatiles in the products (CO by about 60 % and H_2 by 73 %), which confirms more complete combustion of volatiles.

ACKNOWLEDGEMENTS

The authors deeply acknowledge the financial support of the European Regional Development Funding Project No. 1.1.1.1/16/A/004.

REFERENCES

1. European Commission. (2019). *2030 Climate & Energy Framework*. Available at: https://ec.europa.eu/clima/policies/strategies/2030_en
2. Roger, A.S. (2013). Comparative life cycle assessments: carbon neutrality and wood biomass energy. *Resources for the Future DP13-11*, Washington, 1–18. http://www.rff.org/RFF/Documents/RFF-DP-13-11.pdf
3. Vasilev, S., Baxter, D., Andersen, L.K., Vasileva, C.G., & Morgan, T.J. (2012). An Overview of the Organic and Inorganic Phase Composition of Biomass. *Fuel,* 94, 1–33. https://doi.org/10.1016/j.fuel.2011.09.030
4. Koppejan, J., & Cremers, M. (2019). *Biomass Pre-Treatment for Bioenergy*. Policy report published by IEA Bioenergy. Available at: https://www.ieabioenergy.com/wp-content/uploads/2019/04/Pretreatment_PolicyReport.pdf
5. Wang, L., Littlewood, J., & Murphy, R.J. (2013). Environmental Sustainability of Bioethanol Production from Wheat Straw in the UK. *Renewable and Sustainable Energy Reviews,* 28, 715–725. https://doi.org/10.1016/j.rser.2013.08.031 , Available at:https://www.sciencedirect.com/science/article/pii/S1364032113005716
6. Barmina, I., Kolmičkovs, A, Valdmanis, R, Vostrikovs, S., & Zake, M. (2018). Thermo-chemical conversion of microwave activated biomass mixtures. *JPCS-IOP-MMP*, Journal IOP Conf. Series: Materials Science and Engineering, doi:10.1088/1757-899X/355/1/012018, Available at: https://iopscience.iop.org/article/10.1088/1757-899X/355/1/012018

7. Barmina I., Valdmanis R., & Zake M. (2018). The Effects of Biomass Co-Gasification and Co-Firing on the Development of Combustion Dynamics. *Energy, 146*, 4–12. DOI: 10.1016/j.energy.2017.04.140
8. Pedersen, L.S., Nielsen, H.P., Kiil, S., Hansen, L.A., Dam-Johansen, K., Kildsig, F., ... & Jespersen, P. (1996). Full-Scale Co-Firing of Straw and Coal. *Fuel, 75,* 1584-1590. https://doi.org/10.1016/0016-2361(96)82642-1
9. Houshfar, E., Løvås, T., & Skreiberg, Ø (2012). Experimental Investigation on NOx Reduction by Primary Measures in Biomass Combustion: Straw, Peat, Sewage Sludge, Forest Residues and Wood Pellets. *Energies,* 5, 270–290; doi:10.3390/en5020270.
10. Lawton, J., & Weinberg, F. (1969). *Electrical aspects of combustion*. Oxford, UK: Clarendon Press, ISBN 0198553412.
11. Blades, A.T. (1976). Ion Formation in Hydrocarbon Flames. *Can J Chem, 54* (18), 2919−2924, https://www.nrcresearchpress.com/doi/pdfplus/10.1139/v76-413
12. Chien, Y., & Dunn-Rankin, D. (2018). Electric Field Induced Changes of a Diffusion Flame and Heat Transfer near an Impinging Surface, *Energies, 11,* 1235; doi:10.3390/en11051235.
13. Ryu, S.K., Kim, Y.K., Kim, M.K., Won, S.H., & Chung, S.H. (2010). Observation of Multi-Scale Oscillation of Laminar Lifted Flames with Low-Frequency AC Electric Fields. *Combust. Flame,* 157, 25–32. https://doi.org/10.1016/j.combustflame.2009.10.001 Available at: https://www.sciencedirect.com/science/article/abs/pii/S001021800900279X
14. Barmina, I., Kolmickovs, A., Valdmanis, R., Zake, M., Vostrikovs, S., Kalis, H., & Strautins, U. (2019). Electric Field Effect on the Thermal Decomposition and Co-combustion of Straw with Solid Fuel Pellets, *Energies, 12,* 1522; https://doi.org/10.3390/en12081522
15. Barmina, I., Purmalis, M., Valdmanis, R., & Zaķe, M. (2016). Electrodynamic Control of the Combustion Characteristics and Heat Energy Production. *Combustion Science and Technology, 188* (2), 190–206, DOI: 10.1080/00102202.2015.1088010. URL: http://www.tandfonline.com/doi/full/10.1080/00102202.2015.1088010
16. Colannino, J. (2013). *Electrodynamic Combustion Control TM Technology*, A ClearSign White Paper; ClearSign Combustion Cooperation: Seattle, WA, USA. Available at: http://www.ctgn.qc.ca/images/bulletins/bulletin_vol4no3/pdf/ind_ha_clearsign_01.pdf
17. Greene, S.A. (1963). *A Literature Survey of Ions in Flames*, Report No. TDR-169(S3153-01) TN-5, Ballistic Systems Division Air Force Systems Command, United States Air Force, California, 1–23.
18. Yang, H., Yan, R., Chen, H, Lee, D.H, & Zheng, Ch. (2007). Characteristics of Hemicellulose, Cellulose and Lignin Pyrolysis, *Fuel, 86,* 1781–1799. https://doi.org/10.1016/j.fuel.2006.12.013
19. Barmina, I., Kolmickovs, A., Valdmanis, R., & Vostrikovs, S. (2019). Electrodynamic control of straw co-firing with propane. In *Engineering for Rural Development conf*, 22–24 May 2019 (pp. 1319–1324), Jelgava, Latvia: Latvia University of Life Sciences and Technologies. DOI: 10.22616/ERDev2019.18. N022.